UPSTREAM CONTROL AND DOWNSTREAM RESPONSES OF p53 ARE INVOLVED IN ITS TUMOR SUPPRESSION FUNCTIONS UPON GENOTOXIC STRESS

Inaugural-Dissertation
to obtain the academic degree
Doctor rerum naturalium (Dr. rer. nat.)

submitted to the Department of Biology, Chemistry and Pharmacy
of Freie Universität Berlin

by

ANA FINZEL PÉREZ

from Gijón (Asturias, Spain)

2016

The present work was done from October 2011 to June 2016 in the research group of Prof. Dr. Alexander Löwer at the Max Delbrück Center (MDC) for Molecular Medicine in Berlin-Buch.

First reviewer: Prof. Dr. Alexander Löwer
Second reviewer: Prof. Dr. Petra Knaus

Date of defence: 13.12.2016

ACKNOWLEDGMENTS

First of all I want to thank Prof. Dr. Alexander Löwer not only for giving me the opportunity to work in his lab, but also for his support and understanding during the hard times, for his trust, and for his patience with my questions and inestimable help during the writing of this thesis.

I also would like to thank Prof. Dr. Petra Knaus for her willingness to read and evaluate this thesis.

A very special thank you goes to the Löwer´s lab, especially to Andrea (vielen Dank, nicht nur für deine große Hilfe mit den Experimenten, sondern auch für dein Verständnis), Jette (meine liebe Oghetta), my informatics-problems-savior Caibin, meine Lieblingsorganisatorin und hilfsbereite Dhana, our Greek postdoc Ilias (thanks for your support and advice), Elena (Gordi), Marcel (our cool bioinformatician guy, vielen, vielen Dank für deine Hilfe mit den Analysen) and Gitta (danke für deine Hilfe mit den Zellen). Thanks for your help, but also for the laughs, the “mouse hunt”, the Glühwein stand, the cakes, even for the flood, and for so many other unforgettable memories.

Furthermore, I thank Dr. Stefan Kempa (technology platform Proteomics/Metabolomics, MDC Berlin) for the interesting collaboration and for his help and input. I want to express my gratitude to several members of his group: Guido Mastrobuoni, Christine Zasada, Nadine Royla, Jenny Grobe, Julia Diesbach, Tobias Opialla and especially to Fabian Bindel. I thank you all for your time, patience and help at different steps of the experiments, analysis and/or thesis writing.

I would also like to thank the Genomics technology platform (Prof. Dr. Wei Chen, MDC Berlin), especially Madlen Sohn; Antje Hirsekorn from the Ohler´s lab for introducing me into the RNA-seq world and for always being so kind, and Altuna Akalin (Bioinformatics Platform, MDC Berlin) for his help with the RNA-seq analysis and for answering so many questions.

Outside of work, a special thank you goes to my friends for the fun, the tasty food, the nice talks and their support.

ACKNOWLEDGMENTS

With all my love, I want to thank my family. Mamá, papá, Paula y Dani, gracias por vuestro cariño y amor, por vuestro apoyo, por creer en mí siempre, por las risas y los momentos bonitos, que son tantos. Sois la mejor familia que puedo imaginar.

Finalmente ringrazio te, Davide. Grazie per la tua pazienza, grazie per prenderti cura di me, grazie per il tuo amore, grazie per camminare sempre al mio fianco, mano nella mano e cuore a cuore.

DIRECTORY

1 INTRODUCTION

1.1 p53 is a cellular gatekeeper

The p53 protein was discovered almost forty years ago (DeLeo et al., 1979; Lane and Crawford, 1979; Linzer and Levine, 1979), and ten years later it was characterized as a tumor suppressor (Baker et al., 1989; Finlay et al., 1989). p53 is one of the most studied human genes, as loss of its function is a common feature in most tumors (Muller and Vousden, 2013), either through mutations in p53 or perturbations by other mechanisms such as DNA tumor viruses (Levine, 2009). p53 has been called "the guardian of the genome" (Lane, 1992) or "cellular gatekeeper" (Levine, 1997) because it is a transcription factor that plays a prominent role in responding to a wide range of cellular stress signals that cells could encounter during malignant progression, for example genotoxic damage, oncogene activation or hypoxia (Vousden and Prives, 2009).

1.1.1 Functional domains of p53

The p53 protein consists of 393 amino acids and is divided into three functional domains (Bode and Dong, 2004) (Figure 1). The N-terminal transactivation domain interacts with several transcription factors and the E3 ubiquitin-protein ligase mouse double minute 2 (Mdm2). The DNA binding core domain binds to promoter sites containing two copies of the consensus sequence 5´- RRRC(A/T)(A/T)GYYY-3´ (R=A,G; Y=C,T) separated by 0-13 base pairs (bp) (el-Deiry et al., 1992). p53 is also capable of binding to half- and three quarter-consensus sites (Jordan et al., 2008), but with lower affinity than to its consensus sequence. The C-terminal domain contains the tetramerization domain that permits oligomerization of the protein – it is in its tetrameric conformation when p53 is active and binds to DNA (Chène, 2001) –, the nuclear localization and export signals (NLS and NES, respectively), and a regulatory domain that seems to regulate the DNA binding core domain.

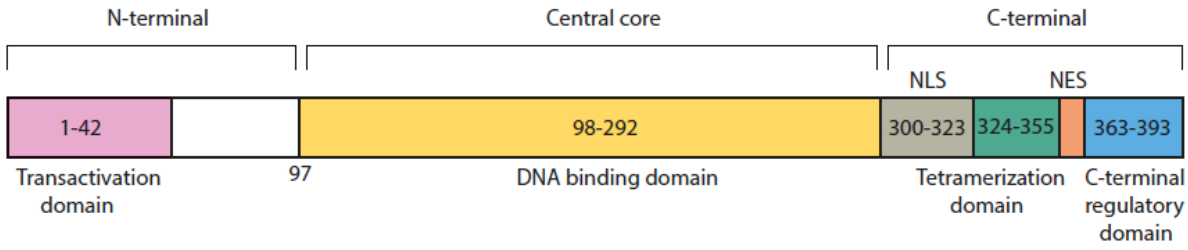

Figure 1. Functional domains of p53. Numbers indicate residue number. Modified from (Bode and Dong, 2004)

1.1.2 p53 is activated upon stress

In the traditional model of p53 activation, p53 levels are kept low under non-stressed conditions by its interaction with Mdm2. Mdm2 ubiquitinates p53 on the C-terminal domain and promotes p53 proteasomal degradation (Haupt *et al.*, 1997; Kubbutat *et al.*, 1997). After stress induction, p53 is phosphorylated by different kinases on serine residues (e.g. Ser15) within the N-terminal transactivation domain. These phosphorylations inhibit the interaction between p53 and Mdm2 and stabilize p53, which interacts then with target gene promoters in a sequence-specific manner and activates transcription together with the general transcription machinery (Kruse and Gu, 2009). However, the classical model is not sufficient to completely explain p53 activation, as p53 stabilization, DNA binding and transcriptional activation steps are actually more complex than originally anticipated (Kruse and Gu, 2009). Cellular localization, oligomerization and concentration are crucial elements that control p53 activity (Gu and Zhu, 2012; Rajagopalan et al., 2011). Under non-stressed conditions, p53 levels and activity are downregulated by ubiquitin-mediated proteasomal degradation by Mdm2 (Kubbutat et al., 1997), by a decrease in nuclear p53 levels due to nuclear export by exposure of either p53 or Mdm2 NES (Stommel et al., 1999; Tao and Levine, 1999; Zhang, 2001), and by a repression of chromatin-associated p53, mediated by p53 key negative regulators, Mdm2 and mouse double minute 4 (Mdm4). Under stress conditions, p53 is stabilized and accumulates in the nucleus by different means, which include p53 phosphorylation by kinases and acetylation by p300-CBP (CREB-binding protein) cofactor on the C-terminal domain, which prevent Mdm2-p53 interaction; Mdm2 phosphorylation and p300-CBP-mediated acetylation, which inhibit Mdm2 activity; suppression of p53 nuclear export, as p53 tetramerization occludes its NES (Stommel et al., 1999), and promotion of nuclear import (Marchenko et al., 2010). Apart from increasing p53 stability, cellular stress also promotes antirepression (Kruse and Gu, 2009): p53 is intrinsically active and bound to several gene promoters but continuously repressed by Mdm2 and Mdm4. p53 post-translational modifications such as phosphorylation and acetylation are needed for repression release (Kruse and Gu, 2009) (Figure 2).

Interaction of p53 with some coactivators, together with antirepression, is enough to activate genes highly responsive to p53, which contain high affinity-binding sites (e.g. genes involved in reversible cell cycle arrest). On the contrary, promoters of genes involved in terminal cell fates, e.g. apoptosis, have lower affinity-binding sites (Weinberg et al., 2005). That´s why, antirepression is insufficient to induce expression of apoptotic genes, and promotion of this irreversible cell fate actually requires additional stimulation: combinations of specific cofactors and coregulators need to be recruited to the target promoters, while Mdm2 and Mdm4

corepressors need to be completely removed. These specific cofactors modify p53 at many specific sites through acetylation, methylation, neddylation and sumoylation on the different domains. Moreover, they also modify the surrounding histones and other transcription factors needed for p53 function (Kruse and Gu, 2009).

Interestingly, depending on interaction with coactivators or corepressors, p53 either activates or represses target gene expression (Kruse and Gu, 2009). In addition, various types of stress require different modes for p53 regulation. The high number of possible variations of these modifications acts like a barcode, promoting DNA specific responses depending on the type of damage or stress.

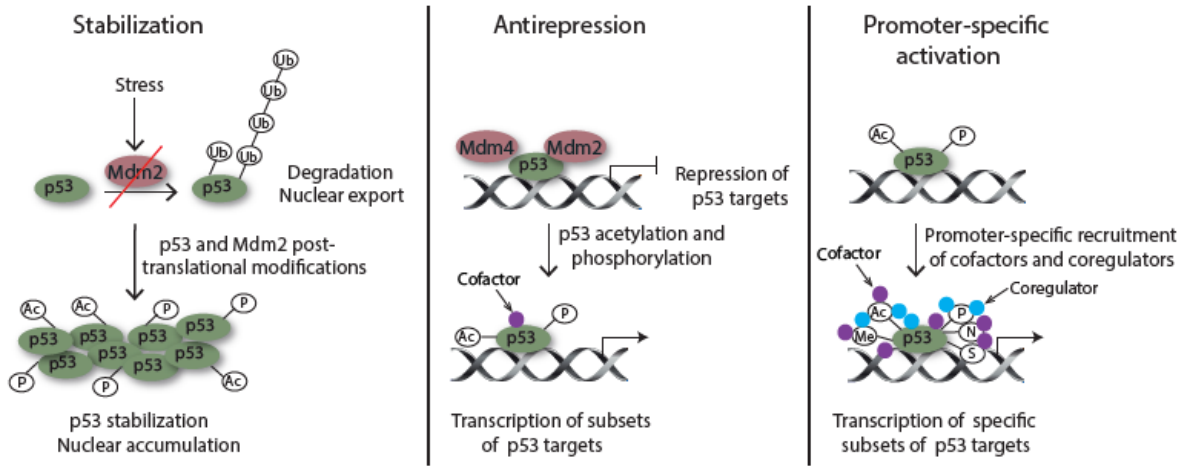

Figure 2. Model for p53 activation. Ub stands for ubiquitylation, P for phosphorylation, Ac for acetylation, N for neddylation, S for sumoylation and Me for methylation. Modified from (Kruse and Gu, 2009).

1.2 Response to double strand breaks

p53´s best characterized function is the response to DNA damage. The DNA damage response (DDR) is an essential process that protects the integrity of the genome and prevents cancerogenic transformations. In mammalian cells, sophisticated mechanisms evolved to sense various kinds of DNA damage and adjust cellular physiology by arresting the cell cycle, activating repair mechanisms or inducing senescence and apoptosis (Ciccia and Elledge, 2010). Among the most dangerous DNA lesions are double strand breaks (DSBs), as they can lead to chromosomal aberrations and cellular transformation when left unrepaired. Three kinases belonging to the phosphatidylinositol 3-kinase (PI3K)-like kinase family coordinate the response to DSBs: ataxia telangiectasia-mutated (ATM) (Harper and Elledge, 2007), ataxia telangiectasia and Rad3-related (ATR) (Cimprich and Cortez, 2008) and DNA-dependent protein kinase catalytic subunit (DNA-PKcs) (Chiruvella *et al.*, 2013). The activation of these

nuclear serine/threonine kinases follows a complex pattern that changes over time and depends on the nature of the induced breaks and the repair pathways employed (Ciccia and Elledge, 2010). ATM is activated immediately upon damage and mediates repair of DSBs by both canonical non-homologous end joining (cNHEJ) and homologous recombination (HR) (Lavin et al., 2006). DNA-PKcs activation, in contrast, is restricted to breaks repaired by cNHEJ. ATR is activated at later stages of the response by the presence of single-stranded DNA, which is mainly exposed during HR.

1.2.1 Homologous recombination

Homologous recombination repair pathway is only available during S and G2 phases. Upon DNA damage, the MRE11A-RAD50-NBN or MRN complex is one of the first in being recruited to the break sites (Figure 3). Then, this complex activates ATM (Williams et al., 2007) by promoting its autophosphorylation. Active ATM phosphorylates, among other substrates, the histone H2A.X adjacent to the breaks forming ɣH2A.X (Fernandez-Capetillo et al., 2004). The adaptor protein MDC1 (mediator of DNA damage checkpoint 1) binds to ɣH2A.X (Stucki et al., 2005), and a positive feed-back loop is formed through the MDC1 interaction with NBN and ATM (Lou et al., 2006) that extends H2AX phosphorylation to distances up to one to two megabases around the breaks. The formation of extensive ɣH2A.X regions is important for sustaining the DDR and maintaining factors involved in repair at the breaks sites, such as NBN, tumor protein p53 binding protein 1 (TP53BP1) or breast cancer 1 (BRCA1) (Celeste et al., 2002). The maintenance of the response is achieved through recruitment of a complex network of chromatin modifying enzymes, such as ubiquitin ligases. For example, ATM-dependent phosphorylation of MDC1 is recognized by the ubiquitin ligase ring finger protein 8, activating an ubiquitination cascade and finally recruiting BRCA1 (Ciccia and Elledge, 2010). The large multi-protein complexes assembled around break sites in a γ-H2AX- and MDC1-dependent manner are necessary to distribute the damage signal throughout the nucleus and to promote appropriate repair mechanisms.

The next step is DNA repair itself. First, resection of the two 5´ends is performed by the bloom syndrome RecQ like helicase and three exonucleases, exonuclease 1, MRE11A – component of the MRN complex –, and RBBP8 (retinoblastoma binding protein 8), whose interaction with BRCA1 facilitates resection (Cruz-García et al., 2014). Breaks resection forms single-stranded DNA regions that activate ATR, kinase that regulates RAD51 recruitment. The RAD51-coated nucleoprotein filaments invade the undamaged sister strands (Baumann et al., 1996) forming a

displacement loop. There are several models explaining the last steps that lead to damage resolution (not shown).

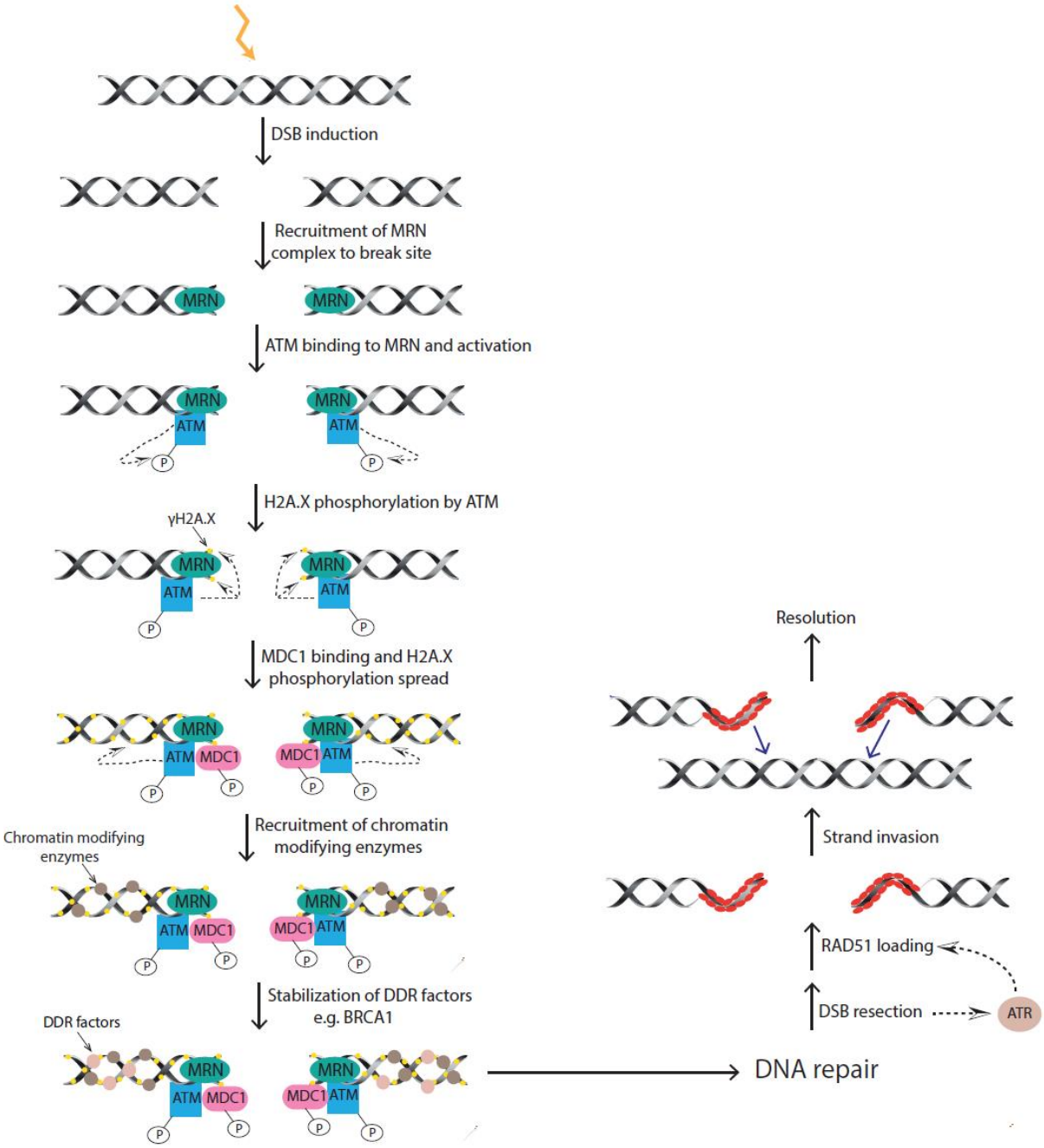

Figure 3. Homologous recombination repair pathway. P stands for phosphorylation. Based on (Ciccia and Elledge, 2010; Lopez-Contreras and Fernandez-Capetillo, 2012).

1.2.2 Canonical non-homologous end joining

cNHEJ is simpler than HR, it can take place in any cell cycle stage and is more error-prone. Upon DNA damage, DSBs are sensed by a heterodimer of Ku70 and Ku80 proteins (Doherty and Jackson, 2001), which stabilizes the two DNA ends and attracts DNA-PKcs (Figure 4). DNA-PKcs becomes active and phosphorylates Artemis, involved in end-processing.

Interestingly, DNA-PKcs phosphorylation by ATM is necessary for Artemis phosphorylation and recruitment (Jiang et al., 2015). Upon phosphorylation, Artemis acquires endonuclease activity, needed for opening closed hairpins in which the two strands of the break have linked together. DNA-PKcs also phosphorylates the complex formed by XRCC4 and ligase IV (LigIV) that rejoins the ends (Martin and MacNeill, 2002) with the help of the XRCC4-like factor (XLF) (Mahaney et al., 2009). LigIV provides the catalytic activity, while XRCC4 stimulates its activity. This complex can access the breaks only upon DNA-PKcs autophosphorylation and dissociation from the DNA (Allen et al., 2003; Jiang et al., 2015).

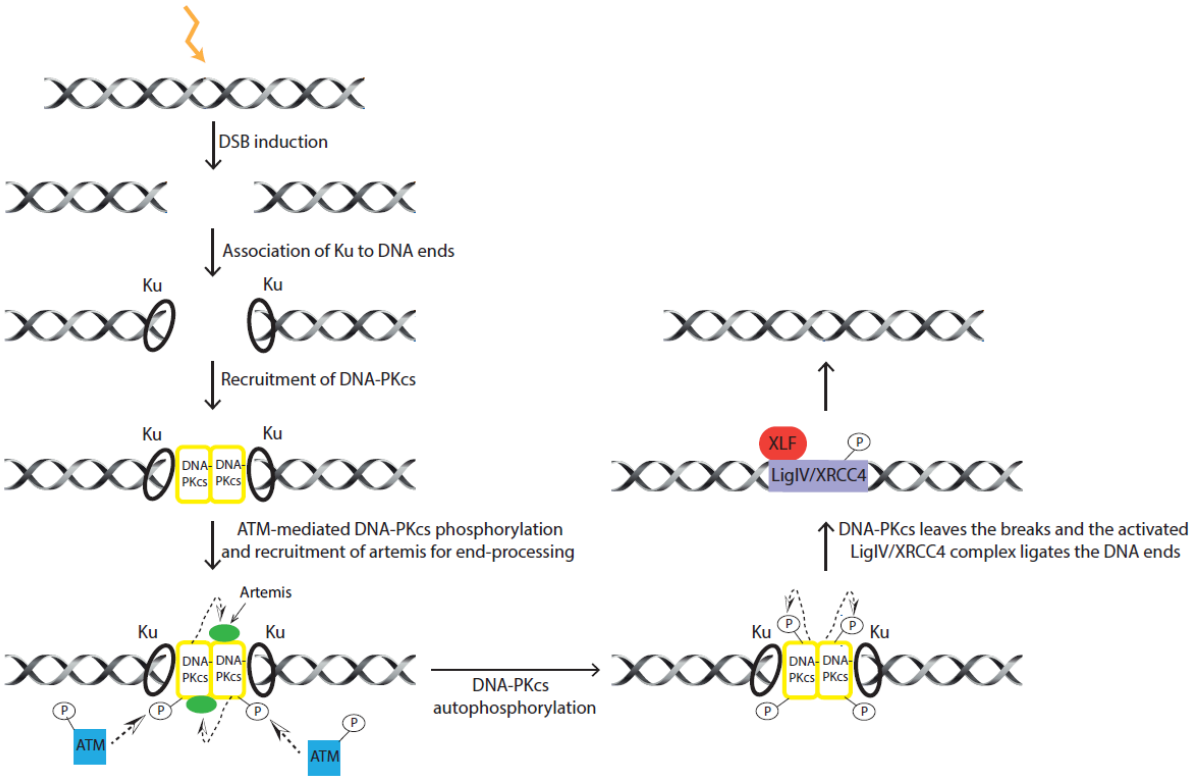

Figure 4. **Canonical non-homologous end joining.** P stands for phosphorylation. Based on (Ciccia and Elledge, 2010; Lopez-Contreras and Fernandez-Capetillo, 2012).

1.2.3 p53 is activated upon genotoxic stress

In addition to organizing repair of DSBs, PIK3-like kinases relay damage signals to p53. Under non-stressed conditions, p53 is kept at low levels by Mdm2-mediated proteasomal degradation. When a cell encounters DNA damage, ATM, ATR and DNA-PK phosphorylate p53 and Mdm2. In addition, ATR and ATM activate the checkpoint kinases Chk1 and Chk2, respectively, which modify p53 as well (Kruse and Gu, 2009). Together, these phosphorylations prevent binding of p53 to Mdm2. p53 accumulates in the nucleus and acts as a transcription factor promoting the expression of genes involved in several processes, such as DNA repair, cell cycle arrest, apoptosis and senescence in order to maintain genome integrity (Vousden and Prives, 2009).

p53 accumulation occurs as a series of discrete pulses upon genotoxic stress (Lahav et al., 2004). The timing of the first pulse maximum occurs approximately two to four hours after damage induction, and the timing between maximum of two consecutive pulses is about seven hours. Interestingly, genetically identical cells have different number of pulses, but their mean duration and height are constant and independent of the degree of DNA damage (Lahav et al., 2004). However, the mean number of pulses increases with the amount of damage applied.

What is the molecular mechanism behind this stereotyped nature of p53 pulses? Upon damage, p53 starts accumulating and promotes expression not only of genes involved in cell cycle arrest or apoptosis, but also of two negative regulators, Mdm2 and Wip1 (wild-type p53-induced phosphatase 1). Once Mdm2 protein concentration increases, p53 response is terminated through a negative feedback loop. However, this interaction is not sufficient to explain sustained p53 oscillations. A second feedback loop exists between p53 and Wip1, phosphatase that reverses not only p53 phosphorylation by PI3K-like kinases (Lu et al., 2007), but also dephosphorylates ATM (Shreeram et al., 2006) and Chk2 (Fujimoto et al., 2006; Oliva-Trastoy et al., 2007) (Figure 5). That´s why, Wip1 is the protein responsible for creating pulses in the upstream signaling kinases (phosphorylated ATM and Chk2) that drive p53 pulses (Batchelor et al., 2008). When p53 levels go down after the first pulse, phosphorylated ATM levels start accumulating again if the damage is still present. ATM activates then p53, which in turn promotes Mdm2 and Wip1 expression, leading to a second pulse (Batchelor et al., 2008).

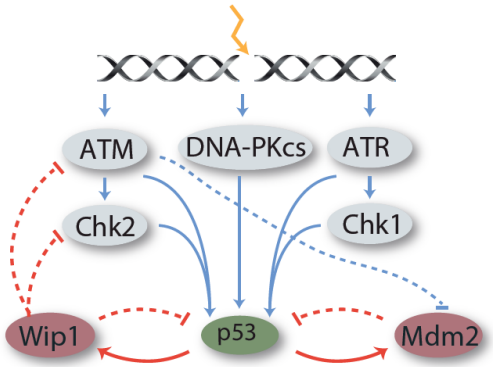

Figure 5. Schematic overview of the p53 network in response to double strand breaks.

In summary, these two interlinked negative feedback loops shape the dynamic response of p53 to DSBs, resulting in pulsatile protein accumulations or dynamics with uniform amplitudes and durations (undamped oscillations), independent of the degree of damage. What is the meaning or function of p53 pulses? Activation of p53 is not only depending on increased concentrations, but also on post-translational modifications necessary for activating specific sets of genes, as previously explained. It could happen that the information encoded by p53 modifications on

the first pulse needs to change in the second pulse in order to activate a different group of genes. Degradation of p53 is the simplest way for "deleting" the information and allowing synthesis of new unmodified p53 (Lahav, 2004).

1.3 Importance of p53 single cell studies

The fact that p53 pulses show undamped oscillations was first described in single cell studies using time-lapse fluorescent microscopy and transgenic fluorescent cell lines (Lahav et al., 2004). Until that time, p53 was thought to undergo damped oscillations after DNA damage, as it was shown that the second p53 pulse showed a smaller amplitude when compared to the first one (Lev Bar-Or et al., 2000). In that study, p53 accumulation was analyzed on cell populations by western blot.

The difference observed between population and single cell studies can be explained because different cells can exhibit different number of pulses, and because synchronicity upon the first p53 pulse is lost (Purvis and Lahav, 2013) (Figure 6).

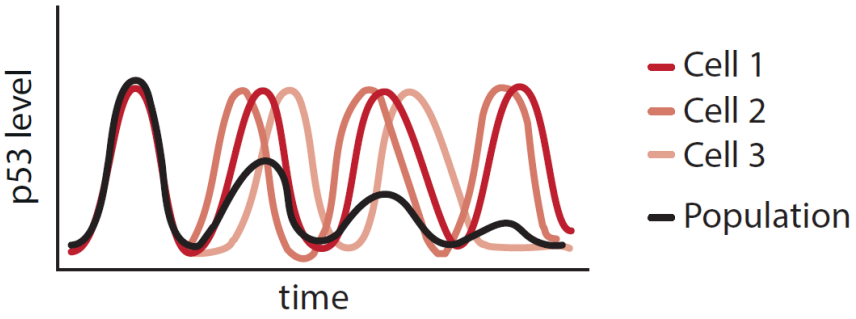

Figure 6. Cell population studies can obscure dynamics of individual cells. p53 pulses upon genotoxic stress have uniform amplitudes and durations. Loss of synchrony and different number of pulses among individual cells explain the damped oscillations observed in the population. Modified from (Purvis and Lahav, 2013).

The importance of performing studies at the single cell level is highlighted by the recently proposed hypothesis that biological information is not only encoded in the structural components of a cell, but also in the dynamics of signaling molecules (Behar and Hoffmann, 2010). Regarding p53, the importance of its dynamics in regulating cell fate decisions has been previously described. In Purvis et al., p53 pulsing behavior was transformed into a sustained response by adding Nutlin-3, a small molecule that binds to Mdm2 and inhibits p53 degradation (Vassilev et al., 2004). This change in dynamics was enough to increase the number of cells undergoing senescence upon genotoxic stress due to a higher expression of the p53 target genes p21, involved in cell cycle arrest (El-Deiry et al., 1993), and YPEL3 (Kelley et al., 2010) and

promyelocytic leukemia (De Stanchina et al., 2004), involved in senescence. In Borcherds et al., the binding affinity between p53 and Mdm2 was increased by mutating conserved proline residues to alanines on the N-terminal domain. These genetic modifications led to earlier and shorter p53 pulses upon DNA damage, provoking reduced levels of p21 expression and a subsequent decrease in arresting cells (Borcherds et al., 2014).

1.4 p53 and metabolism

The role of p53 as a tumor suppressor has been attributed to transcriptional activation of genes involved in apoptosis or in a permanent inhibition of cell proliferation (senescence) (Kruiswijk et al., 2015), terminal cell fates that eliminate tumor cells and block cancer progression. However, in recent years it has become evident that p53 is also involved in regulating transcription of genes involved in cellular homeostasis, such as DNA repair and metabolism.

Nutrients are taken up by cells and metabolized in order to produce energy and increase cell biomass to support cell growth. It is therefore not surprising that cancer cells need to adjust their metabolism in order to maintain a high rate of cell proliferation (Garber, 2006). In fact, reprogramming of cellular metabolism has been recently considered as an emerging hallmark of cancer (Hanahan and Weinberg, 2011).

Glucose is a key nutrient used for energy production (conserved as adenosine triphosphate, ATP) and for synthesis of macromolecules. Glucose is oxidized in the cytoplasm by the glycolytic pathway to pyruvate, producing two molecules of ATP from one molecule of glucose. This process is anaerobic, but in the presence of oxygen, pyruvate enters the tricarboxylic acid (TCA) or citric acid cycle in the mitochondria and is further oxidized. This oxidation produces nicotinamide adenine dinucleotide (NADH) and flavin adenine dinucleotide ($FADH_2$), which carry electrons to the electron transport chain, composed of four complexes (I, II, III and IV). There, ATP is produced through oxidative phosphorylation (OXPHOS)/mitochondrial respiration. Approximately 36 molecules of ATP are generated per molecule of glucose when it is completely oxidized; two are produced during glycolysis, and the rest are acquired from OXPHOS. Many cancer cells, even under aerobic conditions, primarily use glycolysis for energy production (Warburg effect, (Warburg, 1956)). This reprogramming is seemingly counterintuitive, as cells have to compensate the lower efficiency of glycolysis in ATP production. In order to deal with that, cancer cells upregulate glucose transporters, mainly GLUT1 (glucose transporter type 1), which increases glucose import into cytosol (DeBerardinis et al., 2008; Hsu and Sabatini, 2008; Jones and Thompson, 2009). What

are the advantages conferred by the glycolytic switch? One hypothesis is that an increase in glycolysis enables more glycolytic intermediates to be used for nucleotide, amino acid, and fatty acid production, needed to produce a new cell (Potter, 1958; Vander Heiden et al., 2009). How does p53 control metabolism? Does this regulation contribute to its tumor suppressor function? p53 has been reported to downregulate glycolysis by promoting the expression of TP53-induced glycolysis regulator (TIGAR) (Bensaad et al., 2006; Jen and Cheung, 2005) (Figure 7). TIGAR degrades fructose-2,6-bisphosphate, an allosteric effector of the glycolytic enzyme 6-phosphofructo-kinase-1. Moreover, p53 directly downregulates gene expression of glucose transporters GLUT1 and GLUT4 (Schwartzenberg-Bar-Yoseph et al., 2004), and indirectly of GLUT3 (Kawauchi et al., 2008). It also downregulates pyruvate dehydrogenase kinase 2 (PDK2) expression (Contractor and Harris, 2012), which inhibits pyruvate dehydrogenase (PDH) complex. This complex transforms pyruvate into acetyl coenzyme A (CoA) that feeds into the TCA cycle.

p53 also controls OXPHOS by promoting the expression of SCO2 (Matoba et al., 2006), involved in the biogenesis of one subunit of complex IV, and by upregulating the expression of apoptosis-inducing factor, mitochondrion-associated, 2 (AIFM2), needed to maintain the integrity of mitochondrial complex I (Stambolsky et al., 2006; Vahsen et al., 2004). Moreover, p53 induces the expression of glutaminase 2 (GLS2), a mitochondrial enzyme that catalyzes the hydrolysis of glutamine to glutamate. Glutamate is transformed into α-ketoglutarate that feeds into the citric acid cycle, promoting OXPHOS and subsequent ATP production (Hu et al., 2010; Suzuki et al., 2010). p53 also contributes to TCA cycle and OXPHOS maintenance by promoting mitochondrial fatty acid catabolism (β-oxidation), which produces acetyl-CoA, NADH and $FADH_2$. The carnitine palmitoyltransferase/acyltransferase 1C (CPT1C) is a p53 target gene (Sanchez-Macedo et al., 2013) involved in the transport of long-chain fatty acids into mitochondria. Moreover, conversion of malonyl CoA – a negative regulator of carnitine acyltransferase – to acetyl CoA is catalyzed by malonyl-CoA decarboxylase (MLYCD), another p53 target (Liu et al., 2014). Finally, lipin 1, positively regulated by p53, acts as a a transcriptional co-activator of genes involved in β-oxidation (Assaily et al., 2011; Finck et al., 2006).

Inhibition of glycolysis and promotion of OXPHOS by all these means help to curb the acquisition of the Warburg effect (Liang et al., 2013; Vousden and Prives, 2009). That´s why, metabolic control is considered another way for p53 to execute its tumor suppressor function.

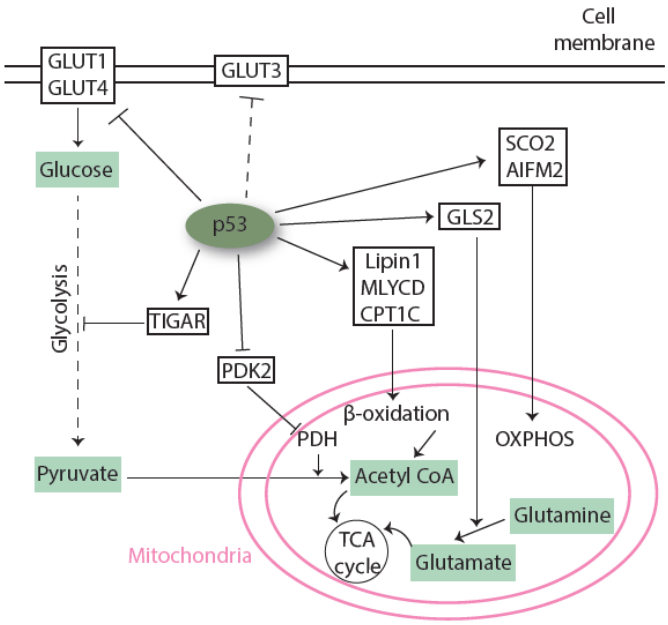

Figure 7. p53 regulates cellular metabolism by inhibiting glycolysis and promoting OXPHOS. Modified from (Kruiswijk et al., 2015; Liang et al., 2013)**.**

How are the canonical p53 responses – senescence and apoptosis – integrated together with its metabolic functions? The emerging model is that p53 is involved in two different mechanisms: under stress conditions, it first promotes cell survival by inducing cell cycle arrest to give time to the cells to repair the damage (for example DNA breaks). Moreover, metabolism regulation further prevents tumor-promoting changes. But if the stress does not resolve or the damage cannot be repaired, then p53 drives apoptosis or senescence (Vousden and Prives, 2009) (Figure 8).

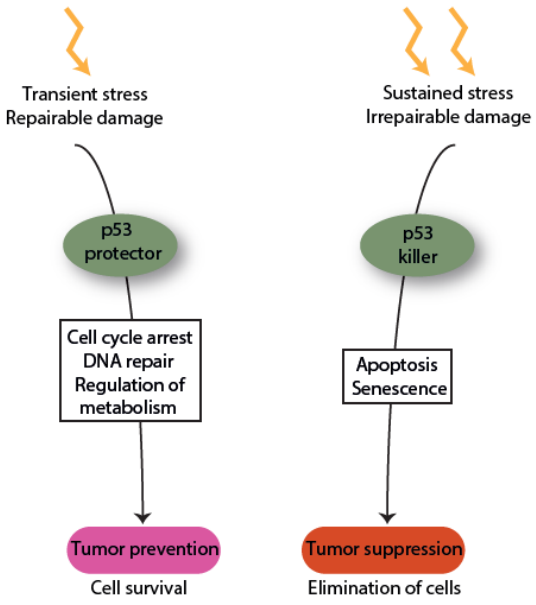

Figure 8. Dual mechanisms of p53. Under low stress conditions or repairable damage, p53 acts as a cell protector and promotes survival. It prevents tumorigenic transformations by inducing cell cycle

arrest and DNA repair, and by regulating metabolism. Under sustained stress or irreparable damage, p53 promotes apoptosis or senescence in order to eliminate the cells. Modified from (Vousden and Prives, 2009).

1.5 Aims of the study

p53 exerts its tumor suppressive functions acting as a transcriptional factor and promoting or repressing hundreds of target genes. Apart from inducing apoptosis and senescence upon cellular stress, p53 has recently emerged as a regulator of homeostasis, being control of metabolism an example of how p53 inhibits tumor-promoting changes. However, the way p53 exerts its non-canonical activities is not completely known (Liang et al., 2013). A better understanding of p53 homeostatic target genes could show us new targets for a more efficient cancer therapy. In fact, targeting cancer metabolism has emerged during the past decade as a promising strategy for developing novel antineoplastic agents (Galluzzi et al., 2013). In order to understand in a systematic way how p53 controls its downstream response, a combined analysis of the cell proteome by liquid chromatography-tandem mass spectrometry (LC-MS/MS) and the transcriptome by RNA-sequencing (RNA-seq) upon p53 knock down in a breast cell line was performed. In addition, it was decided to treat these cells with ionizing ɣ-irradiation (IR), which causes DSBs, as induction of DNA damage is used as cancer treatment during chemo- and radiotherapy, and combination of metabolic modulators with conventional therapies is a promising strategy to fight tumor cells (Zhao et al., 2013).

p53 regulates the transcriptional responses of its target genes, and these responses are indirectly regulated by the upstream PIK3-like kinases, as they control p53 dynamics. Initial studies using *in-vitro* models, xenografts and first clinical trials have demonstrated that inhibition of ATM, ATR or DNA-PKcs could increase cancer treatment efficiency by sensitizing cancer cells (Davidson et al., 2013; Weber and Ryan, 2015). However, to gain a deeper understanding of the molecular mechanisms underlying the sensitizing effect of these inhibitors, it is necessary to understand how the individual kinases regulate p53 and to which extent they function independently from each other or modulate each other's activity in regard to p53 activation, which is at present unclear. For this purpose, several fluorescent reporter cell lines were used in combination with live-cell time-lapse microscopy and automated image analysis. Cells were pharmacologically perturbed, and p53 response was followed upon induction of double strand breaks with ɣ-IR in individual cells with high temporal and spatial resolution.

2 MATERIALS AND METHODS

2.1 Cell culture

All A549 (human non-small cell lung cancer) and U-2 OS (human osteosarcoma) cell lines were maintained in McCoy´s 5A (GE Healthcare Life Sciences) + 10% fetal calf serum (FCS) (Thermo Fisher Scientific); all MCF10A cells (non-transformed human breast epithelial) in Dulbecco's Modified Eagle Medium:Nutrient Mixture F-12 (DMEM/F-12) (Thermo Fisher Scientific) + 5% horse serum (HS) (PAN-Biotech) + 20 ng/ml epidermal growth factor (EGF) (Peprotech) + 0.5 µg/ml hydrocortisone (Sigma-Aldrich) + 100 ng/ml cholera toxin (Sigma-Aldrich) + 10 µg/ml insulin (Sigma-Aldrich) (Debnath et al., 2003), and MCF7 cells (human breast cancer) in RPMI (Roswell Park Memorial Institute)1640 (Thermo Fisher Scientific) + 10% FCS at 37 °C. All media contained penicillin and streptomycin (Thermo Fisher Scientific). When appropriate, selective antibiotics (400 µg/ml geneticin disulphate (G418) (Carl Roth GmbH + Co. KG), 5 µg/ml blasticidin S hydrochloride (Carl Roth GmbH + Co. KG), 50 µg/ml hygromycin B (Thermo Fisher Scientific) or 0.5 µg/ml puromycin dihydrochloride (Carl Roth GmbH + Co. KG)) were added to maintain transgene expression.

A549, U-2 OS (Chen et al., 2013) and MCF7 (Batchelor et al., 2008) p53-Venus reporter cell lines have been described before. Jette Strasen (Löwer lab) generated p53 fluorescent reporters in MCF10A by infecting cells with lentiviruses encoding a construct where p53 was fused to yellow fluorescent protein Venus (p53-YFP) under the control of the human Ubiquitin C promoter (UbCp) (Figure 9).

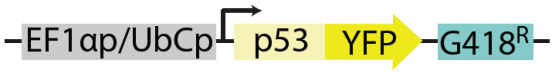

Figure 9. Scheme of the p53 fluorescent reporter construct. p53 was fused to YFP under the control of EF1αp (elongation factor-1 α promoter) for A549, MCF7 and U-2 OS, or under the control of UbCp for MCF10A cells. The construct contained a Neomycin selection marker (resistance to G418 antibiotic).

Nuclear markers were added to reporters by infecting with lentiviruses expressing histone 2B fused to cyan fluorescent protein (CFP) under the control of UbCp (U-2 OS, MCF10A and A549 – Elena Cristiano (Löwer lab) added the nuclear marker to A549 cells), or expressing near-infrared fluorescent protein (iRFP) with a nuclear localization sequence under the control of EF1αp (MCF7). Subsequently, stable clonal cell lines were established and validated.

Both A549 and MCF10A p53 knock down ($p53^{sh}$) cells were created by infecting the wild-type ($p53^{wt}$) corresponding cells with lentiviruses expressing small hairpin RNA (shRNA) against p53 (pRETRO-SUPER-p53, (Brummelkamp et al., 2002)). They were subsequently selected with the corresponding antibiotic and validated.

2.2 Inhibitor and radiation treatments

In experiments shown in section 3.1, treated samples were irradiated with 10 Gy ɣ-IR, while control samples were not irradiated. In experiments shown in section 3.2, media were replaced with fresh ones containing DMSO (Sigma-Aldrich) (control condition) or the inhibitors shown in Table 1, alone or in combination, 30 minutes before irradiating cells with ɣ-IR (2.5, 5, 10 or 20 gray (Gy)) or UV (single burst of 4.5 J/m^2).

ɣ-irradiation was applied using a cesium-137 source (rate 8.9 Gy/min). For ultraviolet (UV) treatment, cells were irradiated by an ultraviolet lamp (254 nm wavelength).

Table 1. Inhibitors used.

Inhibitor (Abbreviation)	Target	Final concentration	Supplier
KU-55933 (ATMi)	ATM	10 µM	Axon Medchem
VE-821 (ATRi)	ATR	2 µM	Selleckchem
NU 7026 (DNA-PKi)	DNA-PKcs	10 µM	Biomol GmbH
NU 7441 (DNA-PKi-2)	DNA-PKcs	1 µM	Axon Medchem
SCR7 (LigIVi)	LigaseIV	100 µM	Xcess Biosciences Inc.
Chk2 Inhibitor II (Chk2i II)	Chk2	10µM	Merck Millipore

2.3 Time-lapse microscopy

Reporter cells were seeded on 3.5 cm poly-D-lysine-coated glass-bottom plates (MatTek Corporation) two days before microscope imaging:

- A549 cells: 1.5exp5-1.75exp5 cells/plate
- MCF10A cells: 1.5exp5 cells/plate
- U2OS: 3exp5 cells/plate
- MCF7: 0.75exp5 cells/plate

The day of the experiment, medium was changed to RPMI 1640 medium without phenol red and riboflavin supplemented with 10% FCS for A549, U-2 OS and MCF7, and 5% HS, 20 ng/ml EGF, 0.5 µg/ml hydrocortisone, 100 ng/ml cholera toxin and 10 µg/ml insulin for

MCF10A. All media contained penicillin, streptomycin, HEPES buffer (10 mM) and GlutaMAX (2 mM) (both from Thermo Fisher Scientific)).

Cells were imaged on a Nikon Ti inverted fluorescence microscope with perfect focus system. Imaging was performed with a Hamamatsu Orca R2 camera, a 20x plan apo objective (numerical aperture (NA) 0.75) and appropriate filter sets (Venus: 500/20 nm excitation, 515 nm dichroic beam splitter, 535/30 nm emission; CFP: 436/20 nm excitation, 455 nm dichroic beam splitter, 480/40 nm emission; iRFP: 650/45 nm excitation, 685 nm dichroic beam splitter, 720/60 nm emission (Chroma)). The microscope was enclosed with an incubation chamber to maintain constant temperature (37°C), CO_2 concentration (5%), and humidity. Cells were imaged every 15 minutes for the duration of the experiment (normally 24 hours) using Nikon Elements software.

2.4 Image analysis

Cells were tracked throughout the duration of the experiment using custom-written MATLAB (MathWorks) scripts based on code developed by the Alon lab (Cohen et al., 2008) and the CellProfiler project (Carpenter et al., 2006). In brief, flat field correction and background subtraction to raw images were applied before segmenting individual nuclei from fluorescence images of the nuclear marker using adaptive thresholding and seeded watershed algorithms. Segmented cells were then assigned to corresponding cells in following images using a greedy match algorithm (Figure 10).

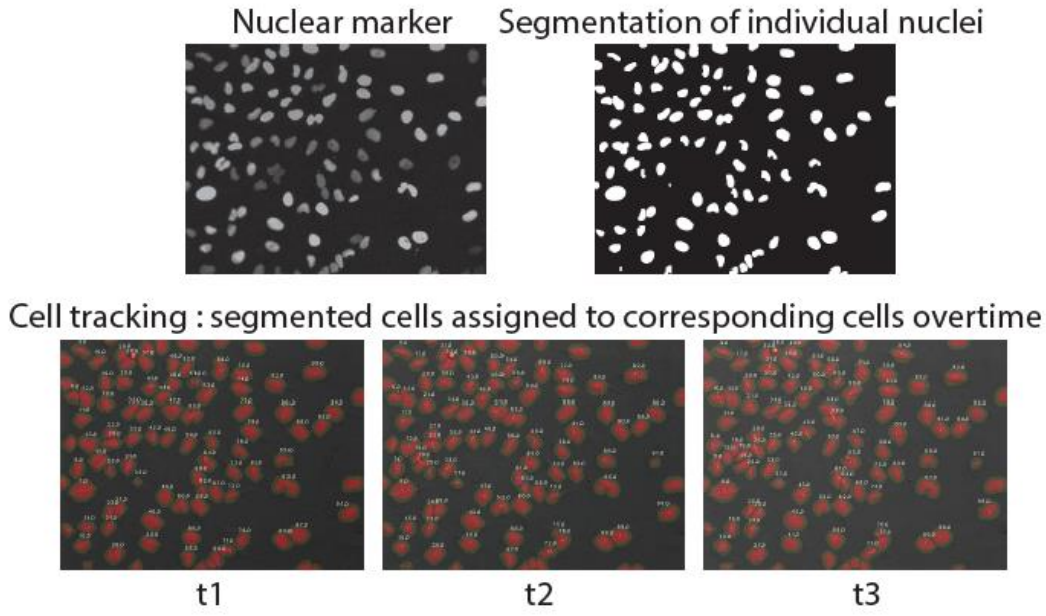

Figure 10. Image analysis example. Cells were segmented according to the nuclear marker; segmented cells were assigned to corresponding cells at following time points.

Finally, the nuclear fluorescence intensity of p53-Venus for each cell over time was quantified, and the resulting single-cell trajectories were computationally analyzed to extract features of p53 dynamics, e.g. relative amplitude or full-width at half-maximum (FWHM) of protein accumulation pulses, as previously described (Loewer et al., 2010). To determine the effect size and its significance for a given treatment, changes of the median pulse width and amplitude were calculated, and permutation testing (1000 permutations) was performed to establish corresponding 90% confidence intervals.

For small interfering RNA (siRNA) experiments, cells were considered to show monotonously increasing p53 dynamics when mean levels during the last 4 hours were 1.3x higher than levels during the first 4 hours. Due to increased noise associated with transfecting cells, an alternative measure for pulse duration (width at 10% of maximum peak levels) was considered as well in these experiments.

2.5 Western blot analysis

MCF10A (6exp5 cells) and A549 (2exp5-2.5exp5 cells) were seeded on 5 cm plates two days prior to the experiment, and harvested at the indicated time points after treatment. They were washed with cold phosphate-buffered saline (PBS), harvested in 2 ml PBS with a cell scraper, and centrifuged during 5 minutes at 4000 RPM; supernatant was aspirated. After the harvesting procedure, cells were lysed for 20 minutes on ice in 40-70 µl of lysis buffer and centrifuged at 4°C during 20 minutes at 14000 RPM; lysate was transferred to a new tube. Protein concentration was determined in technical duplicates with the Pierce BCA Protein Assay Kit (Thermo Fisher Scientific) using a bovine serum albumin (BSA) standard curve (2, 1, 0.5, 0.25, 0.125, 0.0625 and 0 mg/ml). 25 µl of each standard or 2.5 µl of each sample (diluted to 25 µl in H_2O) and 200 µl of Working Reagent (50:1, Reagent A:B) were transferred to a 96-well plate, followed by incubation at 37°C during 25 minutes. Absorbance was measured at 595 nm in a microplate reader (EL800 Universal Microplate Reader, BioTek Instruments, Inc.).

Equal protein amounts (15-20 µg depending on protein concentration) were denatured in sample buffer (NuPAGE LDS Sample Buffer (4X), Thermo Fisher Scientific) and dithiothreitol (DTT). Proteins were separated by electrophoresis on precast gels in MES SDS Running Buffer (NuPAGE, Thermo Fisher Scientific) (see Table 2 for further details). Next, they were transferred to nitrocellulose or polyvinylidene fluoride (PDVF) membranes (Carl Roth GmbH + Co. KG) by electroblotting.

Table 2. Electrophoresis and electroblotting conditions depending on protein size.

Protein size (kDa)	Electrophoresis		Electroblotting		
	Gradient gel	Conditions	Membrane	Conditions	Buffer
<250	4–12% Bis-Tris	35-40 min, 200 volts	nitrocellulose	90 min, 200 mA	Transfer buffer
>250	3-8% Tris-Acetate	150 volts, 1 h	PDVF	Overnight, 150 mA	CAPS

Membranes were blocked for one hour with 5% non-fat dried milk or 5% BSA (Carl Roth GmbH + Co. KG) in tris-buffered saline with Tween20 (TBST) according to the antibodies manufacturer's recommendations, and incubated overnight with primary antibody (see Table 3).

Table 3. Primary antibodies for western blot analysis.

Target	Dilution	Supplier
total p53 (FL-393)	1:2500	Santa Cruz Biotechnology, Inc.
Mdm2 (SMP14)	1:200	Santa Cruz Biotechnology, Inc.
pp53 (Ser15)	1:1000	Cell Signaling Technology
pChk2 (Thr68)	1:1000	Cell Signaling Technology
pChk1 (Ser317)	1:1000	Cell Signaling Technology
pATM (Ser1981)	1:500	Rockland Immunochemicals Inc.
pDNA-PKcs (Ser2056)	1:1000	Abcam
total DNA-PKcs (H163)	1:200	Santa Cruz Biotechnology, Inc.
GAPDH	1:9000	Sigma-Aldrich

The next day membranes were washed in TBST, incubated for one hour with secondary antibody coupled to horseradish peroxidase (HRP, see Table 4) in 5% non-fat dried milk in TBST, and washed again.

Table 4. Secondary antibodies for western blot analysis.

Antibody	Dilution	Supplier
Goat anti-Rabbit IgG Secondary Antibody, HRP conjugate	1:10000	Thermo Fisher Scientific

Goat anti-Mouse IgG Secondary Antibody, HRP conjugate	1:10000	Thermo Fisher Scientific

Protein levels were detected using Amersham ECL Prime Western Blotting Detection Reagent (GE Healthcare Life Sciences). Chemiluminescent images were captured with ChemiDoc XRS System (Bio-Rad Laboratories, Inc.).

Buffers used (all reagents from Carl Roth GmbH + Co. KG, unless otherwise stated):

- PBS

10 mM sodium hydrogen phosphate + 2 mM monopotassium phosphate + 137 mM sodium chloride + 2.7 mM potassium chloride, pH 7.4

- Lysis buffer

50 mM Tris pH 7.5 + 100 mM sodium chloride + 1% Triton X-100 + 0.5% sodium deoxycholate + 0.1% SDS + 50 mM sodium fluoride + 1 mM sodium orthovanadate + 1:100 Protease Inhibitor Cocktail Plus + 1:100 Phosphatase Inhibitor Cocktail (Sigma-Aldrich)

- Transfer buffer

25 mM Tris + 192 mM glycine + 20% methanol

- CAPS buffer

10 mM CAPS pH 11 + 15% methanol

- TBST

50 mM Tris pH 7.5 + 150 mM sodium chloride + 0.1% Tween-20

2.6 RT-qPCR

MCF10A (6exp5 cells) and A549 (2exp5-2.5exp5 cells; for p21 and YPEL3 expression study, 0.5exp5 cells) were seeded on 5 cm plates two days prior to the experiment, and harvested as indicated in section 2.5 at the corresponding time points after treatment. RNA was extracted using either High Pure RNA Isolation Kit (Roche) or InviTrap Spin Cell RNA Mini Kit (STRATEC Biomedical AG) following manufacturer´s protocols. RNA concentration was measured with the NanoDrop 2000c Spectrophotometer (Thermo Fisher Scientific). Next, complementary DNA (cDNA) was generated. The following components were mixed, and heated for 5 minutes at 70°C in a thermocycler (PEQLAB, VWR):

- 500 ng or 1 µg of total RNA (depending on RNA concentration)
- 2 µl of Oligo $d(T)_{23}$ VN (50 µM) (New England Biolabs)
- 1 µl of dNTP solution mix (10 mM) (New England Biolabs)

- Up to 10 µl of DEPC-treated H_2O (Carl Roth GmbH + Co. KG)

Next, the following reagents (all from New England Biolabs) were added, and the resulting mix was incubated at 42°C for one hour:

- 4 µl of 5X ProtoScript II Buffer
- 2 µl of DTT (0.1 M)
- 1 µl of ProtoScript II Reverse Transcriptase
- 1 µl of RNase Inhibitor, Murine

The resulting cDNA was diluted 1:10, and quantitative PCR was performed in triplicates. 3 µl of cDNA were mixed with 9.5 µl of primer mix and 12.5 µl of SYBR Green reagent (Roche).

- Primer mix

  6.4 µl forward primer (100 µM) + 6.4 µl reverse primer (100 µM) + 987.2 µl DEPC-treated H_2O

  The final concentration of each primer in the reaction mix was 243.2 nM.

Quantitative PCR was performed on a StepOnePlus PCR machine (Applied Biosystems) with the following thermal profile:

1) 95°C for 10 minutes

2) 40 cycles: 95 °C for 15 seconds, 60 °C for one minute

Table 5. Primers used in RT-qPCR. Oligonucleotide primers used in SYBR green RT-qPCR for several human genes. β-actin was used as reference gene. All primers were from Eurofins Genomics.

Primer		Primer sequence 5'→3'
p21	forward	TGG ACC TGT CAC TGT CTT GT
	reverse	TCC TGT GGG CGG ATT AG
p53	forward	TGA CTG TAC CAC CAT CCA CTA
	reverse	AAA CAC GCA CCT CAA AGC
RRM2B	forward	GGT CTT ATG CCA GGA CTC AC
	reverse	CAA TGA TCT CCC TGA CCC TTT C
SESN1	forward	AGA TGA GGC AGT TAC AGG AAT G
	reverse	ATG ACG AGA TAC AGC TCT TGC
Mdm2	forward	AGA TGT TGG GCC CTT CGT GAG AA
	reverse	GCC CTC TTC AGC TTG TGT TGA GTT
KLK10	forward	CTG CCC AGC ATC CAG CTG TCT AC
	reverse	CTG GGC ATC TGG ATC AGC AGG AG
Wip1	forward	ATA AGC CAG AAC TTC CCA AGG

	reverse	TGG TCA ATA ACT GTG CTC CTT C
YPEL3	forward	GTG CCT ACC TCT TCA ACT CAG
	reverse	TGC TCT CAA AGG CCT GTT C
DNA-PKcs	forward	CAG GTG CCA ATC CAG CAG TC
	reverse	CGT GCC ACA GCC ACA TAG TC
NBN	forward	ATG GAG GCC ATA TTT CCA TGA C
	reverse	CAA GCA GCC AGA ACT TGG AAG
MRE11A	forward	ACG TTT GTA ACA CTC GAT GAA
	reverse	CTG GAA TTG AAA TGT TGA GG
RBBP8	forward	TGC TGG TTC TCA TGA GCC AAT AA
	reverse	TCT GCT CCC GGA TCT ATA CTC CAC
RAD50	forward	GAG ATT TCC CTC CTG GAA CC
	reverse	ACA TCA CGA AAT TGC AGA CG
β-actin	forward	GGC ACC CAG CAC AAT GAA GAT CAA
	reverse	TAG AAG CAT TTG CGG TGG ACG ATG

2.7 Cell proliferation assay

0.1exp5 cells were seeded 1.5 days before being treated with DMSO or DNA-PKi and irradiated with 5 Gy ɣ-IR. Media was changed every day, and the same randomly chosen cells were imaged at day 1, 2 and 3 after irradiation by using gridded dishes and a Nikon Eclipse inverted microscope with a 4x objective. Initial numbers and fraction of dividing cells were manually quantified for each condition.

2.8 Immunofluorescence

1exp5 cells were seeded on coverslips coated with poly-L-lysine (Sigma-Aldrich) in 6-well plates two days prior to the experiment. At the corresponding time points, cells were washed with PBS and fixed with 2% paraformaldehyde in PBS for 10 minutes. Cells were washed again in PBS, permeabilized with 1 ml of Triton X-100 in PBS during 20 min and blocked with 1 ml of 10% goat serum (PAN-Biotech) in PBS for 30 min. Next, cells were incubated with phospho-histone H2A.X (Ser319, JBW301, Merck Millipore) at 1:500 dilution in 1% BSA/PBS overnight at 4°C. Cells were washed with 0.1% Triton X-100/PBS, incubated with secondary antibody coupled to Alexa Fluor 647 (Thermo Fisher Scientific) at 1:500 dilution in 1% BSA/PBS for 30 min, and washed with 0.1% Triton X-100/PBS. Finally, nucleus was stained

with 2 µg/ml Hoechst 33342 (Thermo Fisher Scientific) in 0.1% Triton X-100/PBS for 5 min, and cells were washed with PBS. Slides were embedded in Prolong Antifade (Thermo Fisher Scientific). Images were acquired with a 60x plan apo objective (NA 0.75) using appropriate filter sets (Alexa Fluor 647: 620/60 nm excitation, 660 nm dichroic beam splitter, 700/75 nm emission; Hoechst 33342: 387/11 nm excitation, 409 nm dichroic beam splitter, 447/60 nm emission (Chroma)). Automated segmentation was performed in MATLAB using algorithms from CellProfiler (Carpenter et al., 2006).

2.9 siRNA treatment

Cells were seeded on 6-well plates (see Table 6 for details; transfection protocol was optimized for each siRNA in order to get the best knock down efficiency). The next day, co-transfection complexes were prepared by adding the corresponding siRNA and 7.5 µl of TransIT-X2 Dynamic Delivery System (Mirus Bio LLC) to 250 µl of Opti-MEM I Reduced Serum Media (Thermo Fisher Scientific). This mix was incubated for 15-30 minutes at room temperature. Then, it was added drop-wise to different areas of the well, and the plate was gently rocked. One or two days later, cells were replated onto 5 cm plates (2.5exp5 cells; for RT-qPCR and western blot) or onto 3.5 cm poly-D-lysine-coated glass-bottom plates (1.75exp5 cells; for microscopy). For RAD50 knock down, a second transfection was done two days after the first one; the next day, cells were replated. Two days after seeding the cells in 5 and 3.5 cm plates, they were harvested as indicated in section 2.5 or used for time-lapse microscopy, respectively. The transfection protocol used for scrambled siRNA varied depending on the protocol used for the targeted genes. The sequence of the control siRNA was CGU ACG CGG AAU ACU UCG ATT (Zheng et al., 2013).

Table 6. Conditions used for transfection of the different siRNAs. * Two days after the first transfection, a second transfection was carried out. One day later, cells were replated. ** Different transfection protocols were tried for knocking down NBN. The experiment presented in the results section corresponds to the protocol showed here.

siRNA target	Cells/well seeded in 6-well plate	Number of siRNAs used	siRNA final concentration	Repeated transfection *	Days waited after transfection and before replating
DNA-PKcs	2exp5	2	25	No	1
RAD50	1.5exp5	1	50	Yes	1
MRE11A	2exp5	1	25	No	2

RBBP8	2exp5	1	25	No	2
NBN **	2exp5	1	25	No	2

RAD50, MRE11A, RBBP8 and NBN siRNAs were from Thermo Fisher Scientific (s791, s8960, s11849 and s9291, respectively). Scrambled siRNA, as well as DNA-PKcs siRNAs (AGG GCC AAG CUG UCA CUC UTT and AGA GUG ACA GCU UGG CCC UTT, (Serrano et al., 2012)) were from Eurofins Genomics.

2.10 RNA-seq experiment workflow

3exp5 cells were seeded on 5 cm plates two days prior to the experiment, and harvested as indicated in section 2.5 at the corresponding time points after treatment (Figure 11):

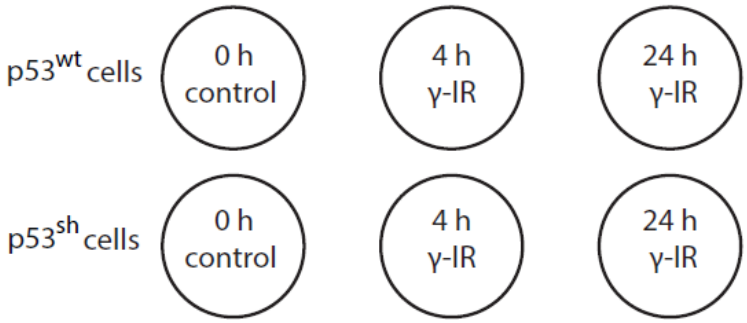

Figure 11. Samples harvested for RNA-seq. There were three different conditions for each cell line (MCF10A $p53^{wt}$ and $p53^{sh}$): non-irradiated cells, and irradiated with 10 Gy and harvested 4 and 24 hours later.

Next, total RNA was isolated using High Pure RNA Isolation kits (Roche). In order to assess RNA quality, Agilent RNA 6000 Nano Kit in combination with Agilent 2100 Bioanalyzer (Agilent Technologies) was used as indicated in manufacturer´s protocol. This bioanalyzer is based on a combination of microfluidics capillary electrophoresis and fluorescence detection, and it is able to record the size distribution of molecules (in this case RNA) in a digital manner. The Agilent technology generates a value called RIN that indicates the integrity of the RNA analyzed using the electrophoretic tracing (Schroeder et al., 2006). A RIN of 10 indicates a non-degraded RNA sample, while a value of 1 represents extensive degraded RNA. The RIN algorithm takes into consideration several features, such as area under the peaks of 18S (svedberg unit) and 28S ribosomal RNA (rRNA) compared to the total area under the curve, or the height of the 28S peak (Figure 12).

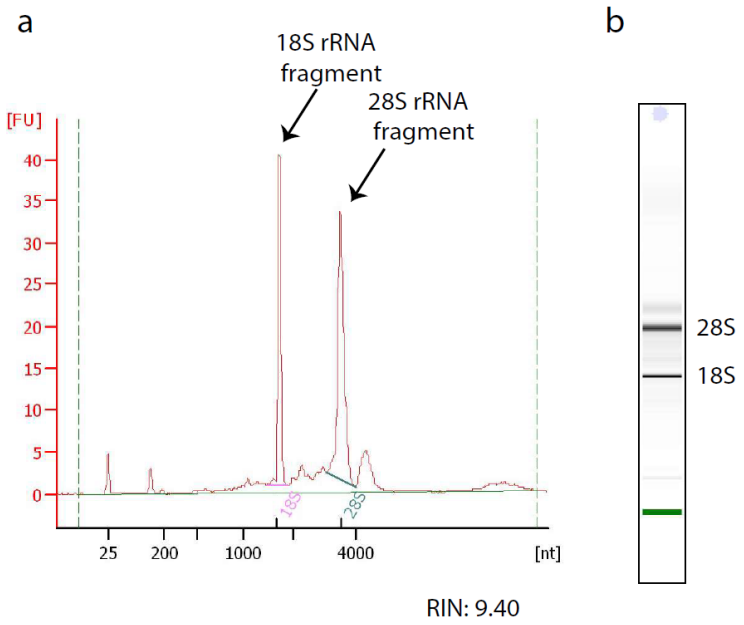

Figure 12. Agilent RNA 6000 Nano Kit data. (a) Typical electropherogram for total eukaryotic RNA with two ribosomal peaks, and the assigned RIN value. (b) Virtual gel representing band intensities of 18S and 28S rRNAs.

All samples used for this study had at least a RIN of 8.50. Once the quality of the samples was checked, RNA concentration was measured with the Qubit 2.0 Fluorometer and Qubit RNA HS Assay Kit (Thermo Fisher Scientific), and samples were prepared in a process called library preparation. Among the different techniques available to sequence whole transcriptomes in a high-throughput manner (Wang et al., 2009), RNA-sequencing on the Illumina platform was chosen. The starting amount of total RNA was one microgram.

Illumina protocol for the TruSeq RNA Library Preparation Kit v2 comprises the following steps ("TruSeq RNA Sample Preparation v2 Guide - Illumina," 2014):

1. Purification of the polyA messenger RNA (mRNA) molecules using poly-dT attached magnetic beads.
2. Fragmentation and priming (with random hexamers) of the mRNA.
3. Synthesis of first strand cDNA using reverse transcriptase and random primers.
4. Removal of the RNA and synthesis of second strand cDNA, generating double strand (ds) cDNA.
5. Repair ends converting the overhangs (from fragmentation) into blunt ends by using a 3' to 5' exonuclease and a polymerase.
6. Adenylation of 3' ends: an adenine is added to the 3´ ends to avoid ligation to one another during the next step.

7. Ligation of adapters: distinct indexing adapters are ligated to the 3' ends of each strand of the ds cDNA. The adapters contain a thymine on the 3' ends, providing an overhang to ligate cDNA strand and adapter.

   The adapter ligation allows DNA fragments to bind to the flow cell for next generation sequencing. Moreover, it "barcodes" samples allowing different libraries to be mixed and simultaneously sequenced.
8. Enrichment of DNA fragments: DNA fragments that have adapters on both ends are enriched and the amount of DNA is amplified via PCR.

After library preparation, DNA concentration was measured using the Qubit 2.0 Fluorometer and Qubit dsDNA BR Assay Kit (Thermo Fisher Scientific). In order to assess library quality, Agilent DNA 1000 Kit in combination with Agilent 2100 Bioanalyzer was used (Agilent Technologies) according to manufacturer´s protocol, which again uses a capillary electrophoresis system. DNA size distribution was examined (Figure 13), and the peak in the different samples was centred around 250-300 bp, as expected ("TruSeq RNA Access Library Prep Kit Support - Questions & Answers," 2016).

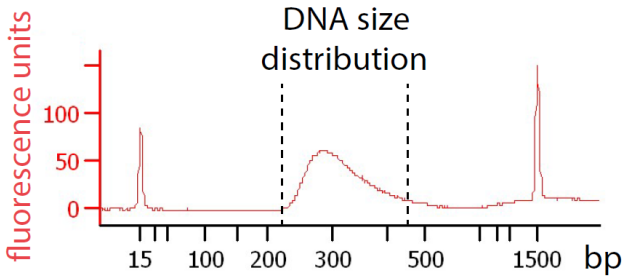

Figure 13. Agilent DNA 1000 Kit data. Typical electropherogram and size distribution of TruSeq RNA Sample Preparation v2 library.

The following procedure was carried out by the Genomics technology platform (Prof. Dr. Wei Chen, MDC Berlin). After library validation, cluster generation was performed on the Illumina cBot ("Specification Sheet: Sequencing - cBot Illumina," 2011) according to manufacturer´s indications. Samples were pooled together, the ds cDNA was denatured into single strands and concentration adjusted to 7 pM. Then, the DNA templates were randomly attached to the surface of the Illumina flow cell on the cBot by hybridization to a dense lawn of immobilized primers, complementary to the adapters. DNA polymerase was used to copy the templates by 3' extension from the hybridized primers. The original templates were denatured and the copies remained immobilized on the surface (Figure 14a), which were then amplified by isothermal bridge amplification, creating millions of clonal clusters inside the flow cell (Figure 14b). Each

cluster of ds DNA bridges was then denatured and the reverse DNA strand was removed. The bound oligonucleotides and the 3' ends of the forward strands were blocked to avoid any interference with the upcoming sequencing. The sequencing primers were hybridized on unbound ends to the adapter of each single stranded molecule in the clusters (Figure 14c).

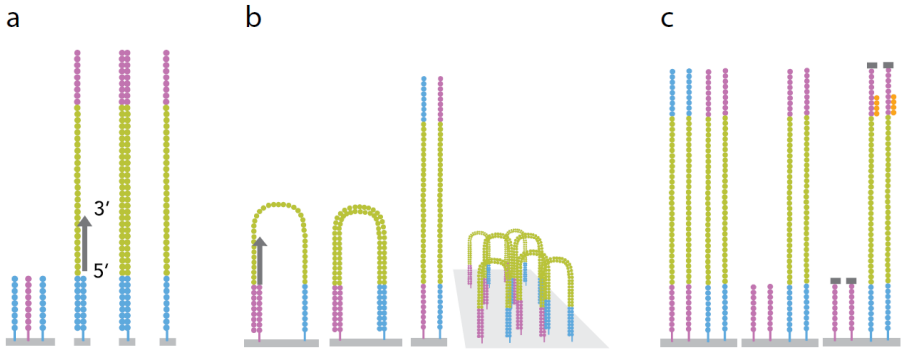

Figure 14. Cluster generation from single-molecule DNA. Modified from ("Specification Sheet: Sequencing - cBot Illumina," 2011).

Finally, the DNA was sequenced on the Illumina HiSeq 2000 by using the sequencing by synthesis technology ("Technology Spotlight: Illumina Sequencing - Illumina Sequencing Technology," 2010) (Figure 15). For this experiment, single-read runs and read length of 100 bp were chosen.

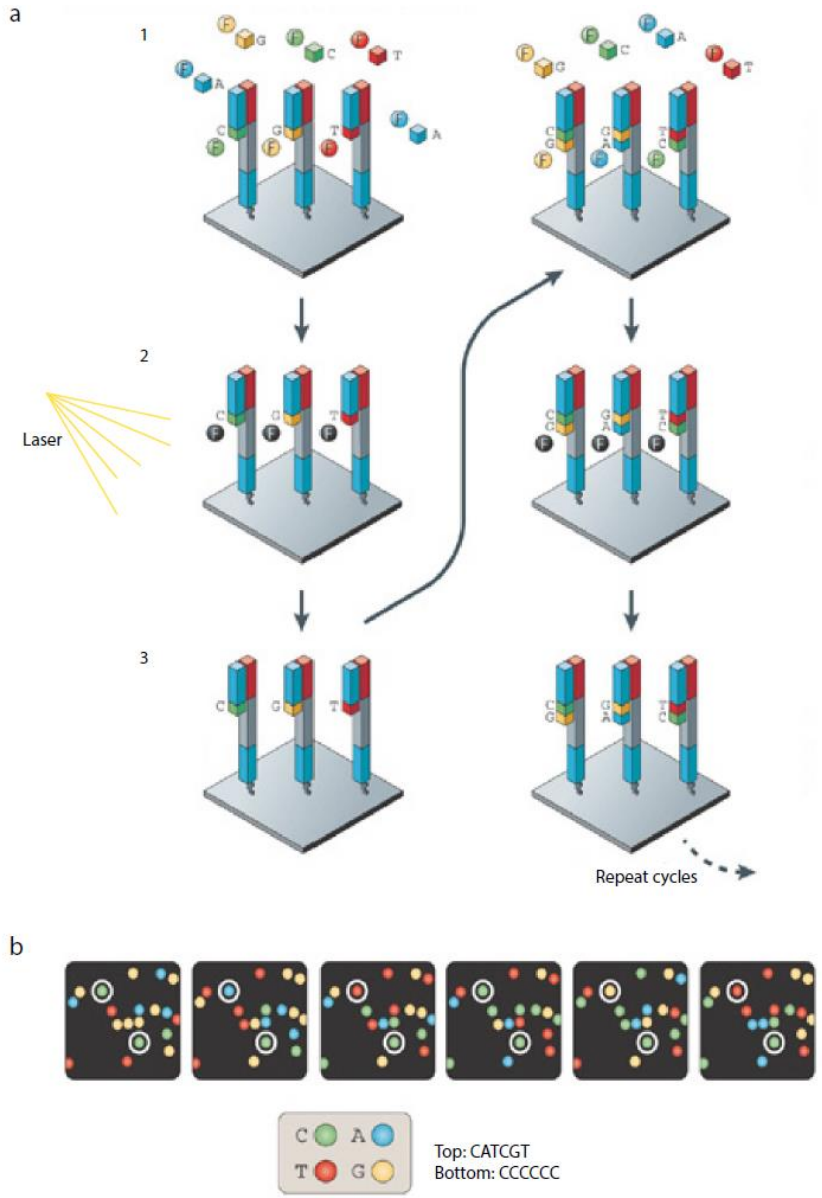

Figure 15. Sequencing by synthesis method. This technology uses four fluorescently labeled (F) nucleotides in order to sequence the previously generated clusters. (a) During each sequencing cycle, a single labeled dNTP is added to each nucleic acid chain. Every dNTP carries a reversible terminator (Bentley et al., 2008) that prevents multiple additions in one cycle. The identity of the incorporated base is identified after laser excitation. Then, the terminating group and the dye are enzymatically cleaved, and the next cycle starts. (b) After laser excitation of the four different dyes, the fluorescence emitted by each cluster is captured and the identity of the subsequently added nucleotides determined. Modified from (Metzker, 2010).

2.11 RNA-seq data analysis

The raw reads obtained from the sequencing were mapped to the human reference genome with the software STAR (Dobin et al., 2013), identifying 18800 genes. FastQ quality control on raw sequence data was performed using FastQC package ("FastQC - Babraham Bioinformatics," 2016). Then, data was normalized and transformed into a quantitative measurement for gene

expression. For this purpose, the RPKM (reads per kilo base per million mapped reads) approach was used. It quantifies gene expression by normalizing according to transcript length and the total number of sequencing reads (Mortazavi et al., 2008). Dr. Altuna Akalin (Bioinformatics Platform, MDC Berlin) did the mapping, quality control and calculation of the RPKM values.

2.11.1 Calculation of the distance score

Genes were sorted according to the distance between gene expression profiles in the presence and absence of p53 across time points (distance score):

- For each gene and condition log2 (x+1) was calculated, with x = RPKM.
- The difference between log2 values of $p53^{wt}$ and $p53^{sh}$ for each time point was calculated. The reason for not subtracting directly RPKM values from each other is that highly expressed genes might have larger distance, and using log2 fold-change gives a relative distance.
- Absolute values of differences were taken, and these three values for each gene were summed up, obtaining the distance score. Genes were ranked according to it.

Distance score was also calculated for only one time point:

- For each gene and condition log2 (x+1) was calculated, with x = RPKM.
- The difference between log2 values of $p53^{wt}$ and $p53^{sh}$ for a certain time point was calculated.
- Absolute value of the difference for each gene was taken (distance score). Genes were sorted according to it.

Although absolute values were used for sorting the genes according to their p53 dependency, positive and negative values gave information about gene up- or downregulation in $p53^{wt}$ cells.

2.11.2 Functional annotation analysis

The web-based tool DAVID 6.7 (Huang et al., 2009a, 2009b) was used for functional annotation analysis with Gene Ontology as database (Ashburner et al., 2011) and medium classification stringency. The analysis clustered functionally similar terms into groups/clusters of biological processes and ranked the importance (enrichment) of these groups according to the enrichment score (see sections 8.2 and 8.3). This score is the minus log10 transformation of the geometric mean of the enrichment p-values of each term in a cluster. A higher score for a group means that annotation term members in the cluster are playing more important roles in the user´s gene

list. That´s why, the focus was put on groups with enrichment scores ≥ 1.3 (1.3 is equivalent to non-log scale 0.05).

2.12 Proteomics

0.6exp5 cells were seeded on 6-well plates; two days later, they were irradiated, except for the control cells (Figure 16). 24 and 48 hours later cells were washed with ice-cold PBS, harvested, lysed in urea buffer and frozen first in liquid nitrogen and then at -80°C.

- Urea buffer

8 M urea (Carl Roth GmbH + Co. KG) in 100 mM Tris, pH 8.25

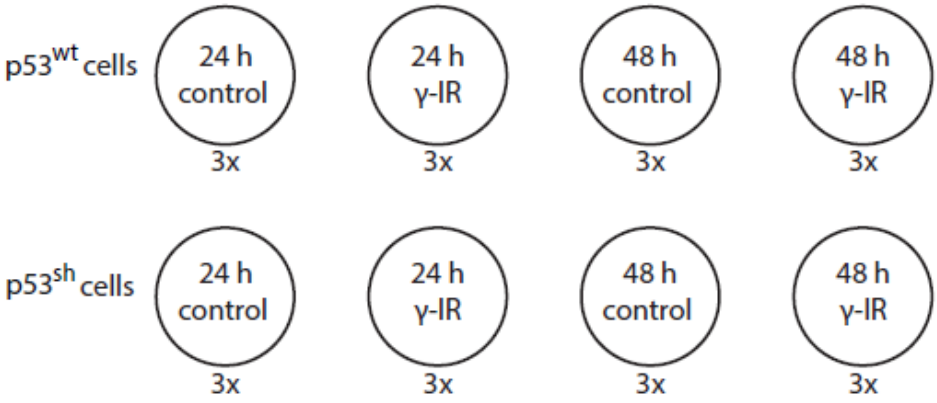

Figure 16. Samples harvested for proteomics. There were four different conditions with biological triplicates for each cell line: MCF10A $p53^{wt}$ and $p53^{sh}$ cells irradiated with 10 Gy and harvested 24 and 48 hours later, and non-irradiated cells, harvested at the same time points.

Dr. Guido Mastrobuoni from the technology platform Proteomics/Metabolomics (Dr. Stefan Kempa, MDC Berlin) did the next steps – in-solution digestion, LC-MS/MS analysis and data processing:

<u>In-solution digestion</u>

Cell debris was removed by centrifugation (14000 x g, 5 min). Protein concentration was determined by Bradford colorimetric assay using a BSA standard curve with eight dilutions ranging from 0 to 2 µg/ml. Absorbance was measured at 595 nm in a plate reader (Infinite M2000, TECAN Group). 100 micrograms of proteins were reduced in 2 mM DTT for 30 minutes at 25 °C in order to convert converts cysteine's disulfide bond into cysteine's free sulfhydryl groups. Free cysteines were alkylated in 11 mM iodoacetamide for 20 minutes at room temperature in the darkness. This step prevents reoxidation of cysteine to form disulfide bonds (Gundry et al., 2010). Next, Lysyl Endopeptidase LysC digestion was performed by adding LysC (Wako Pure Chemical Industries, Ltd) in a ratio 1:40 (w/w) to the sample and incubating it for 18 hours under gentle shaking at 30 °C. After LysC digestion, the samples

were diluted 3 times with 50 mM ammonium bicarbonate solution, and then digestion with trypsin was done using 7 µl of immobilized trypsin (Applied Biosystems) and incubating the samples 4 hours under rotation at 30 °C. Digestion was stopped by acidification (10 µl of trifluoroacetic acid per sample), and trypsin beads were removed by centrifugation. Finally, 15 µg of digest were desalted on STAGE Tips, dried and reconstituted to 20 µl of 0.5 % acetic acid in water (Rappsilber et al., 2003).

LC-MS/MS analysis

5 µl of each sample were injected on a LC-MS/MS system (NanoLC-Ultra, Eksigent (SCIEX) coupled to Q Exactive Plus (Thermo Fisher Scientific)) using a 240 minutes gradient ranging from 5% to 40% of solvent B (80% acetonitrile and 0.1 % formic acid) with solvent A (5 % acetonitrile and 0.1 % formic acid). For chromatographic separation, a capillary of approximately 25 cm long and 75 µm inner diameter was packed with 1.8 µm C18 beads (Reprosil-AQ, Dr. Maisch GmbH). On one end of the capillary nanospray tip was generated using a laser puller (P-2000 Laser Based Micropipette Puller, Sutter Instruments), allowing fretless packing. The nanospray source was operated with spay voltage of 2100 volts and ion transfer tube temperature of 260 °C.

Data was acquired in data dependent mode, with a top10 method (survey MS scan with resolution 70000 at m/z (mass-to-charge ratio) 200, followed by up to 10 MS/MS scans on the most intense ions, intensity threshold 5000). Once selected for fragmentation, ions were excluded from further selection for 45 seconds in order to increase new sequencing events.

Data processing

Raw data was analyzed using the MaxQuant proteomics pipeline (version 1.5.1.2) (Cox and Mann, 2008) and the built-in Andromeda search engine (Cox et al., 2011) with the UniProt human database. Carbamidomethylation of cysteines was chosen as fixed modification (it occurs after treatment with iodoacetamide), oxidation of methionine and acetylation of N-terminus were chosen as variable modifications. The search engine peptide assignments were filtered at 1% false discovery rate and the feature match between runs was enabled; other parameters were left as default. Protein intensities are given as “label-free quantification (LFQ) intensities”, the final output of the MaxLFQ algorithm (Cox et al., 2014). Raw intensities are normalized on different levels to ensure that LFQ intensities across samples reflect the relative amounts of the proteins.

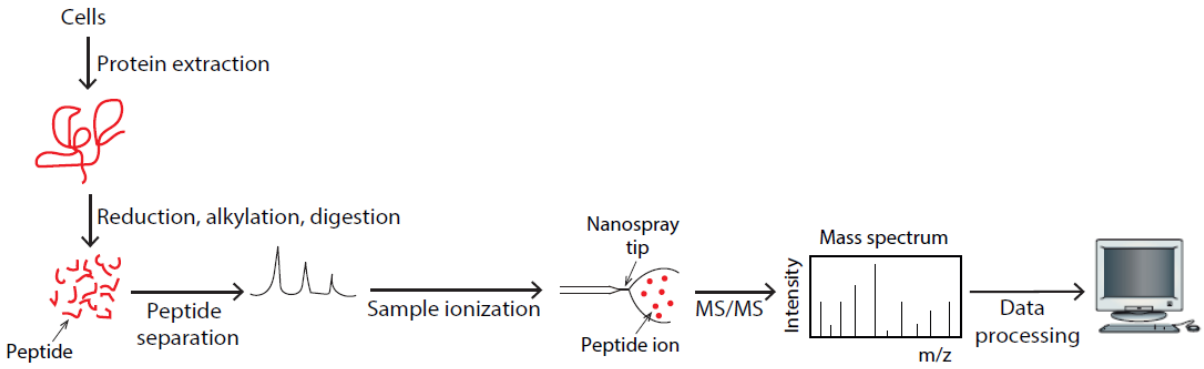

Figure 17. The LC-MS/MS experiment. Sample preparation included protein extraction, reduction, alkylation and digestion. The peptides obtained were first separated by high-performance liquid chromatography. They were subsequently ionized by electrospray ionization creating peptide ions in gas phase that were guided through the mass spectrometer (Q Exactive Plus) and analyzed. Only the 10 ions with the highest intensity every duty cycle were selected for fragmentation by an inert gas (nitrogen). Resulting mass spectra were uniquely matched to peptides sequences in the database using the Andromeda search engine, and relative amounts of proteins were calculated. Modified from (Steen and Mann, 2004).

2.12.1 Data analysis

The total number of proteins identified in at least one sample was 6007. As the lowest non-zero value present in the data was 440000, the lower order of magnitude present in the data, 100000, was used as a pseudocount. Biological triplicates were combined via mean calculation using custom-written MATLAB. Non-irradiated conditions (24 and 48 hours) were considered equal and merged together in $p53^{wt}$ and in $p53^{sh}$ cells in order to simplify the number of controls. These steps were done with the help of Marcel Jentsch (Löwer lab).

2.12.1.1 Calculation of the distance score

Proteins were sorted according to the distance score (see section 2.11.1). In this case x = LFQ intensity. The score was calculated for individual time points: 24 and 48 hours after irradiation, and 24+48 hours together for basal conditions.

Proteins mapped to the corresponding metabolic pathways must show at least two LFQ intensity values bigger than zero (100000) in at least one of the triplicates for the corresponding condition (either basal or 24 or 48 hours after irradiation).

3 RESULTS

3.1 Upon genotoxic stress, p53 controls energy production through mitochondrial respiration and promotes expression of kallikreins

3.1.1 Analysis of the p53 transcriptional response under basal conditions and upon genotoxic stress

In order to get a systematic view of the p53 transcriptome control regarding its non canonical activities, RNA-seq was performed in MCF10A in the presence and absence of p53 (Figure 18) under basal conditions and upon irradiation.

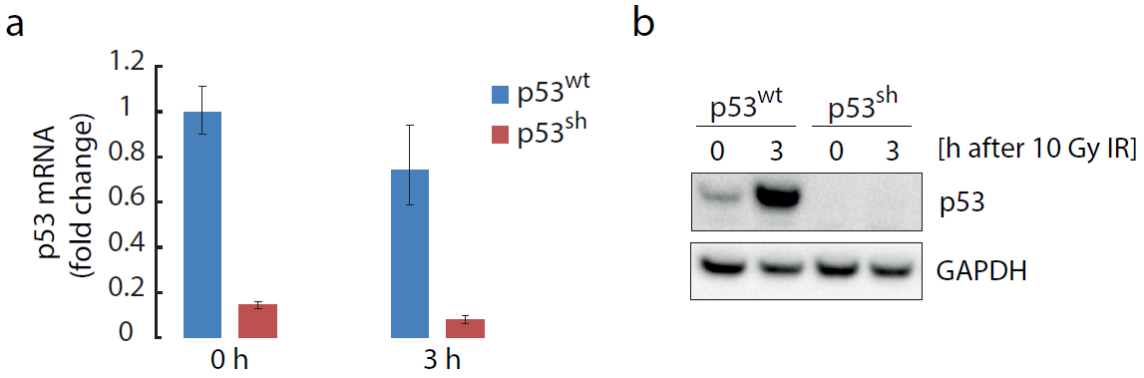

Figure 18. p53 was knocked down successfully. (a) mRNA expression of p53 was measured upon 10 Gy ɣ-IR in MCF10A $p53^{wt}$ and $p53^{sh}$ cells. β-actin was used as an internal control. Error bars indicate standard deviation of technical triplicates. (b) Western blot analysis of p53 upon 10 Gy ɣ-IR in MCF10A $p53^{wt}$ and $p53^{sh}$ cells.

18800 genes were detected after performing the RNA sequencing experiment and analyzing the corresponding data (see section 2.11). The next step was to sort the genes according to their p53 dependency, meaning how gene expression is affected by p53 either in a positive or negative way. How could p53 dependency be assigned to a number? It was observed that canonical p53 target genes – such as p21 (El-Deiry et al., 1993) and ribonucleotide reductase M2 B (RRM2B, (Nakano et al., 2000; Tanaka et al., 2000)) – showed time-dependent expression patterns that were highly divergent between $p53^{wt}$ and $p53^{sh}$ cells (Figure 19).

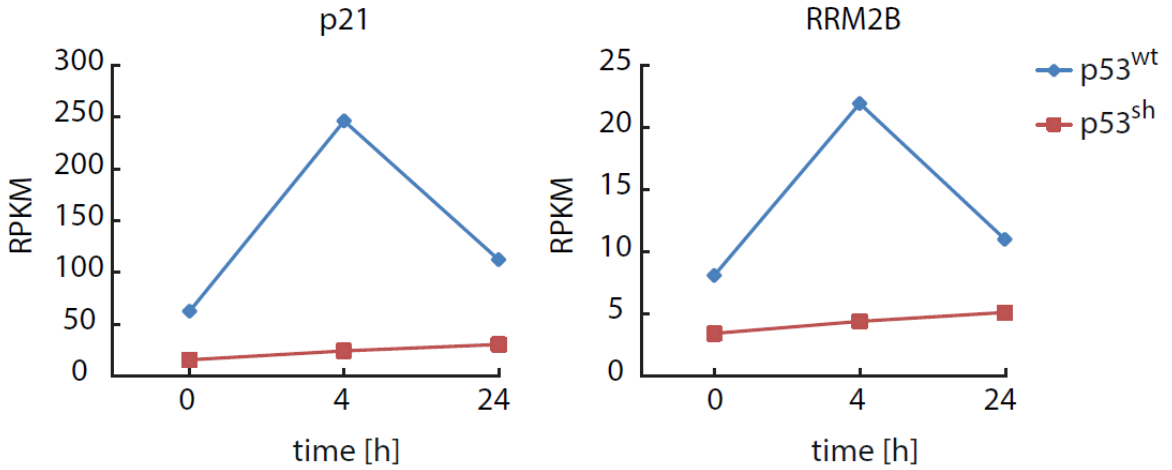

Figure 19. Expression of canonical target genes is higher in p53^{wt} compared to p53^{sh} cells. RRM2B and p21 gene expression was quantified with RPKM in MCF10A p53^{wt} and p53^{sh} cells at basal conditions and 4 and 24 hours after 10 Gy ɣ-IR.

Moreover, genes inhibited by p53, such as cyclin B2 (CCNB2, (Krause et al., 2000)), showed a higher gene expression in p53^{sh} compared to p53^{wt} cells (Figure 20).

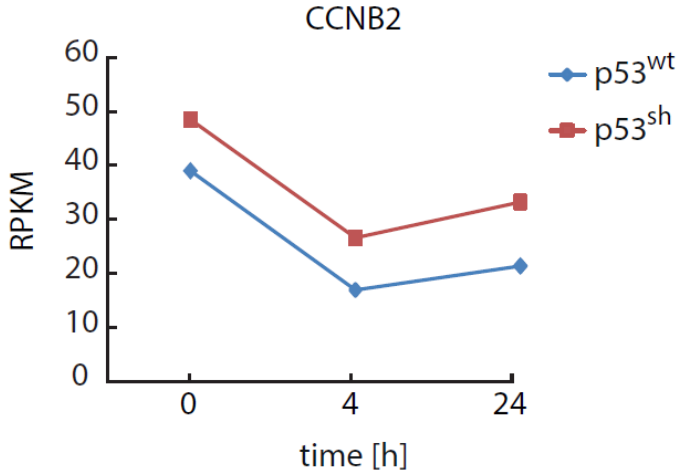

Figure 20. Expression of CCNB2, a p53-repressed gene, is higher in the p53^{sh} compared to p53^{wt} cells at all time points. CCNB2 gene expression was quantified with RPKM in MCF10A p53^{wt} and p53^{sh} cells at basal conditions and 4 and 24 hours after 10 Gy ɣ-IR.

Based on these observations, genes were sorted according to the integrated distance between gene expression profiles for p53^{wt} and p53^{sh} across all time points (distance score, see section 2.11.1). Time course gene expression patterns that were highly divergent between p53^{wt} and p53^{sh} had high distance.

The distance scores ranged from 9.04 (for the gene on the first position, GDF15, a known p53 target gene (Tan et al., 2000)), to almost 0 (no difference between p53 presence and absence). As a validation of the method for sorting the genes, the distance score of 399 known p53 target genes validated in published RNA-seq and ChIP (chromatin immunoprecipitation) data

(Menendez et al., 2013; Nikulenkov et al., 2012)) was plotted and compared to the score of the remaining genes (Figure 21). As expected, p53 targets showed a significantly higher distance score.

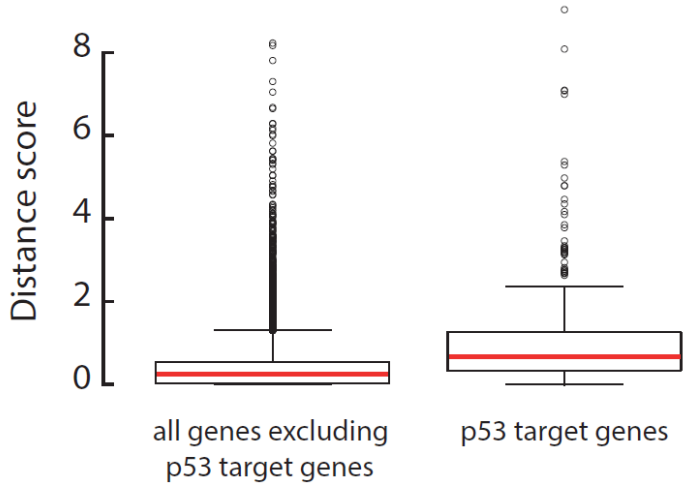

Figure 21. p53 target genes have a significantly higher p53 dependency. Distance score of known p53 target genes compared to distance score of all genes except p53 target genes was plotted. Red lines indicate medians of distributions; boxes include data between 25th and 75th percentiles; whiskers extend to maximum values within 1.5x the interquartile range; circles represent outliers. p-value < 2.2e-16 (Wilcoxon rank-sum test). Plot and statistical test done by Dr. Altuna Akalin.

Moreover, RT-qPCR was performed for several p53 target genes at 0, 4 and 24 hours after ɣ-IR. These genes, that as expected showed a high divergence between p53^{wt} and p53^{sh} (Figure 22), also had high distance scores: p21 was sorted to position 7 of 18800 genes, Mdm2 was at position 36, RRM2B at position 55 and sestrin 1 (SESN1, (Velasco-Miguel et al., 1999)) at position 94. This further confirmed the validity of the distance score for analyzing the data.

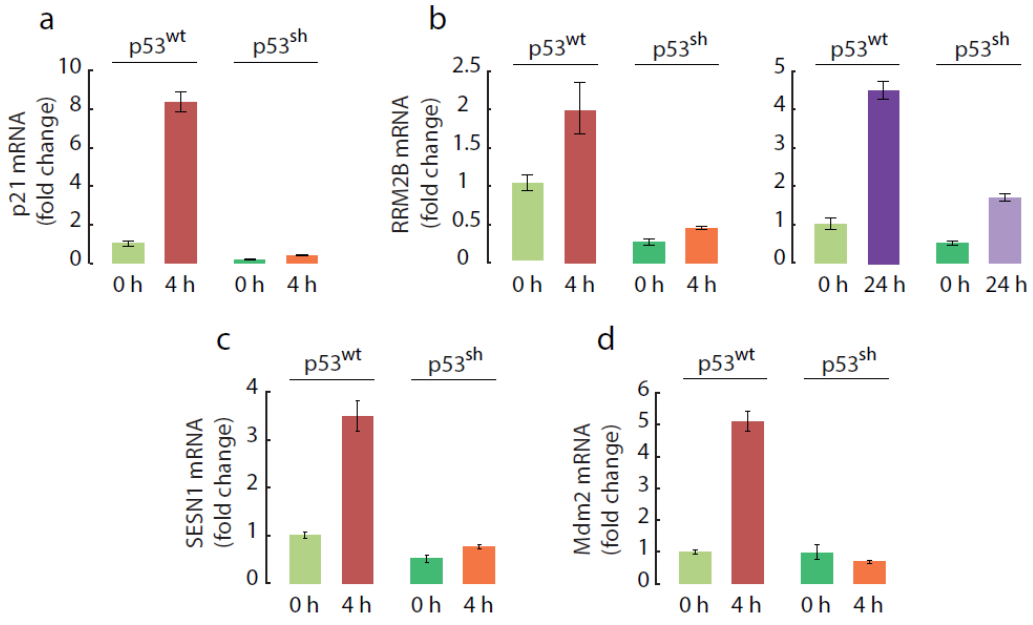

Figure 22. p53 target genes expression is much higher in the p53^{wt} than the p53^{sh} cell line under both basal conditions and irradiation. mRNA expression was measured in MCF10A p53^{wt} and p53^{sh} cells under basal conditions or upon 10 Gy ɣ-IR for (a) p21, 0 and 4 hours after irradiation; (b) RRM2B 0, 4 and 24 hours after irradiation; (c) SESN1, 0 and 4 hours after irradiation; (d) Mdm2, 0 and 4 hours after irradiation. β-actin was used as an internal control. Error bars indicate standard deviation of technical triplicates.

3.1.1.1 Functional annotation analysis of genes with high p53 dependency highlights an enrichment of genes involved in fatty acid metabolism

In order to facilitate biological interpretation of the differentially expressed transcriptome between the presence and absence of p53, gene enrichment analysis for biological process was performed for the top 15% of genes (2820) with the highest distance scores (see section 2.11.2). The analysis resulted in 233 clusters of biological processes. The focus was put on the first 34 clusters (enrichment scores ≥1.3, see section 8.2). They were manually grouped in:

1) Cell fate and DNA damage including terms such as cell cycle, regulation of apoptosis, cell cycle checkpoint, DNA repair, regulation of cell growth and chromosome segregation (44%);
2) Others, where diverse unrelated clusters were included. Some of the terms present in the clusters were epidermis development, response to hormones, angiogenesis and cell adhesion (50%);
3) 6% of the clusters were related to fatty acid metabolism (Figure 23).

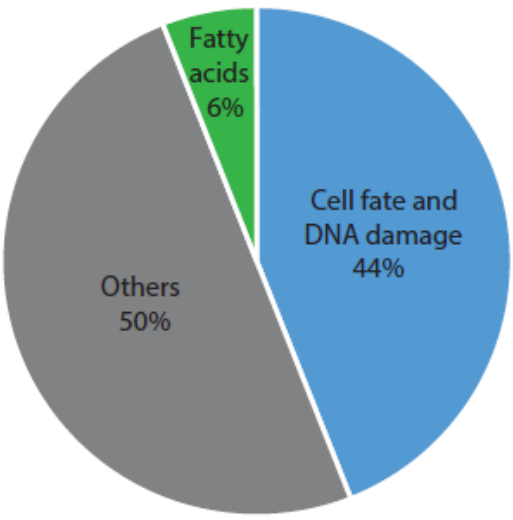

Figure 23. Categories obtained after performing functional annotation analysis. The most statistical significant clusters obtained by gene enrichment analysis of the top 15% of genes with the highest distance scores in MCF10A cells were grouped in three categories: cell fate and DNA damage, fatty acid metabolism and others.

It was not surprising that a high number of clusters were related to cell fate and to DNA damage, as cells were challenged with genotoxic stress and had to respond properly to it; moreover, p53 is well known to regulate proliferation and apoptosis (Meek, 2004) and is involved in the response to DNA damage.

Although further studies in the clusters related to hormones, angiogenesis, etc. may be interesting, it was decided to focus on p53´s role in regulating metabolism first. During the 1920s, the first indication that cancer cells have a distinct metabolism compared to normal cells emerged: Otto Warburg observed that unlike the majority of normal cells which depend on oxidation of pyruvate in mitochondria to produce energy (aerobic process), cancer cells primarily used glycolysis even under normal oxygen concentrations (Warburg effect, (Warburg, 1956)). However, the field of tumor cell metabolism has been largely ignored for many decades, as researchers focused on the genetic of tumorigenesis. Nonetheless, in recent years there has been a renewed interest in the study of the unique metabolism of cancer, and individual links between tumor suppressor genes (such as p53) and cell metabolism have been identified. However, there are few studies that systematically investigate this relationship and its temporal characteristics.

3.1.1.2 Fatty acid metabolism is controlled by p53 mainly at later time points

RNA-seq data suggested a role of p53 in controlling fatty acid metabolism. Does this regulation happen under both basal conditions and upon genotoxic stress, or only upon DNA damage induction? Are there differences on gene expression at different time points after irradiation?

In order to answer these questions, the distance scores for each time point were separately calculated. For example, when calculating the distance scores for PDK2, whose gene expression has been reported to be downregulated by p53 (Contractor and Harris, 2012), it showed up among the top 15% of genes with highest p53 dependency only 24 hours after irradiation, as would be expected from its RPKM values (Figure 24).

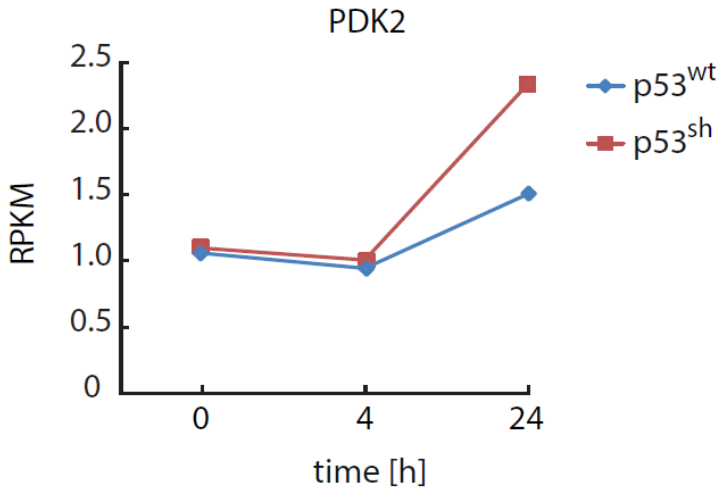

Figure 24. Expression of PDK2, a p53-repressed gene, is higher in $p53^{sh}$ compared to $p53^{wt}$ cells 24 hours after irradiation. CCNB2 gene expression was quantified with RPKM in MCF10A $p53^{wt}$ and $p53^{sh}$ cells at basal conditions and 4 and 24 hours after 10 Gy ɣ-IR.

Once the individual distance scores were calculated, gene enrichment analysis for biological process was performed at individual time points. Under basal conditions, there were no clusters involved in fatty acid metabolism with enrichment scores ≥ 1.3. Four hours upon genotoxic stress, only 2.5% of the clusters were related to fatty acid metabolism (one out of 40 groups), but at later times (24 hours after irradiation) the percent increased up to 11.1% (2 out of 18 clusters, see section 8.3).

3.1.2 Combination of RNA sequencing and proteomics data points to a role of p53 in controlling energy production upon irradiation

Given the results of RNA-seq suggesting a function for p53 in controlling cell metabolism, it was decided to further study this issue by performing a systematic analysis at the protein level upon p53 knock down putting the focus on changes in metabolic pathways, and combining the resulting data with the previous analysis.

In the RNA-seq data, fatty acid metabolism seemed to be regulated by p53 mainly 24 hours after irradiation. p53-dependent effects on the metabolism may show up also at even later time points; therefore, protein levels were measured 24 and 48 hours after irradiation in MCF10A $p53^{wt}$ and $p53^{sh}$ cells by proteomics (see section 2.12). There were 6007 proteins identified after performing the experiment and analyzing the data. As done before for RNA-seq data, individual distance scores for non-irradiated conditions and irradiation (24 and 48 hours) were calculated, and the proteins were sorted accordingly. Again, only the 15% of the proteins with the highest distance scores for each condition were considered.

Fatty acid metabolism is a broad concept that includes different terms such as synthesis of eicosanoids, fatty acid catabolism (β-oxidation) and fatty acid synthesis. In both RNA-seq and proteomics datasets several genes/proteins involved in the β-oxidation pathway were identified. Moreover, it was realized that among the top 15% there were also a high number of genes and proteins linked – as the β-oxidation pathway – to energy production. For these reasons, the focus was put on the analysis of genes/proteins belonging to the fatty acid catabolism and other energy processes, which were manually mapped to the corresponding pathways, either under basal or irradiated conditions (Figure 25). The references consulted for plotting the metabolic pathways and doing the mapping of genes and proteins are listed in section 6.1.

The TCA cycle is a key metabolic pathway that takes place inside the mitochondria. It is the final common pathway for the oxidation of glucose, fatty acids and amino acids. During this series of reactions, electrons are removed from acetyl CoA (coming from the previously mentioned glucose and fatty acid carbon fuels) and used to form NADH and $FADH_2$, which carry the electrons to the electron transport chain. Electrons pass then through four complexes (I, II, III and IV) and are finally transferred to O_2, forming H_2O (oxidative phosphorylation/mitochondrial respiration). During this process, protons are pumped out of the mitochondrial matrix. The electrochemical proton gradient generated across the inner membrane drives protons back through the ATP synthase, generating ATP. The TCA cycle coupled to oxidative phosphorylation provides the most part of energy used by aerobic cells. ATP synthase is composed of different subunits, such as mitochondrially encoded ATP synthase 8 (MT-ATP8). Regarding the electron transport chain, all NDUFs (NADH dehydrogenase (ubiquinone)) depicted, as well as mitochondrially encoded NADH dehydrogenase 4 (MT-ND4), are either (accessory) subunits or involved in assembly of complex I; succinate dehydrogenase complex assembly factor 1 (SDHAF1) and mitochondrial nucleoid factor 1 (MNF1) are involved in complex II or III assembly, respectively, and cytochrome c oxidase asembly factor (COX20) is involved in the assembly of complex IV.

Glycolysis takes place in the cytoplasm, and it is a series of reactions that metabolizes one molecule of glucose to two molecules of pyruvate (not shown). This process is anaerobic, but in the presence of oxygen, pyruvate is transported inside the mitochondrial matrix and is then transformed into acetyl CoA by the pyruvate dehydrogenase complex. This complex is inhibited by different pyruvate dehydrogenase kinase (PDK) isozymes, and positively regulated by pyruvate dehydrogenase phosphatase catalytic subunit 1 (PDP1).

Moreover, proline degradation, which takes place inside the mitochondria and is catalyzed by PRODH (proline dehydrogenase 1) and aldehyde dehydrogenase 4 family member A1 (ALDH4A1), produces glutamate that is converted to α-ketoglutarate and enters the cycle.

Fatty acids are also connected to the TCA cycle. Hydrolysis of triglycerides and cholesteryl esters in the lysosome by lipase A (LIPA) is one way to obtain free fatty acids inside the cell. Long-chain fatty acids (more than 12 carbon atoms) require activation by covalent modification via acyl CoA synthetases on the outer mitochondrial membrane. The resulting acyl CoAs pass through large pores in the outer membrane to the mitochondrial intermembrane space. There, they are conjugated to carnitine by carnitine acyltransferase I (CPT1B isoform shown), which is inhibited by malonyl CoA. Conversion of malonyl CoA to acetyl CoA is catalyzed by MLYCD, and acetyl-CoA carboxylase (ACC) converts acetyl CoA back to malonyl CoA. AMP-activated protein kinase (AMPK), which consists of different subunits such as PRKAG2 and PRKAB1, is positively regulated by SESN1 and SESN2 and it inhibits the activity of ACC. Acyl carnitine produced by CPT1 is shuttled by a translocase across the inner mitochondrial membrane. Carnitine acyltransferase II converts acyl carnitine back to acyl CoA. Only long-chain fatty acids need carnitine-mediated transport; medium- and short-fatty acids can enter by diffusion and are activated by acyl CoA synthetases in the matrix (not depicted). Acyl CoA enters then the β-oxidation/fatty acid degradation pathway. Although the enzymes are different depending on the size of the acyl CoA, the reactions taking place are the same: oxidation, hydration, oxidation and thiolysis (the depicted enzymes ACADVL and HADHA are involved in the metabolism of long-chain fatty acids, and are bound to the inner mitochondrial membrane). The last step of the degradation pathway produces acetyl CoA and an acyl CoA shortened by two carbon atoms, which undergoes another cycle of β-oxidation. The molecule of acetyl CoA produced in each cycle enters the TCA cycle to be further oxidized. Moreover, a molecule of NADH - which donates its electrons to the mitochondrial respiratory chain- and a molecule of $FADH_2$ are produced. The electrons from $FADH_2$ are transferred to the mitochondrial respiratory chain by the electron transfer flavoprotein dehydrogenase (ETFDH). During the β-oxidation of unsaturated fatty acids, the action of auxiliary enzymes such as 2,4-dienoyl-CoA reductase 1 (DECR1) is needed. Lipin 1 is a transcriptional co-activator of genes involved in β-oxidation.

Although most β-oxidation occurs in the mitochondria, oxidation of very long-chain or 2-methyl-branched fatty acids happens in peroxisomes. The oxidation in these organelles halts at octanoyl CoA, which is converted into the corresponding carnitine ester and enters the mitochondria to further undergo β-oxidation. One enzyme involved in the oxidation of fatty

acids in peroxisomes is 2,4-dienoyl-CoA reductase 2 (DECR2). Peroxisome proliferator activated receptor gamma (PPARG) is a nuclear receptor activated by peroxisome proliferators, and it positively controls transcription of genes involved in peroxisomal β-oxidation.

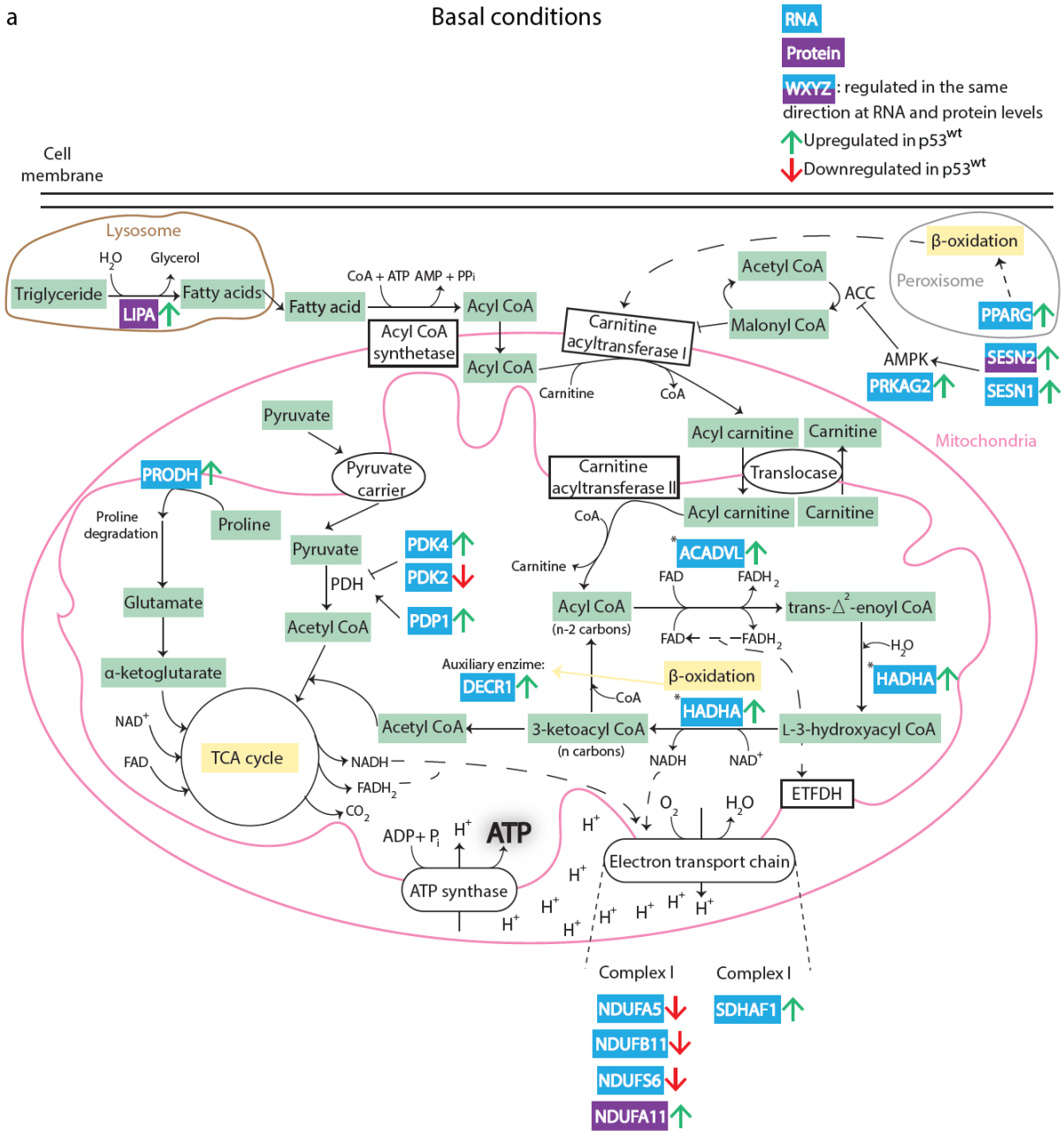

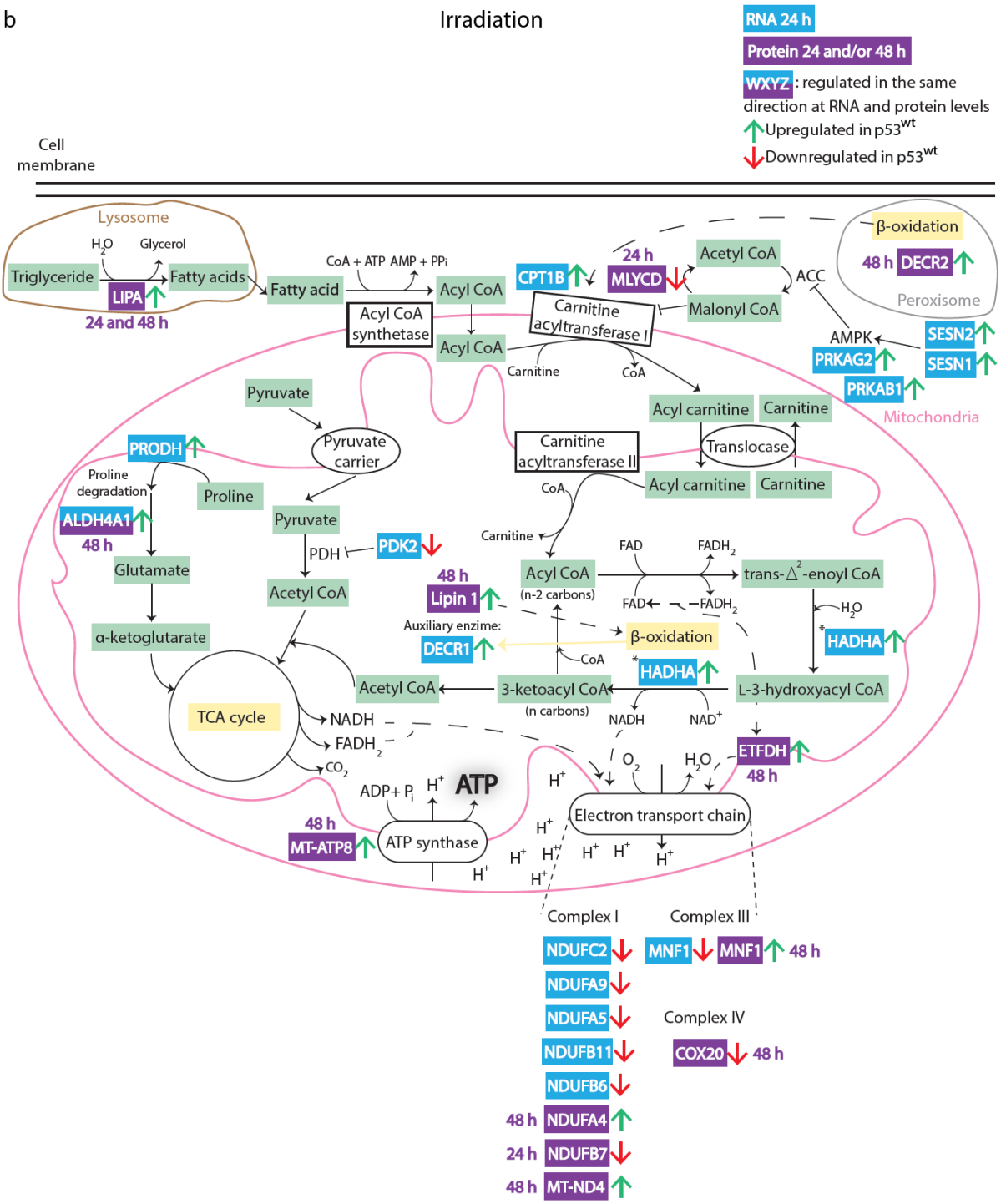

Figure 25. Fatty acid catabolism and other pathways linked to ATP production. Mapping of the 15% of genes and proteins in MCF10A cells with the highest distance scores under (a) basal conditions; (b) 10 Gy ɣ-IR 24 hours after irradiation for genes, and 24 and/or 48 hours for proteins. Pi stands for inorganic phosphate, and PPi for inorganic pyrophosphate.

What happens to the metabolism when comparing presence and absence of p53 in cells? Under basal conditions, there was not a very clear picture (Figure 25a). On one side, fatty acid catabolism could be upregulated in the $p53^{wt}$ cell line since there was an increase in gene or

protein expression for HADHA, ACADVL, LIPA, PPARG and DECR1 (its promoter has two p53 binding sites ("EpiTect ChIP qPCR Primers - SABiosciences, QIAGEN," 2016a)). Moreover, SESN1 and SESN2, known p53 target genes (Budanov et al., 2002; Velasco-Miguel et al., 1999) and positive regulators of AMPK, and the AMPK subunit PRKAG2, were upregulated by p53 at the transcriptional and/or protein level. The first step of proline degradation (PRODH is a p53 target gene (Polyak et al., 1997)) was also upregulated. However, three out of four genes involved in the electron chain were downregulated in the $p53^{wt}$ cells. Although NDUFB11 promoter has been reported to have five p53 binding sites ("EpiTect ChIP qPCR Primers - SABiosciences, QIAGEN," 2016b), in this study the gene was downregulated by p53. It could be that these binding sites do not regulate NDUFB11, but another gene in the vicinity through distant regulatory control. Regarding pyruvate dehydrogenase regulation, it was not clear if it was positively or negatively regulated: PDP1 and PDK4 gene expression was upregulated in $p53^{wt}$ cells (PDK4 promoter has been suggested to be p53 responsive (Harris et al., 2009)), while PDK2 was downregulated by p53, as previously reported (Contractor and Harris, 2012).

After irradiation, the picture was different (Figure 25b). Regarding fatty acid metabolism, the lipase LIPA was upregulated at the protein level in $p53^{wt}$ cells 24 and 48 hours after irradiation; CPT1B, AMPK subunits PRKAG2 and PRKAB1 (known p53 target gene (Jen and Cheung, 2005)), as well as SESN1 and SESN2, were transcriptionally upregulated by p53, but MLYCD protein was downregulated 24 hours after ɣ-IR. However, MLYCD decreased levels could be indirectly compensated by an increased expression of sestrins and AMPK subunits. MLYCD has been reported to be positively controlled by p53 in response to nutrient deprivation (Liu et al., 2014). It may be that different stresses promote a different MLYCD regulation by p53.
HADHA and DECR1, enzymes of the β-oxidation, were upregulated at the RNA level by p53. Moreover, lipin 1 – a p53 target gene (Assaily et al., 2011)) –, DECR2 and ETFDH proteins showed higher levels in the $p53^{wt}$ cell line 48 hours after irradiation.
Regarding the TCA cycle, pyruvate entry into the cycle was positively controlled by p53, as PDK2 gene was inhibited. In addition, proline degradation was also promoted by PRODH and ALDH4A1 upregulation, known p53 target genes (Polyak et al., 1997; Yoon et al., 2004).
Five proteins belonging to the electron transport chain were among the top 15%. From these five, three were upregulated in $p53^{wt}$ cells 48 hours after irradiation (NDUFA4, MT-ND4 and MNF1); NDUFB7 was downregulated by p53 24 hours after ɣ-IR and COX20 after 48 hours. All genes involved in OXPHOS were downregulated. However, these reduced levels could be

compensated by the remaining upregulated proteins and by an increase in β-oxidation and in fluxes feeding into the TCA cycle. The fact that p53 regulates genes involved in OXPHOS in an opposite way in regard to the overall tendency is interesting and needs further investigation, as well as the different regulation of MNF1 at the transcriptional and protein level by p53.

Finally, one subunit of the ATP synthase was positively controlled by p53 48 hours after irradiation.

Interestingly, upregulation by p53 of metabolic proteins happened mainly 48 hours after irradiation. It could be that p53 directly promotes gene transcription, as it happens for ALDH4A1 (Yoon et al., 2004), but an additional mechanism regulates mRNA translation or degradation, which would delay accumulation of proteins. Thus, only 48 hours after irradiation significant differences between $p53^{wt}$ and $p53^{sh}$ would appear. In fact, ALDH4A1 gene was upregulated by p53 24 hours after DNA damage induction, but protein levels were different between presence and absence of p53 only after 48 hours. However, this hypothesis is hard to prove with the current data, as most part of the depicted genes were either not detected or out of the top 15% in proteomics data, and most part of the depicted proteins were not on the top 15% in RNA-seq data.

In summary, RNA-seq and proteomics data together showed that p53 promoted energy production through the electron transport chain for days upon genotoxic stress, especially by controlling the expression of genes and proteins involved in fatty acid β-oxidation.

3.1.3 Kallikrein expression is p53-dependent

As explained in section 3.1.1, distance scores for the RNA-seq data were calculated across all time points and genes were sorted according to them. Although gene enrichment analysis for biological process did not result in any cluster specific for the kallikrein family (probably due to the low number of correlated genes present on the top 15%), it was observed that distance score of two kallikrein-related peptidases, KLK10 and KLK5, occupied position third and ninth of 18800, respectively. Moreover, the serine peptidase inhibitor, Kazal Type 6 (SPINK6), a potent inhibitor of KLK5 (Meyer-Hoffert et al., 2010), was at the second position. When the distance score was calculated separately for the different time points (explained in 3.1.1.2), SPINK6 and KLK10 were the first two genes with highest p53 dependency under basal conditions. Four hours after irradiation, they were still within the 15 genes with highest p53 dependency. More interesting, 24 hours after irradiation, apart from KLK10 and SPINK6, three additional kallikreins, KLK5, KLK7 and KLK8, were among the top 15 genes. The absolute

values of the distance scores were all positive for the different time points and genes, meaning that these kallikreins and SPINK6 were positively regulated by p53 (Table 7).

Genes	Distance score all (rank)	Distance score 0 h (rank)	Distance score 4 h (rank)	Distance score 24 h (rank)
KLK10	8.17 (3)	2.37 (2)	2.63 (8)	3.17 (5)
KLK8	5.41 (24)	1.44 (32)	1.57 (65)	2.40 (14)
KLK7	4.91 (34)	0.89 (161)	1.33 (106)	2.69 (9)
KLK5	7.05 (9)	1.46 (30)	2.13 (19)	3.46 (3)
SPINK6	8.23 (2)	2.67 (1)	2.40 (11)	3.16 (6)

Table 7. Kallikrein and SPINK6 expression is p53-dependent. Distance scores and the corresponding sorting positions for KLK10, KLK8, KLK7, KLK5 and SPINK6 at the different time points after irradiation are shown. The highest distance score at 4 hours was again for GDF15 (4.65), while for 24 hours the highest distance score was 4.32.

Were these genes upregulated in a p53-dependent manner overtime? To address this question, the fold changes of the RPKM values at 4 and 24 hours related to basal conditions were calculated in wild-type cells. Interestingly, kallikreins seemed to be highly regulated by p53 at later time points, as all of them were more strongly induced 24 hours after irradiation (Table 8). SPINK6 did not seem to change upon irradiation.

Genes	$p53^{wt}$ 4 h/$p53^{wt}$ 0 h	$p53^{wt}$ 24 h/$p53^{wt}$ 0 h
KLK10	1.4	3.4
KLK8	1.2	4.5
KLK7	1.5	8.6
KLK5	1.6	6.2
SPINK6	1.3	1.4

Table 8. Kallikreins are upregulated by p53 at later time points upon genotoxic stress. Fold changes for KLK10, KLK8, KLK7, KLK5 and SPINK6 were calculated between their RPKM values 4 or 24 hours after 10 Gy ɣ-IR and their RPKM values at basal conditions in MCF10A $p53^{wt}$.

As a validation of the RNA sequencing results, RT-qPCR for KLK10 was performed in MCF10A in the presence and absence of p53 at 0 and 24 hours after irradiation, and it confirmed a p53-dependent transcriptional activation (Figure 26).

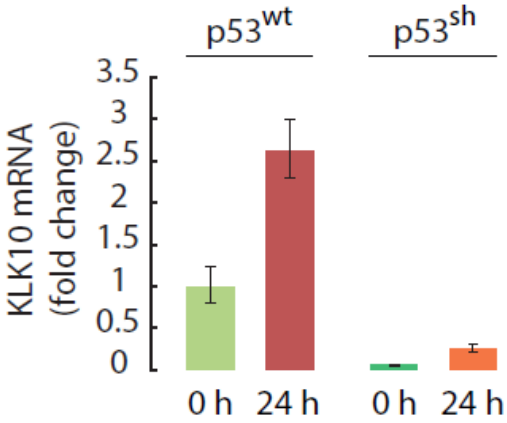

Figure 26. KLK10 expression under both basal conditions and irradiation is much higher in the p53^{wt} than the p53^{sh} cell line. mRNA expression of KLK10 was measured in MCF10A p53^{wt} and p53^{sh} cells under basal conditions or 24 hours upon 10 Gy γ-IR. β-actin was used as an internal control. Error bars indicate standard deviation of technical triplicates.

The human kallikrein family consists of at least 15 structurally related serine proteases with a variety of physiological functions (Borgoño et al., 2004; Yousef, 2001). KLK10 is considered a tumor suppressor in breast cells because its gene expression is downregulated in breast cancer and the transfection of the KLK10 gene into KLK10-negative breast cancer cells significantly inhibits tumor formation in nude mice (Dhar et al., 2001; Goyal et al., 1998; Liu et al., 1996; Yousef et al., 2004). Moreover, KLK5 (Avgeris et al., 2011; Feng et al., 2010; Li et al., 2009; Yousef et al., 2004), KLK8 (Yousef et al., 2004) and KLK7 (Feng et al., 2010; Li et al., 2009) expression is also downregulated in breast cancer.

The results presented here provide the first evidence for a connection between the kallikrein family and p53. Unfortunately, kallikreins were not present in the proteomics data because they are secreted proteins.

3.2 Hyper-activation of ATM upon DNA-PKcs inhibition modulates p53 dynamics and cell fate in response to DNA damage

Due to the complex pattern of kinase activation upon DNA damage, ATM, ATR and DNA-PKcs may play a distinct role in controlling the dynamic response of p53. Moreover, it is also unclear if this control is independent from each other or if they regulate each other's activity. To systematically address these issues, in this study there were used fluorescent reporters, live-cell time-lapse microscopy and automated image analysis in combination with kinases inhibitors to study the p53 response upon ɣ-irradiation in individual cells.

3.2.1 p53 shows pulsatile dynamics upon induction of DSBs

In order to follow the p53 response over time, clonal cell lines stably expressing p53-YFP were employed. These included the transformed cell lines A549, U-2 OS and MCF7 (Batchelor et al., 2008; Chen et al., 2013) as well as the untransformed cell line MCF10A. As previously reported (Lahav et al., 2004), p53 protein accumulated in regular pulses upon genotoxic stress (Figure 27).

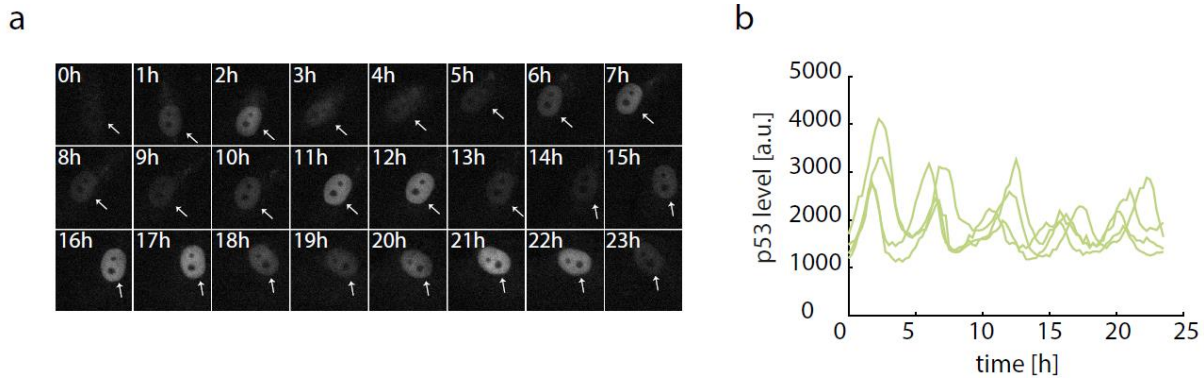

Figure 27. p53 accumulates in uniform pulses upon DSBs induction. (a) Time-lapse microscopy images of A549 cells expressing p53-YFP following treatment with 10 Gy ɣ-irradiation. (b) Individual A549 reporter cells were tracked and the p53 average nuclear fluorescence intensity was measured in cells irradiated with 10 Gy ɣ-IR.

The features used for describing the pulses were width and amplitude (Figure 28), extracted after analyzing hundreds of single cell trajectories.

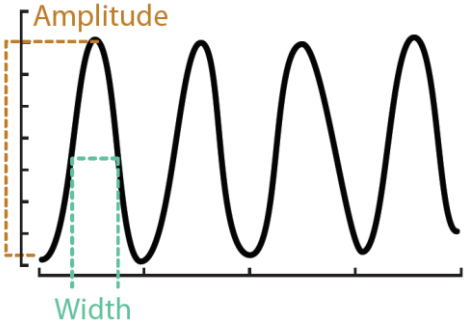

Figure 28. Schematic drawing of the dynamic features (relative amplitude and full-width at half-maximum (FWHM)) of the first p53 pulse.

When p53 dynamics were quantified, the observed constant width and amplitude across pulses further confirmed the previous studies (Figure 29). For this reason, the focus was put on the first pulse.

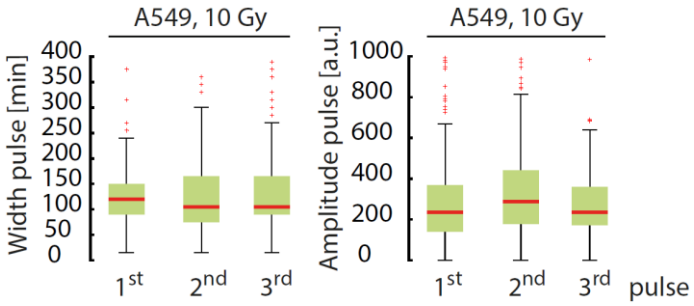

Figure 29. p53 width and amplitude are uniform across pulses. Quantification of the relative amplitude and FWHM of the first, second and third p53 pulses upon 10 Gy ɣ-IR in A549 reporter cells (n > 790 cells per condition). Red lines indicate medians of distributions; boxes include data between 25th and 75th percentiles; whiskers extend to maximum values within 1.5x the interquartile range; crosses represent outliers.

Moreover, feature analysis of the first p53 pulse across increasing doses of ɣ-IR confirmed that in all cell lines tested, width and amplitude were constant and therefore independent of the number of DSBs induced (Figure 30) (Lahav et al., 2004).

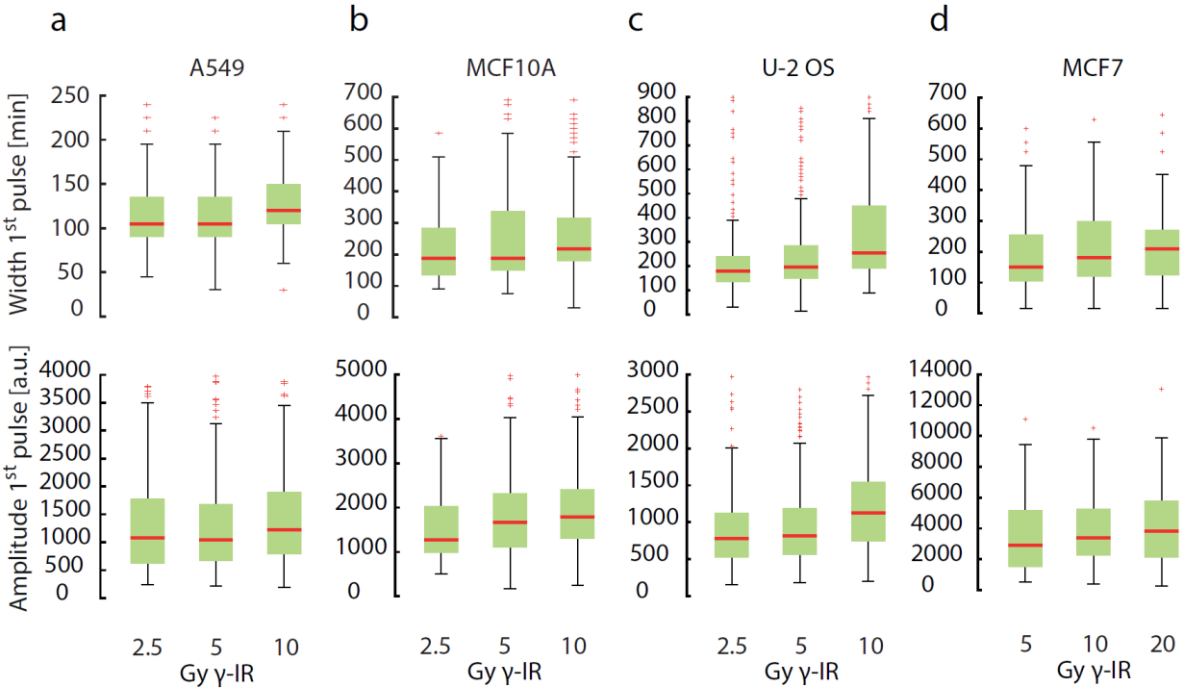

Figure 30. Features of the first p53 pulse are independent of the levels of damage. (a-c) Quantification of the relative amplitude and FWHM of the first p53 pulse upon 2.5, 5 or 10 Gy ɣ-IR for the reporter cells (a) A549 (n > 250 cells per condition); (b) MCF10A (n > 42 cells per condition); (c) U-2 OS (n > 250 cells per condition); (d) Quantification of the relative amplitude and FWHM of the first p53 pulse upon 5, 10 or 20 Gy ɣ-IR for MCF7 reporter cells (n > 85 cells per condition). Red lines indicate medians of distributions; boxes include data between 25th and 75th percentiles; whiskers extend to maximum values within 1.5x the interquartile range; crosses represent outliers.

3.2.2 p53 response is controlled by three PI3K-like kinases

In order to systematically study the role of all three PI3K-like kinases in shaping the p53 response to DSBs, well-characterized small molecule inhibitors were used (ATMi, ATRi and DNA-PKi) (Hickson et al., 2004; Reaper et al., 2011), and their specificity was confirmed using western blot analysis. Chk2 phosphorylation at threonine 68 and ATM auto-phosphorylation at serine 1981 were used as surrogates for ATM activation; Chk1 phosphorylation at serine 317 for ATR activation, and DNA-PKcs phosphorylation at serine 2056 for DNA-PKcs activity. As observed in Figure 31, ATM was not active when using ATMi or a combination of the three inhibitors, but its activation was not affected when using the other two inhibitors alone. The same happened for pChk1 and pDNA-PKcs with ATRi and DNA-PKi, respectively.

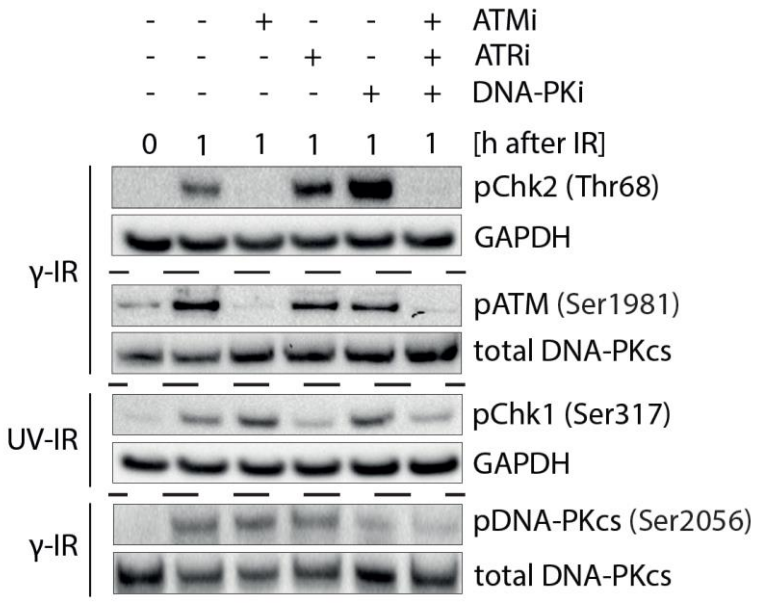

Figure 31. ATM, ATR and DNA-PKcs inhibitors are specific. Western blot analysis showing specificity of ATMi (measured by pATM and pChk2), of ATRi (measured by pChk1) and DNA-PKi (measured by pDNA-PKcs) in A549 cells. Cells were treated with 10 Gy ɣ-IR or 4.5 J/m^2 UV radiation. UV light was used for testing ATRi, as this kind of radiation cross-links consecutive pyrimidine bases and leads to the exposure of single-stranded DNA, structure responsible for ATR activation (Cimprich and Cortez, 2008).

When all three inhibitors were applied together before treating cells with ɣ-IR, a p53 response was no longer observed as expected in single cell trajectories examples (Figure 32).

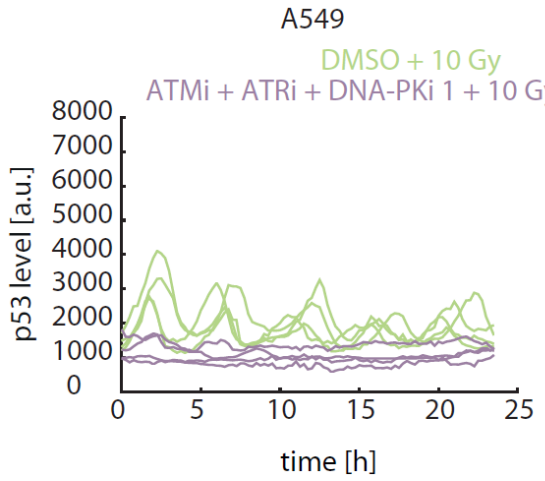

Figure 32. ATM, ATR and DNA-PKcs inhibition abrogates p53 response. Individual A549 reporter cells were tracked and the p53 average nuclear fluorescence intensity was measured in cells untreated or treated with a mix of ATMi, ATRi and DNA-PKi 30 minutes before irradiating cells with 10 Gy ɣ-IR.

To further confirm these results, p53 fluorescence was quantified in both A549 and MCF10A cells at three different time points that approximately define the first pulse: 0, 3 and 5 hours after ɣ-IR (Batchelor et al., 2008; Lahav et al., 2004). In both cell lines, the p53 signal was dramatically decreased when inhibiting the three upstream kinases if compared to the control (Figure 33). These findings further supported the notion that ATM, ATR and DNA-PKcs are necessary for a proper p53 response.

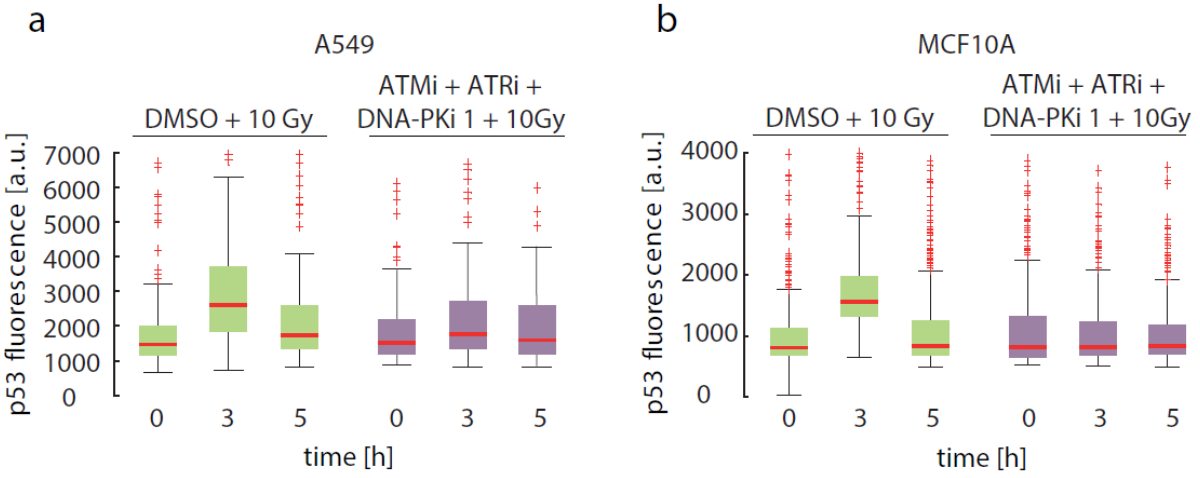

Figure 33. ATM, ATR and DNA-PKcs are needed for a regular p53 induction. Quantification of the p53 average nuclear fluorescence intensity at 0, 3 and 5 hours upon 10 Gy ɣ-IR in reporter cells untreated or treated with a mix of ATMi, ATRi and DNA-PKi for (a) A549 ($n > 120$ cells per condition); (b) MCF10A ($n > 430$ cells per condition). Red lines indicate medians of distributions; boxes include

data between 25th and 75th percentiles; whiskers extend to maximum values within 1.5x the interquartile range; crosses represent outliers.

3.2.3 ATM inhibition has minor effects on p53 dynamics

Next, it was investigated if these kinases act as redundant systems to provide a fail-save relay of the damage input to the p53 system, or if each of them performs a distinct function. First ATM was inhibited, which has been described as the main kinase inducing p53 accumulation upon DSB induction (Ciccia and Elledge, 2010). However, no qualitative differences in p53 pulses were observed (Figure 34).

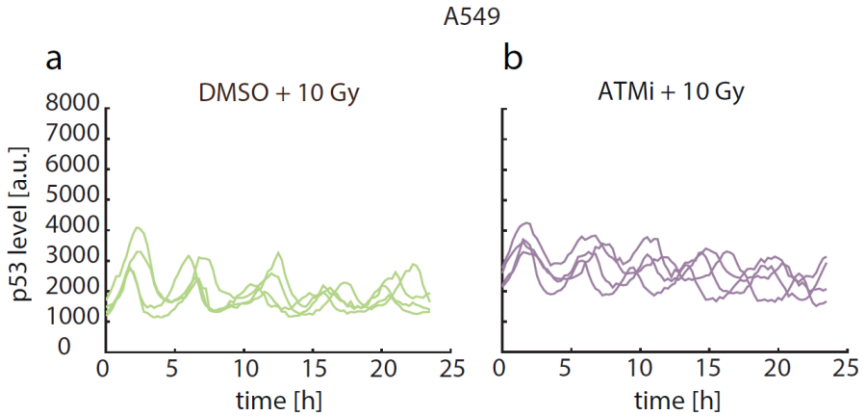

Figure 34. Loss of ATM activity does not lead to noticeable changes in p53 dynamics. Individual A549 reporter cells were tracked and the average nuclear fluorescence was measured upon 10 Gy ɣ-IR in (a) untreated cells; (b) cells treated with ATMi.

When the first p53 pulse was quantified, a small reduction of pulse amplitude was detected, while pulse width remained unaltered (Figure 35). This indicated that under the given experimental conditions loss of ATM activity was compensated by the other PI3K-like kinases, which was consistent with previous studies in ATM-deficient cells (Boehme et al., 2008; Callén et al., 2009; Li and Stern, 2005; Tomimatsu et al., 2009).

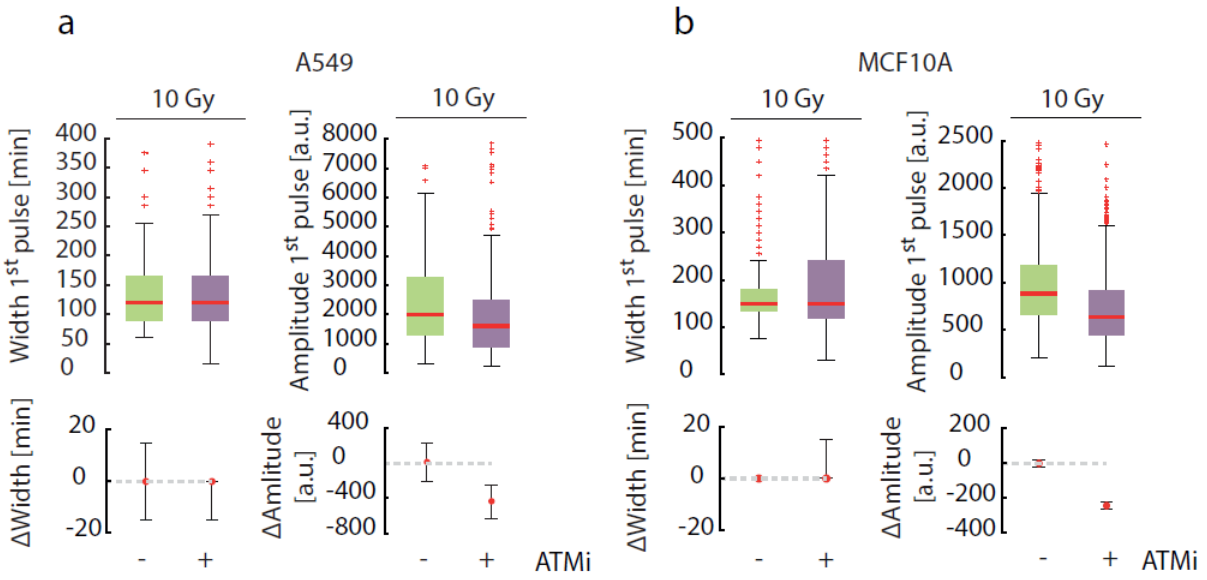

Figure 35. Loss of ATM activity does not greatly alter p53 response. Quantification of the relative amplitude and FWHM and the corresponding statistical analysis of the first p53 pulse upon 10 Gy ɣ-IR in reporter cells untreated or treated with ATMi for (a) A549 (n > 190 cells per condition); (b) MCF10A (n > 570 cells per condition). Red lines indicate medians of distributions; boxes include data between 25th and 75th percentiles; whiskers extend to maximum values within 1.5x the interquartile range; crosses represent outliers. Red dots indicate estimated changes of the median pulse width and amplitude; error bars represent 90% confidence intervals.

3.2.4 ATR inhibition has minor effects on p53 dynamics

Next, ATR was inhibited. Again, regular p53 pulses with only a minor decrease in amplitude were observed (Figure 36). This compensation of ATR's activity was in line with its secondary role during the DSB response, where its function in the presence of ATM is restricted to contributing to damage repair by HR (Cimprich and Cortez, 2008).

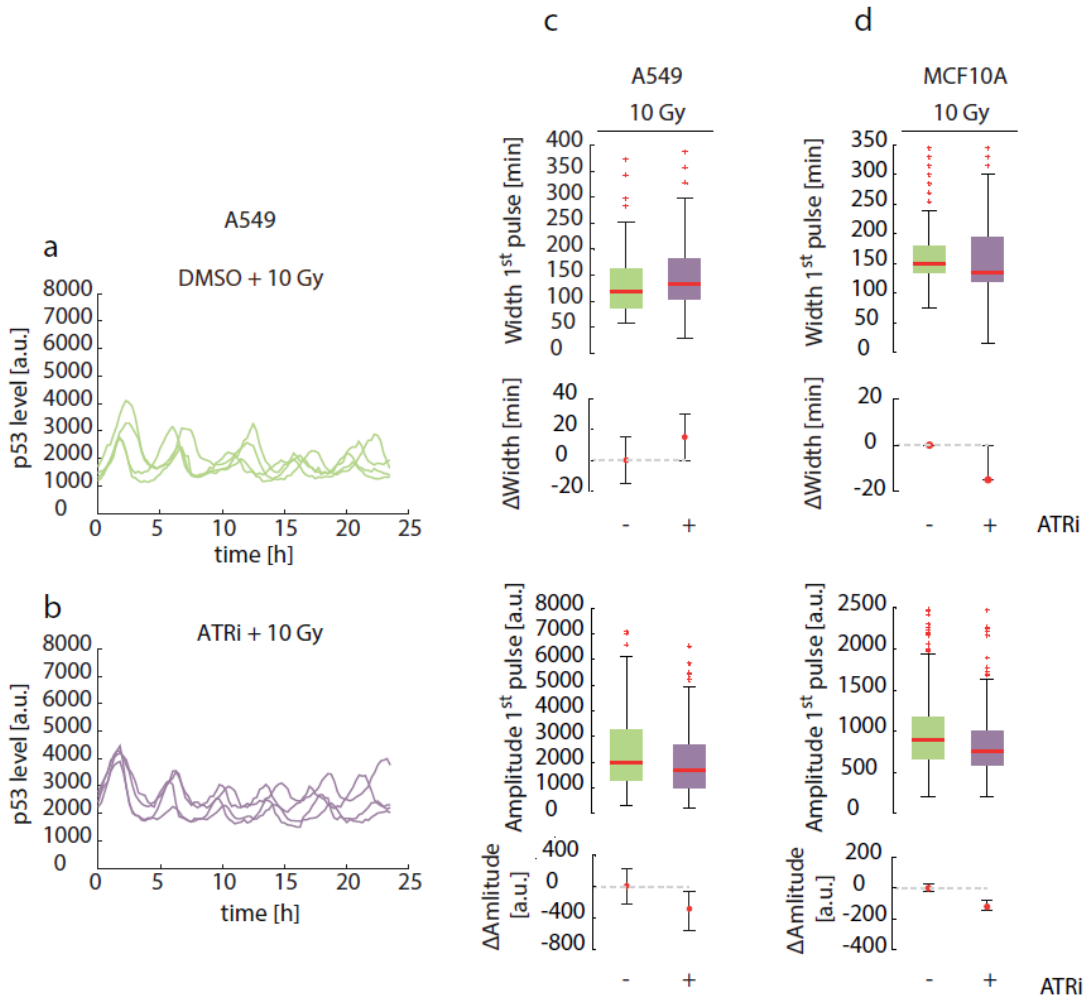

Figure 36. Loss of ATR activity does not greatly alter p53 response. (a-b) Individual A549 reporter cells were tracked and the average nuclear fluorescence was measured upon 10 Gy ɣ-IR in (a) untreated cells; (b) cells treated with ATRi. (c-d) Quantification of the relative amplitude and width and the corresponding statistical analysis of the first p53 pulse upon 10 Gy ɣ-IR in reporter cells untreated or treated with ATRi for (c) A549 (n > 130 cells per condition); (d) MCF10A (n > 330 cells per condition). Red lines indicate medians of distributions; boxes include data between 25th and 75th percentiles; whiskers extend to maximum values within 1.5x the interquartile range; crosses represent outliers. Red dots indicate estimated changes of the median pulse width and amplitude; error bars represent 90% confidence intervals.

3.2.5 DNA-PKcs inhibition induces an amplified p53 response

When finally DNA-PKcs was inhibited, a strong alteration of p53 dynamics upon ɣ-IR at the single cell level was unexpectedly observed (Figure 37).

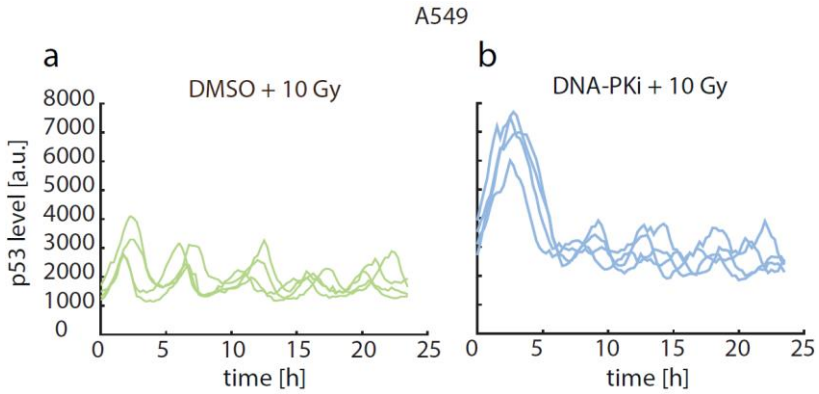

Figure 37. Loss of DNA-PKcs activity changes p53 pulsing behavior. Individual A549 reporter cells were tracked and the average nuclear fluorescence was measured upon 10 Gy ɣ-IR in (a) untreated cells; (b) cells treated with DNA-PKi.

When the first p53 pulse was quantified in different transformed (A549, MCF7 and U-2 OS) and untransformed cell lines (MCF10A), it was confirmed that it was longer and of increased amplitude (Figure 38).

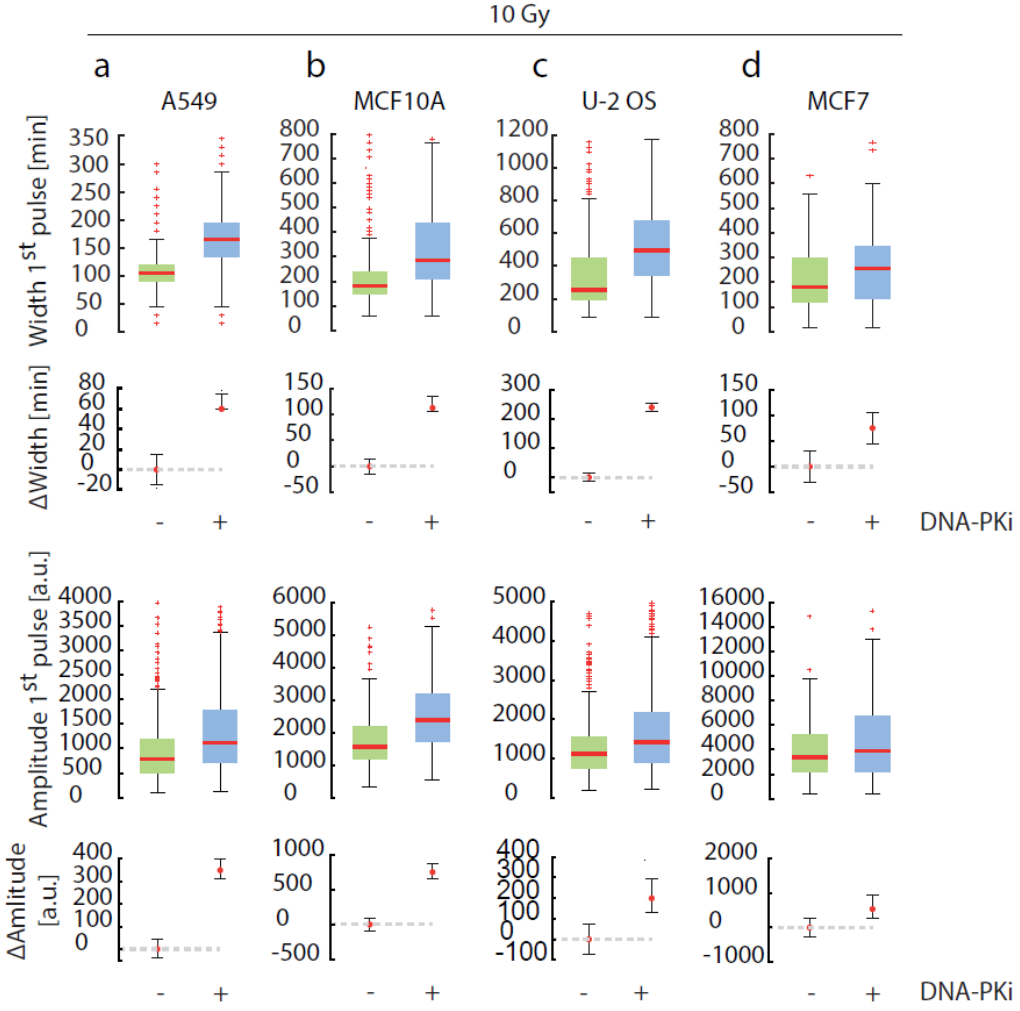

Figure 38. **Loss of DNA-PKcs activity strongly alters first p53 pulse.** Quantification of the relative amplitude and FWHM and the corresponding statistical analysis of the first p53 pulse upon 10 Gy ɣ-IR in reporter cells untreated or treated with DNA-PKi for (a) A549 (n > 790 cells per condition); (b) MCF10A (n > 300 cells per condition); (c) U-2 OS (n > 390 cells per condition); (d) MCF7 (n > 85 cells per condition). Red lines indicate medians of distributions; boxes include data between 25th and 75th percentiles; whiskers extend to maximum values within 1.5x the interquartile range; crosses represent outliers. Red dots indicate estimated changes of the median pulse width and amplitude; error bars represent 90% confidence intervals.

To validate these results, an alternative DNA-PKcs inhibitor was used (DNA-PKi-2) (Hardcastle et al., 2005; Leahy et al., 2004), and a similarly amplified response was observed (Figure 39).

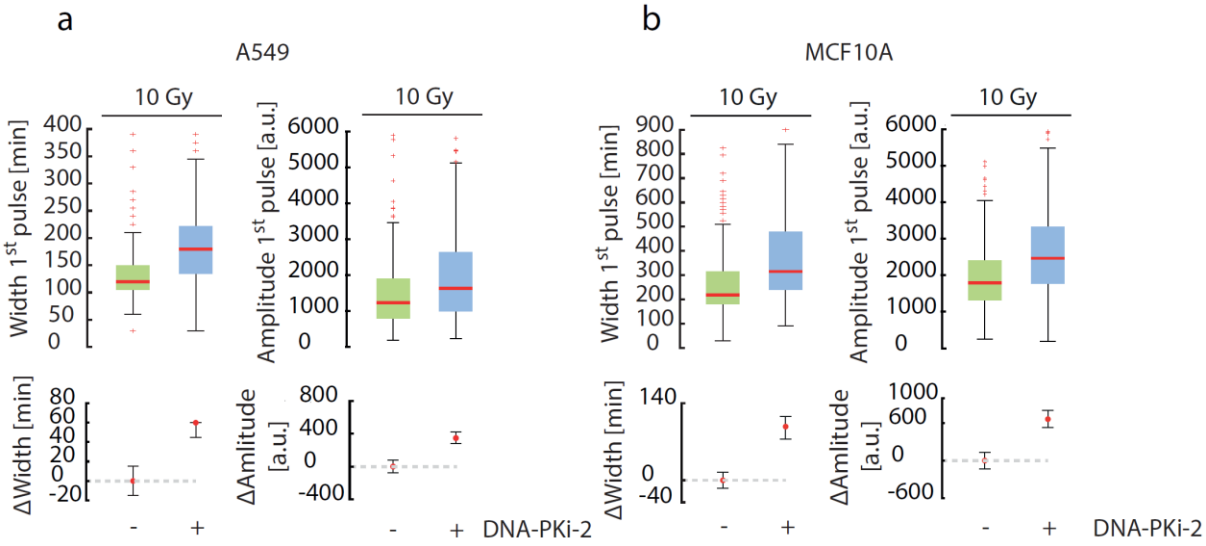

Figure 39. p53 response is also amplified by using an alternative DNA-PKcs inhibitor. Quantification of the relative amplitude and FWHM and the corresponding statistical analysis of the first p53 pulse upon 10 Gy ɣ-IR in reporter cells untreated or treated with DNA-PKi-2 for (a) A549 (n > 260 cells per condition); (b) MCF10A (n > 210 cells per condition). Red lines indicate medians of distributions; boxes include data between 25th and 75th percentiles; whiskers extend to maximum values within 1.5x the interquartile range; crosses represent outliers. Red dots indicate estimated changes of the median pulse width and amplitude; error bars represent 90% confidence intervals.

Moreover, endogenous p53 was analyzed by western blot and higher p53 protein levels and a longer duration of the first response were observed (Figure 40).

Figure 40. Endogenous p53 confirms amplification of the response upon DNA-PKcs inhibition. Western blot analysis of total p53 upon 10 Gy ɣ-IR in cells untreated or treated with DNA-PKi for A549.

Interestingly, after a first altered p53 pulse, the consecutives pulses went back to control levels (Figure 41).

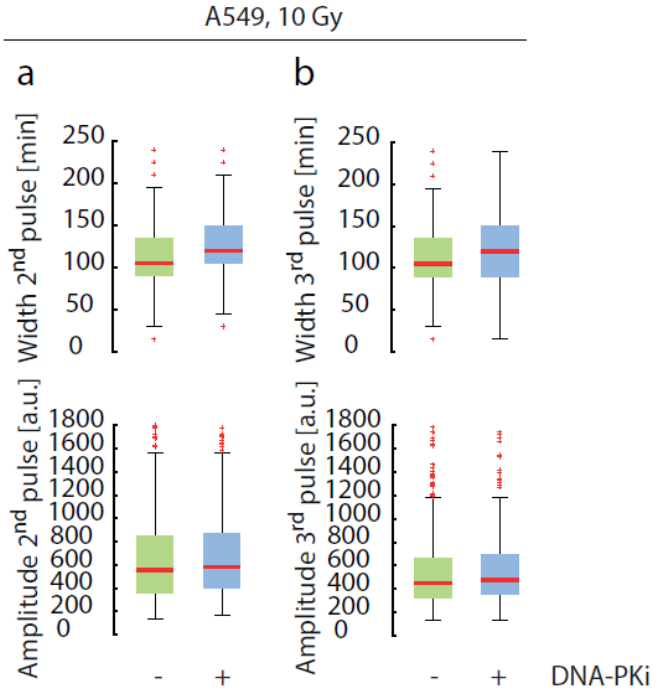

Figure 41. Consecutive pulses of p53 show regular features. Quantification of the relative amplitude and FWHM in A549 reporter cells untreated or treated with DNA-PKi upon 10 Gy ɣ-IR for (a) second pulse; (b) third pulse (n > 790 cells per condition). Red lines indicate medians of distributions; boxes include data between 25th and 75th percentiles; whiskers extend to maximum values within 1.5x the interquartile range; crosses represent outliers.

3.2.6 An increase in unrepaired DSBs is not responsible for changing p53 initial response

How does inhibition of a kinase involved in relaying the damage signal lead to an amplified p53 response? Since DNA-PKcs plays a critical role in cNHEJ and loss of its activity leads to a reduced repair rate (Loewer et al., 2013), it was initially hypothesized that the observed changes in p53 dynamics may occur due to an increase in the number of DSBs. Therefore p53 dynamics were measured in the presence or absence of DNA-PKi after damaging cells with different irradiation doses. In untreated cells, p53 accumulation was hardly changed, even when four times as many DSBs were induced (compare 2.5 Gy to 10 Gy). In contrast, when DNA-PKcs was inhibited, width and amplitude of p53 pulses increased in a dose dependent manner (Figure 42).

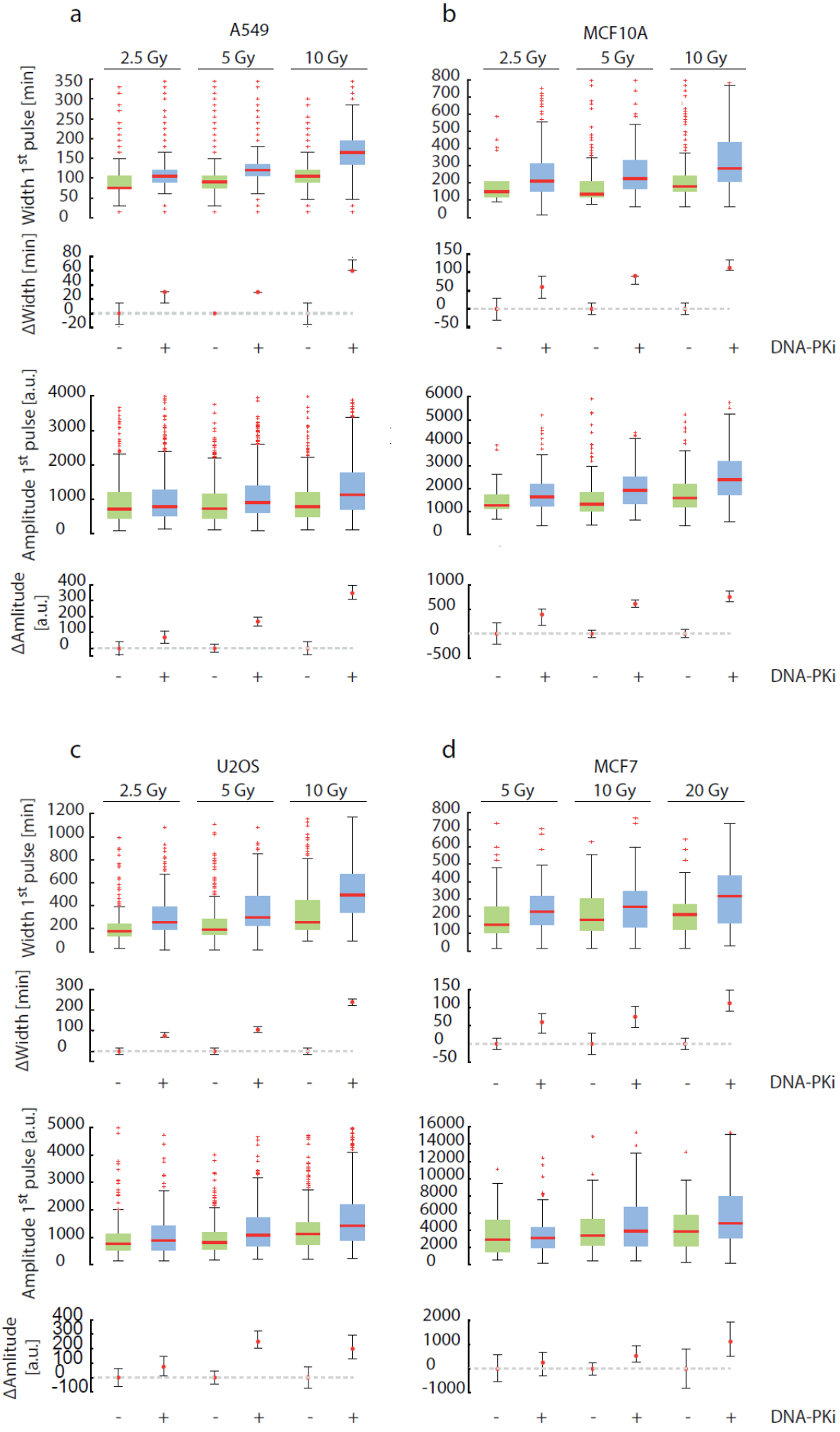
a
A549
2.5 Gy
5 Gy
10 Gy
Width 1st pulse [min]
ΔWidth [min]
Amplitude 1st pulse [a.u.]
ΔAmlitude [a.u.]
DNA-PKi
b
MCF10A
2.5 Gy
5 Gy
10 Gy
DNA-PKi
c
U2OS
2.5 Gy
5 Gy
10 Gy
Width 1st pulse [min]
ΔWidth [min]
Amplitude 1st pulse [a.u.]
ΔAmlitude [a.u.]
DNA-PKi
d
MCF7
5 Gy
10 Gy
20 Gy
DNA-PKi

Figure 42. p53 response is amplified upon DNA-PKcs inhibition in a dose dependent manner. (a-c) Quantification of the relative amplitude and FWHM and the corresponding statistical analysis of the first p53 pulse upon 2.5, 5 or 10 Gy in reporter cells untreated or treated with DNA-PKi for (a) A549 (n > 730 cells per condition); (b) MCF10A (n > 28 cells per condition); (c) U-2 OS (n > 250 cells per condition). (d) Quantification of the relative amplitude and FWHM of the first p53 pulse upon 5, 10 or 20 Gy in cells untreated or treated with DNA-PKi for MCF7 (n > 85 cells per condition). Red lines indicate medians of distributions; boxes include data between 25th and 75th percentiles; whiskers extend to maximum values within 1.5x the interquartile range; crosses represent outliers. Red dots indicate estimated changes of the median pulse width and amplitude; error bars represent 90% confidence intervals

To further investigate whether p53 dynamics were affected by altered DSBs repair, an inhibitor against another component of the cNHEJ pathway was used, ligase IV, which caused a decreased repair rate when applied to cells prior to genotoxic stress (Figure 43, (Srivastava et al., 2012)).

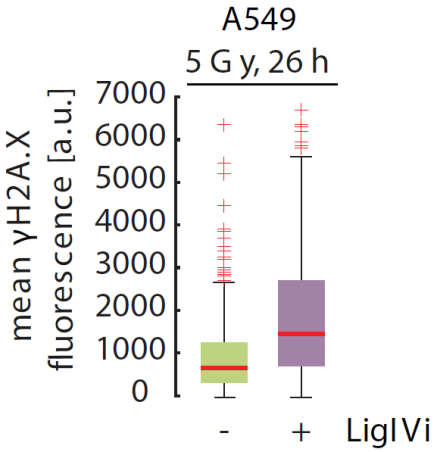

Figure 43. LigIVi inhibits DNA repair. Quantification at 26 hours of the ɣH2A.X average nuclear fluorescence intensity upon 5 Gy ɣ-IR in A549 cells untreated or treated with LigIV inhibitor (n > 340 cells per condition). Red lines indicate medians of distributions; boxes include data between 25th and 75th percentiles; whiskers extend to maximum values within 1.5x the interquartile range; crosses represent outliers.

However, cells treated with this inhibitor did not show changes in p53 dynamics (Figure 44), suggesting that an increase in unrepaired DSBs alone was not sufficient for amplifying the p53 response.

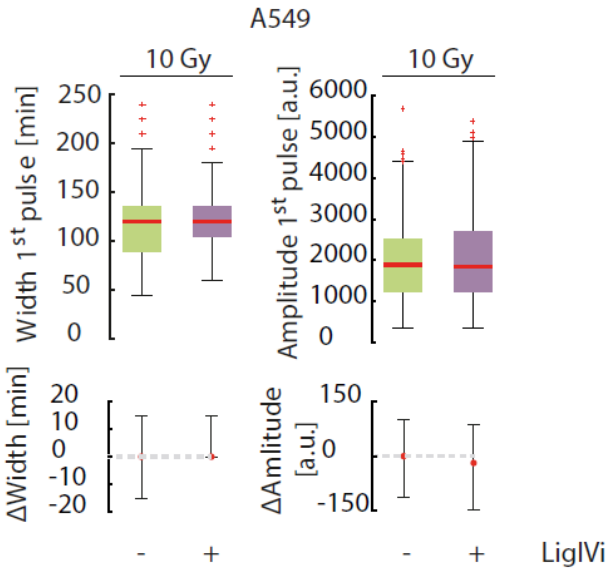

Figure 44. p53 response is not changed upon LigIV inhibition. Quantification of the relative amplitude and FWHM and the corresponding statistical analysis of the first p53 pulse in A549 reporter cells untreated or treated with LigIVi upon 10 Gy ɣ-IR (*n* > 170 cells per condition). Red lines indicate medians of distributions; boxes include data between 25th and 75th percentiles; whiskers extend to maximum values within 1.5x the interquartile range; crosses represent outliers. Red dots indicate estimated changes of the median pulse width and amplitude; error bars represent 90% confidence intervals.

3.2.7 Loss of DNA-PKcs activity modulates the p53 response through prolonged activation of ATM

As an alternative hypothesis, it was considered that inhibiting DNA-PKcs altered the interplay between the PI3K-like kinases. Therefore pair-wise inhibition of all three kinases was performed. When both DNA-PKcs and ATR were inhibited, longer and stronger accumulation of p53 compared to untreated cells was again observed, although slightly decreased compared to DNA-PKcs inhibition alone (Figure 45).

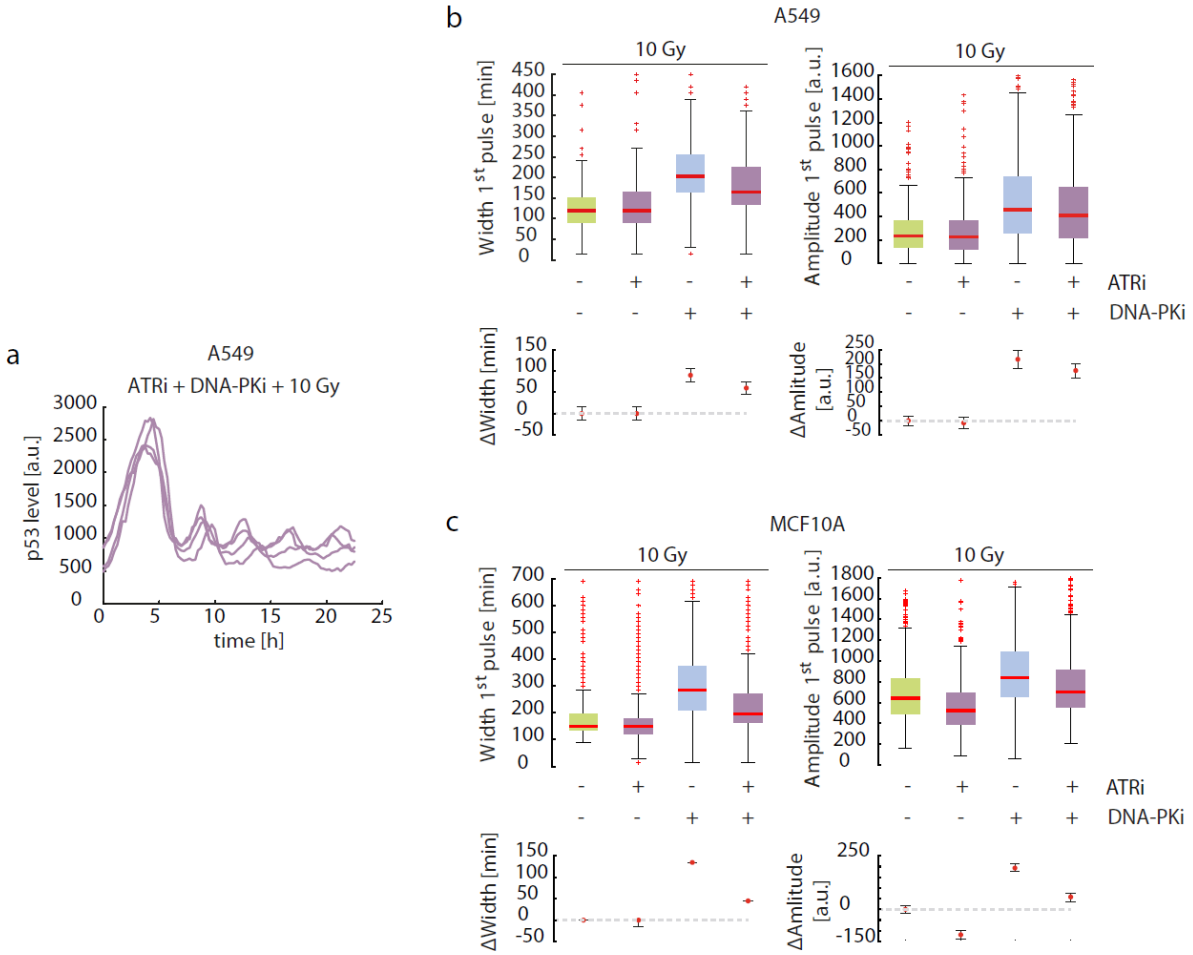

Figure 45. p53 response is still amplified upon inhibition of ATR and DNA-PKcs. (a) Individual A549 reporter cells were tracked and the average nuclear fluorescence was measured upon 10 Gy ɣ-IR in untreated cells or treated with DNA-PKi and ATRi. (b-c) Quantification of the relative amplitude and FWHM and the corresponding statistical analysis of the first p53 pulse upon 10 Gy ɣ-IR in reporter cells untreated or treated with DNA-PKi and ATRi alone or in combination for (b) A549 (n > 280 cells per condition); (c) MCF10A (n > 450 cells per condition). Red lines indicate medians of distributions; boxes include data between 25th and 75th percentiles; whiskers extend to maximum values within 1.5x the interquartile range; crosses represent outliers. Red dots indicate estimated changes of the median pulse width and amplitude; error bars represent 90% confidence intervals.

However, combining DNA-PKi and ATMi before damage induction surprisingly reverted the phenotype of DNA-PKcs inhibition: when the resulting p53 response in living cells was measured, pulse width was reduced from about 200 min for cells treated with DNA-PKi alone back to around 100 min as in controls (Figure 46). The amplitude was similarly reduced.

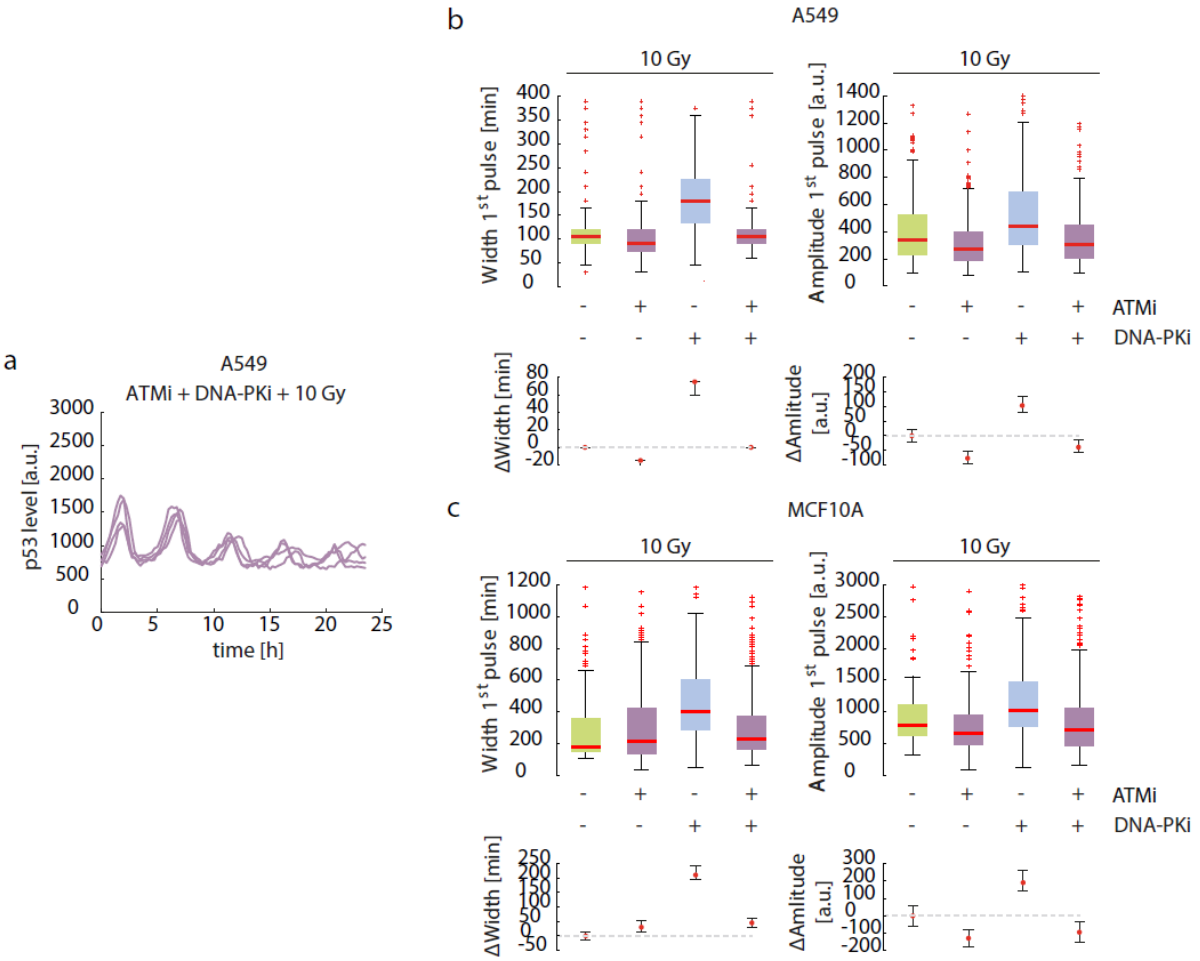

Figure 46. p53 width and amplitude are reduced back to control levels upon inhibition of ATM and DNA-PKcs. (a) Individual A549 reporter cells were tracked and the average nuclear fluorescence was measured upon 10 Gy ɣ-IR in untreated cells or treated with DNA-PKi and ATMi. (b-c) Quantification of the relative amplitude and FWHM and the corresponding statistical analysis of the first p53 pulse upon 10 Gy ɣ-IR in reporter cells untreated or treated with DNA-PKi and ATMi alone or in combination for (b) A549 (n > 260 cells per condition); (c) MCF10A (n > 110 cells per condition). Red lines indicate medians of distributions; boxes include data between 25th and 75th percentiles; whiskers extend to maximum values within 1.5x the interquartile range; crosses represent outliers. Red dots indicate estimated changes of the median pulse width and amplitude; error bars represent 90% confidence intervals.

Inhibiting both ATM and ATR also resulted in a reversion of the increased width and amplitude obtained upon DNA-PKcs inhibition alone, albeit dynamics were slightly more irregular (Figure 47).

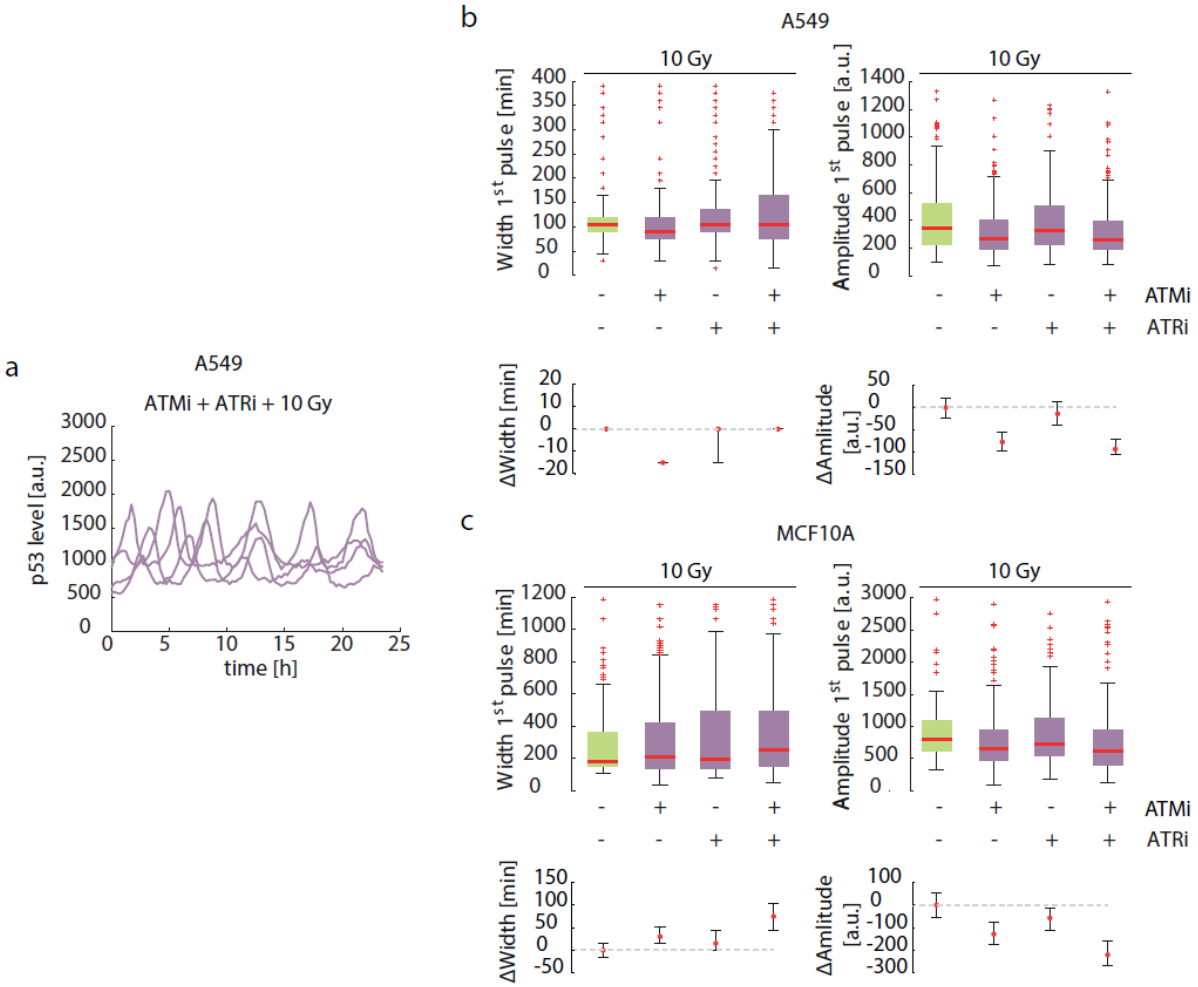

Figure 47. p53 width and amplitude are not amplified upon inhibition of ATM and ATR. (a) Individual A549 reporter cells were tracked and the average nuclear fluorescence was measured upon 10 Gy ɣ-IR in untreated cells or treated with ATRi and ATMi. (b-c) Quantification of the relative amplitude and FWHM and the corresponding statistical analysis of the first p53 pulse upon 10 Gy ɣ-IR in reporter cells untreated or treated with ATRi and ATMi alone or in combination for (b) A549 (n > 260 cells per condition); (c) MCF10A (n > 110 cells per condition). Red lines indicate medians of distributions; boxes include data between 25th and 75th percentiles; whiskers extend to maximum values within 1.5x the interquartile range; crosses represent outliers. Red dots indicate estimated changes of the median pulse width and amplitude; error bars represent 90% confidence intervals.

These results indicate that ATR and DNA-PKcs alone induced regular p53 dynamics and were able to compensate the loss of the other two kinases. In contrast, p53 reacted more strongly to DNA damage when ATM was active in the absence of a functional DNA-PKcs kinase, independently of ATR's state.

It was hypothesized that this amplified p53 response was caused by hyper-activation of ATM in the presence of DNA-PKi. To test this, ATM auto-phosphorylation at Ser1981 and Chk2 phosphorylation at Thr68 were measured as surrogates for ATM's activation state, and an

increase in their levels post damage in the presence of DNA-PKcs inhibitor was observed, which was reverted by ATMi treatment (Figure 48).

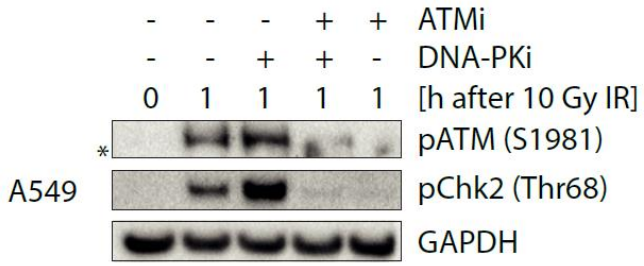

Figure 48. ATM is hyper-activated upon DNA-PKcs inhibition. Western blot analysis of ATM activity in A549 cells untreated or treated with DNA-PKi and ATMi alone, or a combination of both, followed by 10 Gy ɣ-IR. * indicates a nonspecific band.

Levels of phosphorylated Chk2 and p53 over time were then analyzed in the presence and absence of DNA-PKi, and a dramatic increase in the amount and duration of both modifications was observed (Figure 49). At the same time, protein levels of Mdm2, which is auto-degraded in an ATM-dependent manner (Stommel and Wahl, 2004), were severely decreased.

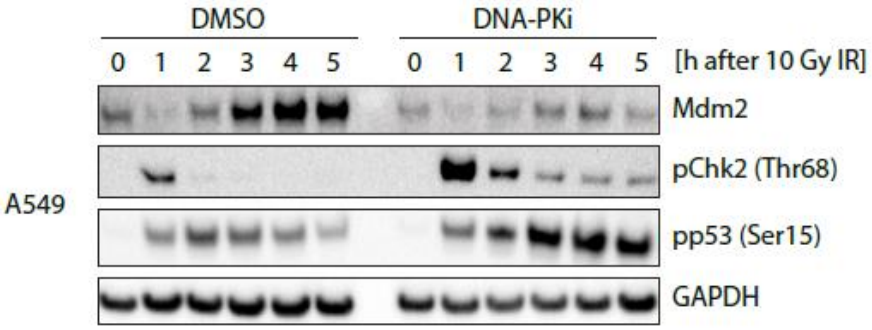

Figure 49. Mdm2, pChk2 and pp53 protein levels are altered upon DNA-PKi treatment. Western blot analysis of Mdm2, pChk2 (Thr68) and pp53 (Ser15) at the indicated time points upon 10 Gy ɣ-IR in cells untreated or treated with DNA-PKi for A549.

In order to verify that lower Mdm2 levels were due to post-translational regulation, its mRNA levels were measured. As expected, only minor differences during the first hours post damage were observed (Figure 50a). In addition, mRNA levels of Wip1, another negative regulator of p53, were measured, obtaining the same result as for Mdm2 (Figure 50b).

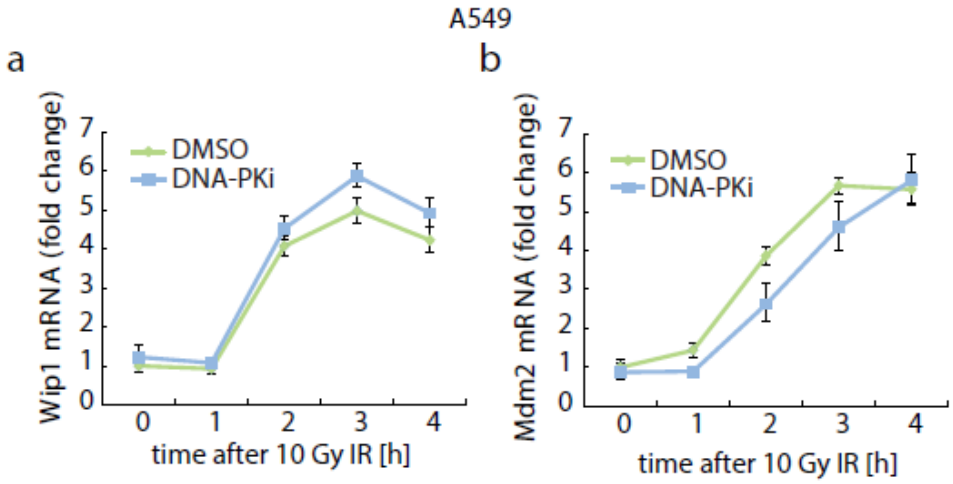

Figure 50. Transcription of p53 negative regulators is not greatly altered upon DNA-PKcs inhibition. mRNA expression of p53 negative feedback regulators (a) Mdm2 and (b) Wip1 was measured upon 10 Gy ɣ-IR in A549 cells untreated or treated with DNA-PKi. β-actin was used as an internal control. Error bars indicate standard deviation of technical triplicates.

As expected, pChk1 levels were not changed upon DNA-PKcs inhibition, further confirming no ATR involvement in ATM hyper-activation (Figure 51).

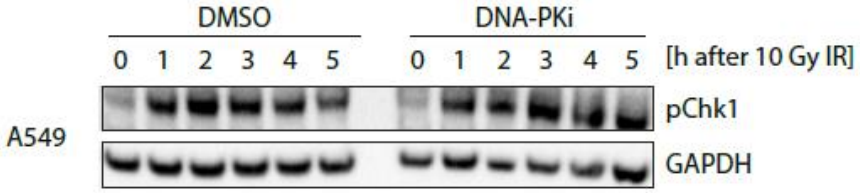

Figure 51. pChk1 protein levels are not altered upon DNA-PKi treatment. Western blot analysis of pChk1 (Ser317) at the indicated time points upon 10 Gy ɣ-IR in cells untreated or treated with DNA-PKi for A549.

To understand if ATM influences p53 dynamics through Mdm2, Chk2 or both, the p53 response in single cells upon simultaneous inhibition of Chk2 and DNA-PKcs was analyzed. As an amplified p53 response under this condition was still observed (Figure 52), it was concluded that increased Chk2 activity is a secondary effect and not involved in altering p53 dynamics.

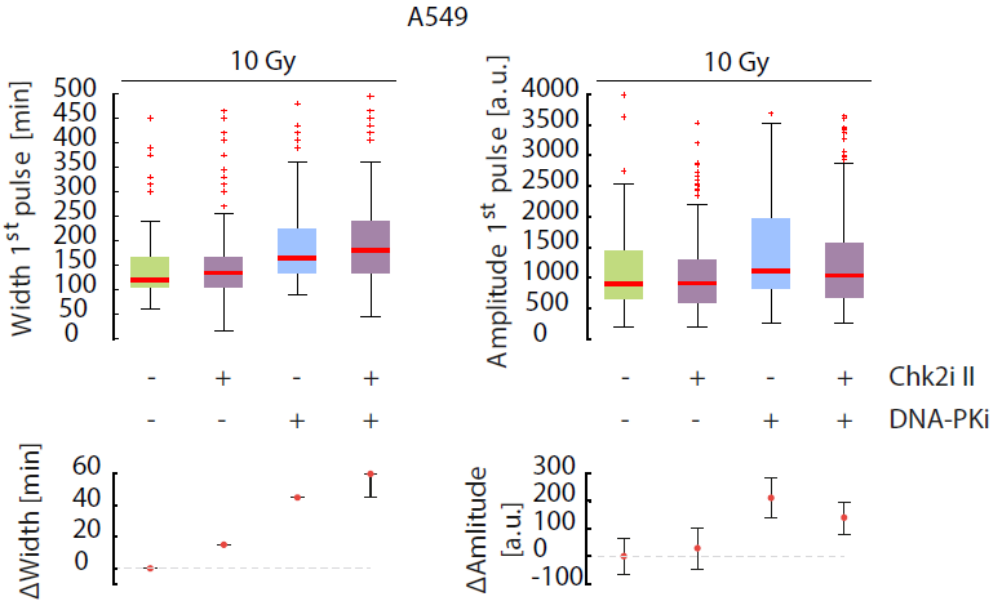

Figure 52. p53 response is still amplified upon Chk2 inhibition. Quantification of the relative amplitude and FWHM and the corresponding statistical analysis of the first p53 pulse upon 10 Gy ɣ-IR in A549 reporter cells untreated or treated with DNA-PKi and Chk2i II alone or in combination ($n > 150$ cells per condition). Red lines indicate medians of distributions; boxes include data between 25th and 75th percentiles; whiskers extend to maximum values within 1.5x the interquartile range; crosses represent outliers. Red dots indicate estimated changes of the median pulse width and amplitude; error bars represent 90% confidence intervals.

3.2.8 There may be a difference between absent DNA-PKcs and catalytically inactive DNA-PKcs

What is the molecular basis of the interplay between DNA-PKcs and ATM? Is there a direct interaction between DNA-PKcs and ATM, for example by a DNA-PKcs-mediated phosphorylation that would inhibit ATM activity? Or is hyper-activation of ATM induced indirectly by a failure of DNA-PKcs to perform its function at the break site? To distinguish between both possibilities, it was tested whether p53 dynamics were altered the same way in the absence of DNA-PKcs as after inhibition of the kinase.

DNA-PKcs was successfully knocked upon transfection of a pair of siRNAs, with a 70% reduction on DNA-PKcs mRNA levels (Figure 53).

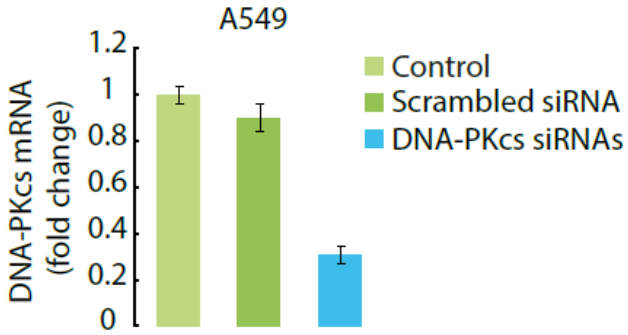

Figure 53. DNA-PKcs was successfully knocked down. Expression of DNA-PKcs mRNA was measured in A549 reporter cells untreated, transfected with scrambled siRNA or with siRNAs against DNA-PKcs. β-actin was used as an internal control. Error bars indicate standard deviation of technical triplicates.

Then, microscope experiments with the transfected cells were performed, and p53 dynamics were studied. Interestingly, in three independent experiments, cells with no DNA-PKcs started with much higher p53 basal levels than the control and scrambled cells, and showed much more often increasing p53 trajectories overtime after irradiation (Figure 54).

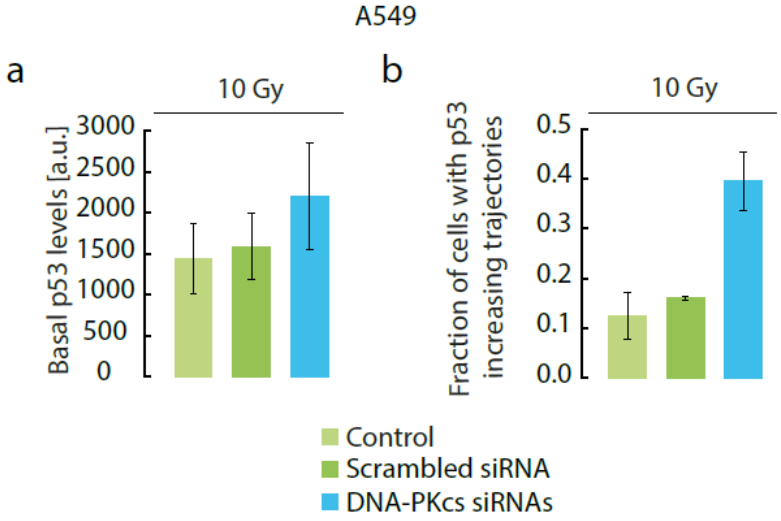

Figure 54. p53 shows altered behavior upon loss of DNA-PKcs. (a-b) A549 reporter cells were transfected with DNA-PKcs–specific or scrambled siRNA and the p53 response to 10 Gy ɣ-IR was measured by time-lapse microscopy. (a) Quantification of mean basal p53 levels before damage; (b) Proportion of A549 cells with monotonously increasing p53. Means of three independent experiments are presented; error bars indicate standard deviation of the mean. (Total number of cells > 260 for each condition)

Surprisingly, knocking down DNA-PKcs by siRNAs only led to an increase in the amplitude of p53 pulses, while the duration of the pulses remained unchanged (Figure 55).

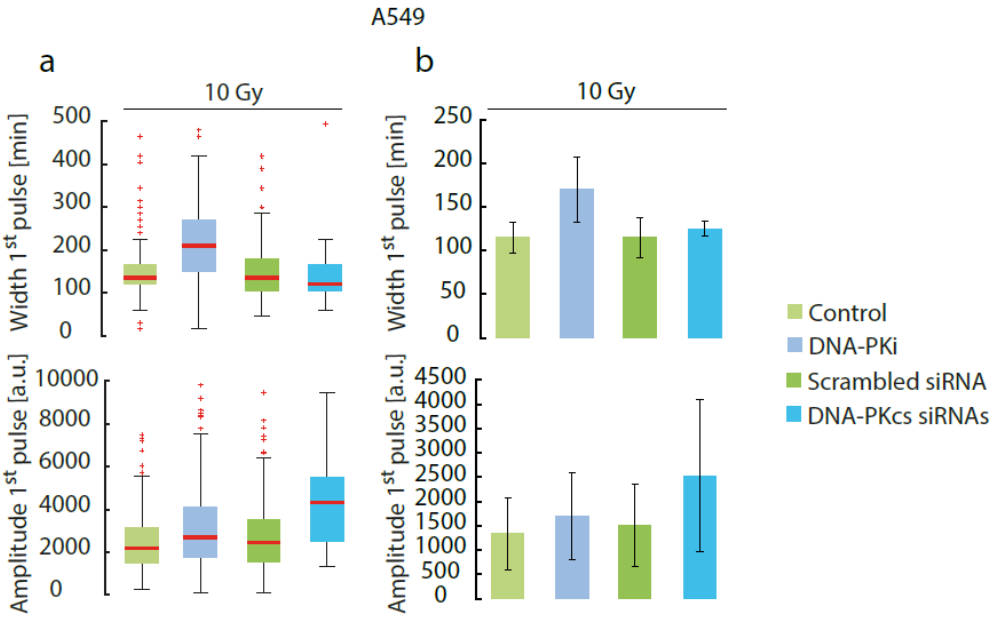

Figure 55. Amplitude of the first p53 pulse is increased upon DNA-PKcs knock down. (a-b) A549 reporter cells were transfected with DNA-PKcs-specific or scrambled siRNA and analyzed by time-lapse microscopy upon 10 Gy ɣ-IR. Relative amplitude and FWHM of the first p53 pulse were quantified. Untreated and DNA-PKi treated cells were included as controls. For this analysis cells showing monotonously increasing p53 levels were excluded. (a) (n > 80 cells per condition). Red lines indicate medians of distributions; boxes include data between 25th and 75th percentiles; whiskers extend to maximum values within 1.5x the interquartile range; crosses represent outliers; (b) Means of three independent experiments are presented; error bars indicate standard deviation of the mean. (Total number of cells > 260 for each condition)

Moreover, no increased activity of ATM upon DNA-PKcs siRNA treatment was observed (Figure 56).

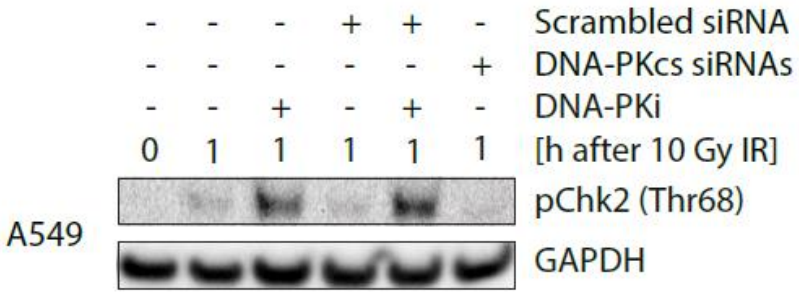

Figure 56. ATM is not hyper-activated upon DNA-PKcs knock down. Western blot analysis of pChk2 (Thr68) (surrogate for ATM activity) upon 10 Gy ɣ-IR in A549 cells untreated or treated with DNA-PKi, transfected with DNA-PKcs-specific or scrambled siRNA.

This indicates that there may be a difference between the presence of an inactive enzyme at the break site and the absence of the protein, suggesting an indirect interaction between ATM and DNA-PKcs.

3.2.9 MRE11A, RBBP8 and RAD50 are not involved in ATM hyper-activation

Assuming that the interaction between ATM and DNA-PKcs is indirect, there should be a third player that hyper-activates ATM. In order to elucidate the mechanism, several proteins involved in the homologous recombination pathway were knocked down using siRNA. Successful knock downs (more than 70%) were obtained for RAD50, RBBP8 and MRE11A (Figure 57).

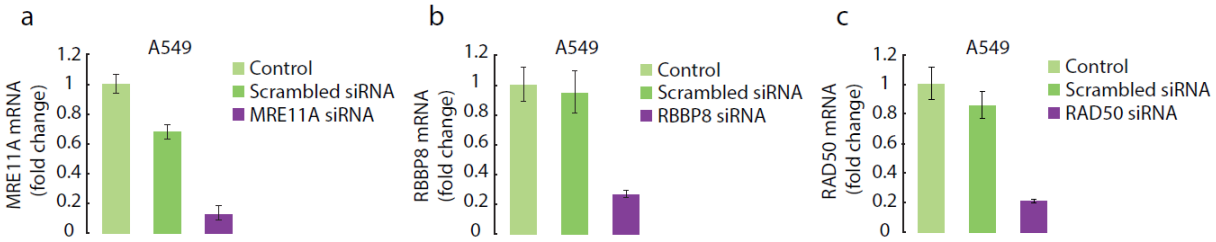

Figure 57. MRE11A, RBBP8 and RAD50 were knocked down successfully. (a-c) Expression of MRE11A, RBBP8 or RAD50 mRNA was measured in A549 cells untreated, transfected with scrambled siRNA or with siRNA against (a) MRE11A; (b) RBBP8; (c) RAD50. β-actin was used as an internal control. Error bars indicate standard deviation of technical triplicates.

When DNA-PKi was applied to the siRNA-treated cells, an ATM hyper-activation was still observed (Figure 58), meaning that MRE11A, RBBP8 and RAD50 were not the third player.

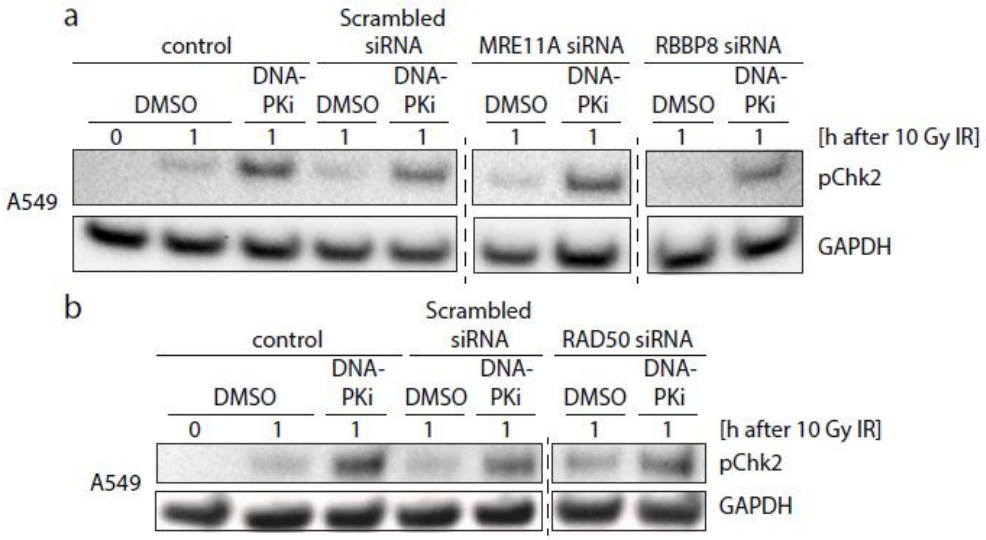

Figure 58. ATM is hyper-activated upon DNA-PKcs inhibition despite MRE11A, RBBP8 or RAD50 knock down. Western blot analysis of pChk2 (Thr68) (surrogate for ATM activity) upon 10 Gy γ-IR in cells untreated or treated with DNA-PKi, transfected with scrambled siRNA or with siRNA against (a) MRE11A or RBBP8; (b) RAD50.

There was no successful knock down obtained for NBN (a component of the MRN complex (van den Bosch et al., 2003)) with any of the transfection protocols tried. The highest efficiency was obtained twice, where NBN was knocked down to around 40-45%. In one of these experiments, an attenuation of pChk2 response upon DNA-PKcs inhibition was observed

(Figure 59). However, in the other experiment ATM hyper-activation was still present (data not shown). Further experiments are needed to get conclusive results.

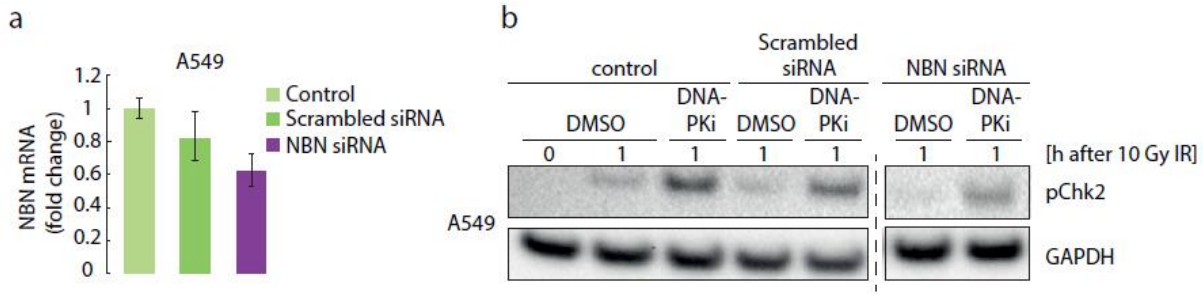

Figure 59. ATM activity may be attenuated upon DNA-PKcs inhibition when knocking down -not efficiently- NBN. A549 cells were transfected with scrambled siRNA or with siRNA against NBN. Untreated cells were included as control. (a) Expression of NBN mRNA was measured. β-actin was used as an internal control. Error bars indicate standard deviation of technical triplicates. (b) Western blot analysis of pChk2 (Thr68) (surrogate for ATM activity) upon 10 Gy ɣ-IR in cells untreated or treated with DNA-PKi.

3.2.10 Modulation of p53 dynamics leads to altered cell fate decision upon DSB induction

Previous studies have shown that changes in p53 dynamics led to altered expression of target genes and cell fate decisions (Borcherds et al., 2014; Purvis et al., 2012). To address whether altered p53 accumulation upon DNA-PKcs inhibition modulates how cells react to DSBs, the induction of the p53 target genes p21, involved in cell cycle arrest (El-Deiry et al., 1993), and YPEL3, involved in senescence (Kelley et al., 2010) was tested. A strongly increased expression of both target genes in the absence of DNA-PKcs activity one and two days after irradiation was observed (Figure 60).

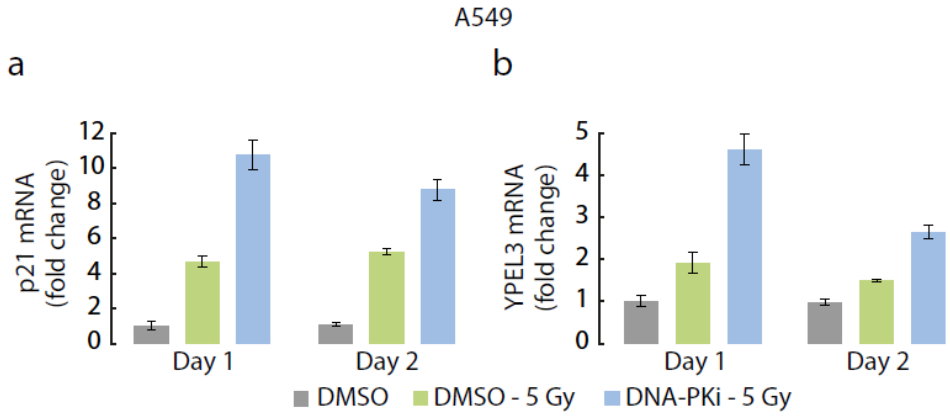

Figure 60. p53 anti-proliferative targets genes are strongly induced upon DNA-PKcs inhibition. mRNA expression of p53 target genes p21 and YPEL3 was measured at day 1 and day 2 in unirradiated A549 cells or upon 5 Gy ɣ-IR in cells untreated or treated with DNA-PKi. β-actin was used as an internal control. Error bars indicate standard deviation of technical triplicates.

Is this sufficient to change the fate of damaged cells? If it is sufficient, is the effect p53-dependent? For answering this last question, a $p53^{sh}$ cell line was created in A549 cells (Figure 61).

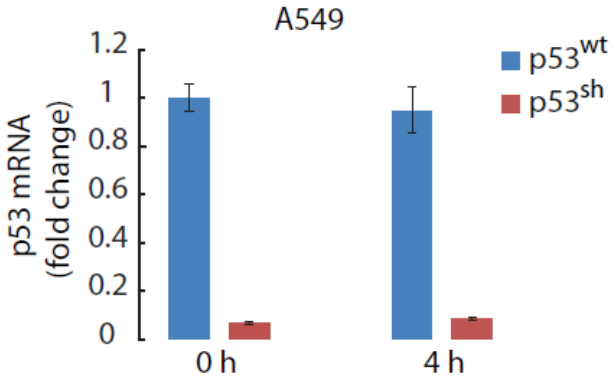

Figure 61. p53 was knocked down successfully. mRNA expression of p53 was measured upon 10 Gy ɣ-IR in A549 $p53^{wt}$ and $p53^{sh}$ d cells. β-actin was used as an internal control. Error bars indicate standard deviation of technical triplicates.

Control and DNA-PKi treated cells were followed for three days after irradiation. A dramatic decrease in the fraction of dividing $p53^{wt}$ cells treated with DNA-PKi was observed, while the majority of cells lacking the tumor suppressor due to siRNA-mediated knock down were able to grow even in the presence of the inhibitor (Figure 62), meaning that the decrease in cell proliferation was mostly driven by p53.

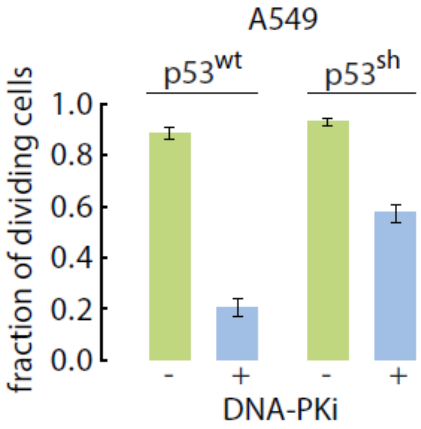

Figure 62. Proliferation upon DNA-PKi treatment is strongly inhibited in $p53^{wt}$ cells. Percentage of dividing A549 cells during 3 days post damage (5 Gy ɣ-IR) in wild-type or p53 knock down conditions both in the presence or absence of DNA-PKi. Error bars indicate standard error of sample proportion. (Initial number of cells > 125 per condition)

In addition, $p53^{wt}$ cells acquired a flattened morphology characteristic for senescence (Figure 63).

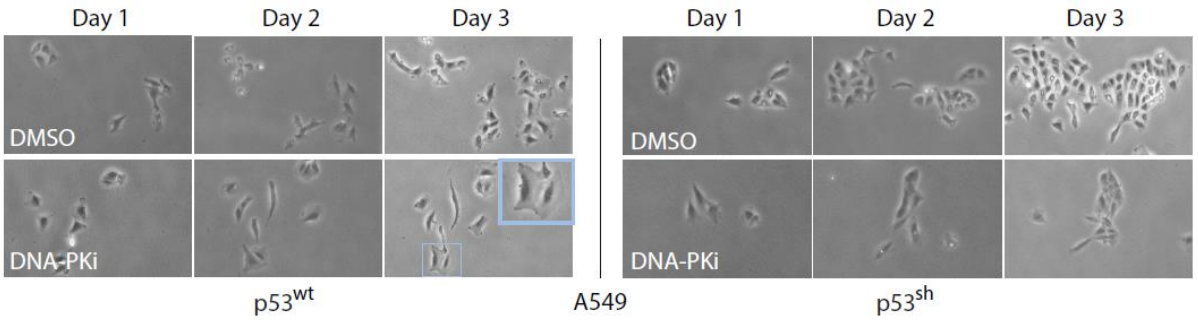

Figure 63. p53^{wt} cells show a senescence-like morphology upon DNA-PKcs inhibition. Representative images of single A549 cells during 3 days upon 5 Gy ɣ-IR in p53^{wt} or p53^{sh} cells untreated or treated with DNA-PKi. Blue boxes highlight the senescence-like phenotype observed in p53^{wt} cells treated with DNA-PKi.

4 DISCUSSION

4.1 p53 promotes energy production through mitochondrial respiration upon DNA damage

p53 is a tumor suppressor activated in the presence of cellular stress (Horn and Vousden, 2007; Vogelstein et al., 2000). Its most well-understood functions are regulating cell cycle arrest, senescence and apoptosis, but p53 has a much broader role, controlling many aspects of cellular homeostasis (Kruiswijk et al., 2015). Previous systematic analysis on p53 have been used to gain novel insights into its non-canonical functions, such as regulation of cell differentiation (Lee et al., 2010) or autophagy (Kenzelmann Broz et al., 2013). In order to further elucidate the role of p53 in regulating homeostasis, a combined systematic analysis of the transcriptome and proteome was performed in the presence or absence of p53, under basal conditions and upon genotoxic stress, in MCF10A, a non-tumorigenic cell line. The RNA-seq analysis revealed, as expected, that many (a 44%) of the most significant clusters obtained by gene enrichment analysis of the 15% of genes with the highest p53 dependency across time points were related to cell fate and DNA damage response. A 6% of the clusters indicated a role for p53 in controlling fatty acid metabolism. It was then decided to further study this interesting result by performing a proteomics experiment. The 15% of the genes and proteins with the highest p53 dependency were mapped to the corresponding metabolic pathways. Under basal conditions, p53 seemed to upregulate some pathways linked to energy production, but downregulate others. This apparent contradiction, together with the low number of proteins present in the data, made very difficult to generate a hypothesis. Metabolism upon irradiation showed a clearer behavior: p53 promoted a general increase in energy production through oxidative phosphorylation, especially by upregulating the expression of genes and proteins related to the fatty acid β-oxidation. To further confirm an increase in OXPHOS through upregulation of pathways such as β-oxidation, an analysis of the mitochondrial fatty acid catabolism could be carried out by using stable isotopically labeled fatty acids, e.g. palmitate (Roe and Roe, 1999; Tyni et al., 2002). This would allow studying the intermediates generated during β-oxidation by tandem mass spectrometry. It is conceivable that $p53^{wt}$ cells would show a higher amount of intermediates than $p53^{sh}$ cells.

4.1.1 A systematic study of the role of metabolism in the response to genotoxic stress

The maintenance of mitochondrial oxidative phosphorylation by p53 through different means (e.g. upregulation of fatty acid catabolism and OXPHOS) has been previously reported (Liang et al., 2013). This can oppose the Warburg effect observed in many cancer cells (Warburg, 1956), which consists of a dependence on glycolysis instead of OXPHOS for energy production. Therefore, metabolic control by p53 has been recently considered as another way of exerting its tumor suppressor function (Liang et al., 2013; Vousden and Prives, 2009).

Although the general functions of p53 in regulating the mentioned pathways were already known, this study has provided further insights into the non-canonical functions of p53 by presenting novel genes and proteins controlled by p53. In fact, for most of them a relation with p53 had never been established. Previous systematic studies showed p53-controlled genes or proteins, among which some were related to energy metabolism. However, no further analysis or functional descriptions were provided. Daoud et al. studied the impact of knocking out p53 in human colon carcinoma cells upon treatment with a specific topoisomerase I inhibitor by cDNA microarray hybridization (Daoud et al., 2003). A few of the p53 responsive genes reported in this study were involved in glucose, fatty acid or amino acid metabolism, but the authors did not comment on that. Sun el al. studied the effect of silencing p53 in nasopharyngeal carcinoma at the proteome level by LC-MS/MS (Sun et al., 2007). They categorized the differentially expressed proteins in groups, and one of them was metabolism. Inside this group, they mentioned cytochrome b5 and valosin containing protein, which are not related to energy metabolism.

The present study has documented for the first time how p53 controls metabolism upon DSB induction in a systematic way.

4.1.2 Future systematic approaches could be done in a breast cancer cell line

This study has given more insights into the non-canonical p53 functions in a non-tumorigenic breast cell line. As well as repair of occurring DNA lesions can prevent the transformation of a normal cell into a cancerous one (Torgovnick and Schumacher, 2015), a change in the metabolism upon dangerous DNA breaks can help preventing tumorigenesis. It would be therefore very interesting to perform a similar systematic analysis in breast cancer cells upon genotoxic stress. It may be that oncogenic signals and induction of DNA damage together could lead to a change in the set of target genes activated and to a shift between “p53 protector” and “p53 killer”.

4.2 Kallikreins are upregulated upon genotoxic stress in a p53-dependent manner

Kallikreins are a family of 15 secreted serine proteases with either trypsin-like and/or chymotrypsin-like specificity (Kalinska et al., 2016). Over the past decade, great advances on KLK research have been made (Prassas et al., 2015). Kallikreins are now known to be involved in diverse mechanistic pathways regulating for example skin desquamation, tooth enamel formation or brain function (Emami and Diamandis, 2007; Lundwall and Brattsand, 2008; Pampalakis and Sotiropoulou, 2007). KLK activity is tightly regulated by different tissue-specific mechanisms and factors, such as endogenous kallikrein inhibitors or micro-environmental pH (Goettig et al., 2010). A disruption in the fine-tuned regulation of KLK activity has been linked to several pathologies, including cancer. In fact, several kallikreins are used are biomarkers in different tumors (Paliouras et al., 2007). For example, KLK3, which encodes prostate-specific antigen (PSA), is extensively used as a biomarker for screening and monitoring treatment of prostate cancer due to its increased serum levels during tumorigenesis (Kote-Jarai et al., 2011). Strikingly, although dysregulated kallikrein expression is clearly associated with cancer (Borgoño et al., 2004), it has not been possible to classify kallikreins as tumor suppressors or promoters, as their function seems to depend on several factors like the tumor model studied (Lawrence et al., 2010).

KLK10, KLK5, KLK7 and KLK8 expression is downregulated in breast cancer (Avgeris et al., 2011; Dhar et al., 2001; Feng et al., 2010; Li et al., 2009; Liu et al., 1996; Yousef et al., 2004). This could indicate that in breast they exhibit tumor suppressive functions. In fact, KLK10 is considered a putative tumor suppressor in breast cells (Goyal et al., 1998). The means by which kallikreins are involved in breast cancer are not always known. For example, both the substrates and physiological functions of KLK10 remain unclear (Hu et al., 2015); in the case of KLK5, its breast cancer suppressing effects are explained by the inhibition of epithelial to mesenchymal transition markers and of the mevalonate pathway (Pampalakis et al., 2014), which is upregulated in several cancers (Zahra Bathaie et al., 2016).

The RNA-seq data highlighted an unknown function of p53 in promoting the expression of different kallikreins upon DSBs induction. It can be hypothesized that their transcription is not directly controlled by p53, but by a downstream transcription factor that is accumulating in a p53-dependent manner at late time points, as kallikrein induction in the presence of p53 is not happening at 4, but at 24 hours after irradiation. ChIP analysis would allow to study if p53 is directly binding to kallikrein promoters.

The upregulation of these kallikreins by p53 provides more evidence for a tumor suppressive function in breast tissue and may represent a novel way for p53 to fight tumorigenesis, although further studies are needed in order to address the mechanistic roles of kallikreins in breast cancer.

4.3 Hyper-activation of ATM upon DNA-PKcs inhibition modulates p53 dynamics and cell fate in response to DNA damage

Ionizing radiation, such as ɣ-irradiation, is a major inducer of DSBs, one of the most dangerous DNA lesions. Defense mechanisms such as cell cycle arrest, apoptosis and DNA repair have evolved in order to maintain genomic stability (Gasser and Raulet, 2006). Three PI3K-like kinases, ATM, ATR and DNA-PKcs, play a critical role in coordinating damage repair by distinct molecular pathways (Chiruvella et al., 2013; Cimprich and Cortez, 2008; Harper and Elledge, 2007). Besides repairing the DNA, cells also need to adjust their physiology to the presence of genotoxic stress. A central step in this process is the activation by ATM, ATR and DNA-PKcs of p53 (Kruse and Gu, 2009), the major tumor suppressor in mammalian cells (Lees-Miller *et al.*, 1990). Do the three kinases act as redundant systems to provide a fail-save relay of the damage input to the p53 system or does each of them perform a distinct function? In order to answer this question, measurement of p53 dynamics in single cells upon pharmacological perturbations was performed in different fluorescent cell lines using live-cell time-lapse microscopy.

4.3.1 ATM activity is compensated by the remaining kinases

In the reporter cell lines used, loss of ATM function was compensated by the remaining kinases. While ATM has been described as the main kinase inducing p53 accumulation upon DSB induction (Ciccia and Elledge, 2010), the observation is consistent with previous reports showing p53 activation either by ATR (Tomimatsu et al., 2009) or DNA-PKcs (Boehme et al., 2008; Callén et al., 2009; Li and Stern, 2005) in ATM-deficient cells.

4.3.2 ATR inhibition has minor effects on p53 dynamics

The structure responsible for ATR activation is single-stranded DNA (Cimprich and Cortez, 2008), originating for example from replication stress or ultraviolet irradiation. During homologous recombination of DSBs, ATR is activated at later time points in an ATM-dependent manner, as end resection reveals a large single-stranded region (Cimprich and Cortez, 2008). The observed compensation of ATR's activity is consistent with the fact that it is not the main kinase responding to DSBs.

4.3.3 DNA-PKcs inhibition amplifies the p53 response

DNA-PKcs activation is restricted to breaks repaired by a single arm of the repair process, cNHEJ (Chiruvella et al., 2013). It was therefore unexpected to observe severe alterations of the p53 response when inhibiting the third PI3K-like kinase. Intuitively, one may hypothesize that inhibiting DNA-PKcs attenuates the p53 response. However, previous studies such as (Callén et al., 2009; Shaheen et al., 2011; Zhu and Gooderham, 2006) did not report any decrease in p53 accumulation. In line with these reports, in this study there was no reduction detected; more strikingly, p53 showed an amplification of its response: a higher amplitude and a longer duration in the first pulse of p53 accumulation across different cell lines and with two different DNA-PKcs inhibitors was observed. Why has this not been reported before? This amplification, although most clearly observed in single-cell analysis with high temporal resolution (due to cell-to-cell variability and noise), can also be detected in population measurements such as western blots, but only when probed at appropriate time points. This may explain why the increase in p53 levels has not been noticed in the previous studies: in Zhu and Gooderham, p53 levels upon DNA-PKcs inhibition were studied twenty-four hours after damaging cells with cryptolepine. At this time point, effect of DNA-PKcs inhibition is not present anymore, as p53 amplification occurred during the first pulse, while the consecutive ones went back to control levels. Regarding Shaheen et al., they damaged cells with doxorubicin and study total p53 six hours later, which may be a too late time point to observe differences on the first p53 pulse. In the same study, they also irradiated cells with 10 Gy and checked p53 levels one hour later, which may be too early.

The present study further confirmed the importance of measurements with high temporal resolution in single cells.

4.3.4 Loss of DNA-PKcs activity, but not loss of DNA-PKcs protein, amplifies p53 response through ATM hyper-activation

How does inhibition of DNA-PKcs lead to an amplified p53 response? DNA-PKcs inhibition reduces the repair rate (Loewer et al., 2013), so the first hypothesis tested was that an increase in unrepaired DSBs could be responsible for the change in p53 dynamics. However, inhibiting another component of the cNHEJ did not contribute to increasing the duration and amplitude of p53 pulses. The second hypothesis considered was that DNA-PKcs inhibition could affect the interplay between ATM, ATR and DNA-PKcs. In fact, in the present study it was shown for the first time that DNA-PKcs inhibition promoted a dose-dependent hyper-activation of ATM upon DSBs induction, which promoted Mdm2 degradation and an increased

accumulation of p53. Altered p53 dynamics clearly depended on this hyper-activation, as concomitant inhibition of ATM reverted the observed phenotype. In order to determine if this new interplay between the two PI3K-like kinases was direct or indirect, DNA-PKcs was knocked down. Cells were clearly stressed under this condition, as an increase in both basal p53 levels and fraction of cells showing monotonous accumulation of p53 instead of regular pulses was observed. This could be due to the fact that before performing the experiment, cells had for several days decreased levels of DNA-PKcs protein and may have accumulate substantial unrepaired damage. Does DNA-PKcs directly interact with ATM to inhibit its activity? While this hypothesis cannot be excluded, the observation that downregulation of DNA-PKcs by siRNA did not lead to hyper-activation of ATM provided strong evidence against it. It seemed as if DNA-PKcs needs to be located at break sites in an inactive form to modulate ATM activity. It was previously shown that catalytically inactive DNA-PKcs prevents end-joining and resolution of associated DSBs by both cNHEJ and HR, as autophosphorylation of the kinase is required for opening access for ligases to the DNA ends (Allen et al., 2003; Jiang et al., 2015). It is conceivable that "immature" breaks blocked by inactive DNA-PKcs would provide a platform for continuous activation of ATM.

Such hyper-activation of ATM by unresolved break sites could serve as an important fail-safe mechanism in the DDR. While most DSBs are rapidly repaired by cNHEJ, there are some insults such as complex break sites consisting of multiple DSBs in close vicinity that cannot be repaired by simple ligation of free DNA ends. It has been previously proposed that during class switch recombination or repair of irradiation-induced DSBs in lymphocytes, if a lesion takes too long to be repaired by cNHEJ, ATM could promote dissociation of DNA-PKcs from the break (Callén et al., 2009). Something similar could occur in this case. Although there are no conclusive studies yet, it is conceivable that even if the pathway chosen for repairing the damage is cNHEJ, the MRN complex could be recruited to the DNA near the Ku- and DNA-PKcs-bound break. It could be also assumed that either the MRN complex – activator of ATM (Lee and Paull, 2005) – or other factors related to MRN could "oversignal" to ATM and hyper-activate it if the damage persists too long without being repaired. ATM could in turn promote autophosphorylation of DNA-PKcs by phosphorylating it at specific sites, and repair could continue through HR. At the same time, ATM hyper-activation would ensure that the presence of the severe damage is transmitted to response pathways such as p53 (Figure 64). Although the results of this study were not conclusive, NBN, one component of the MRN complex, could play a role in ATM hyper-activation. In order to further address this hypothesis, a NBN knock

out cell line could be created, and assess if ATM amplified response still occurs upon DNA-PKcs inhibition.

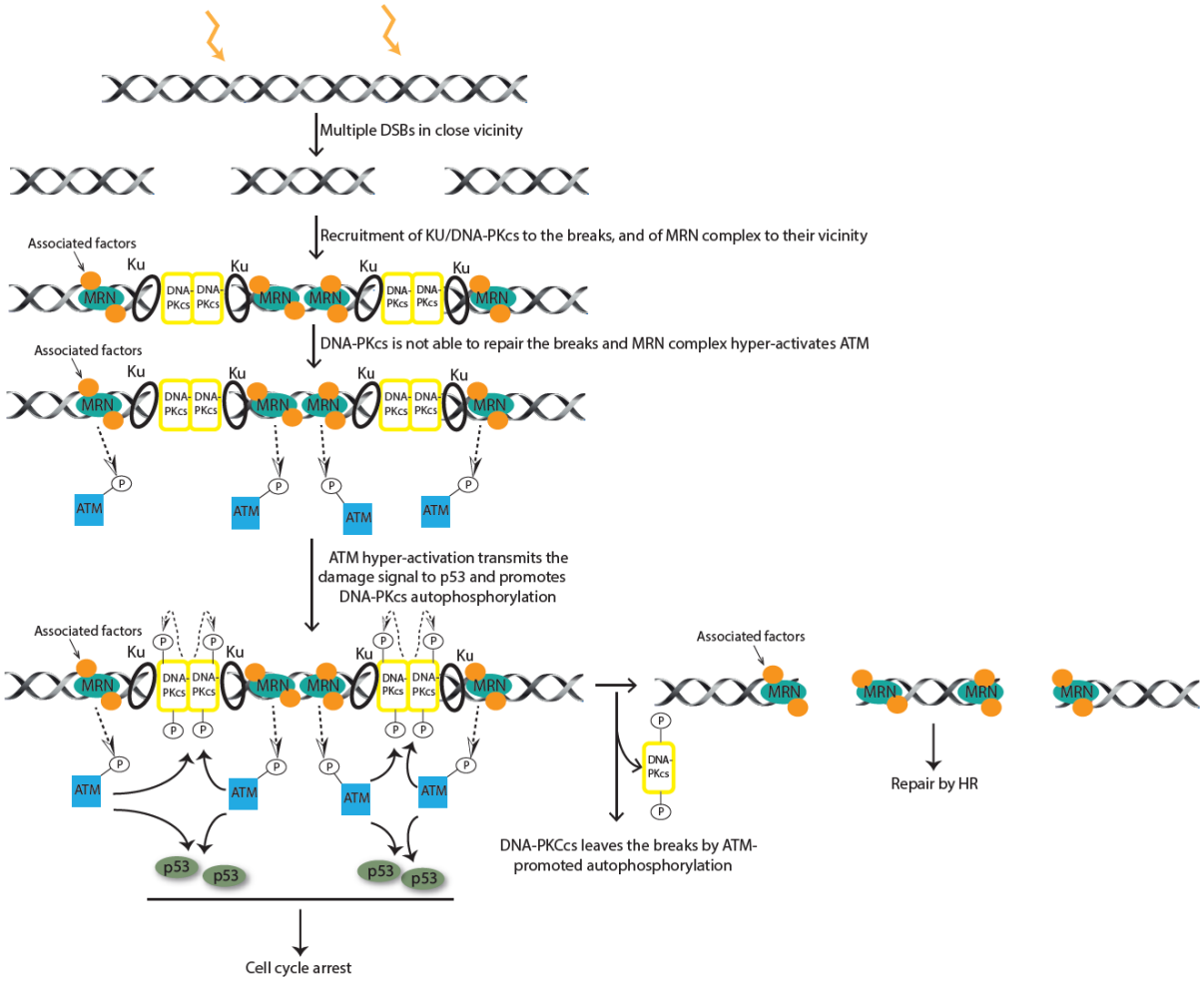

Figure 64. Model proposed for repair of complex break sites. P stands for phosphorylation.

4.3.5 The amplified p53 response in cells treated with DNA-PKi leads to increased cell senescence upon DSB induction

Previous studies have shown that changes in p53 dynamics by genetic or pharmacological perturbations lead to altered expression of target genes and cell fate decisions (Borcherds et al., 2014; Purvis et al., 2012). In Purvis et al., pulsatile behavior of p53 was transformed into a sustained response by adding a small molecule inhibitor, and cells underwent senescence with a higher frequency upon genotoxic stress. Similarly, in this study cells co-treated with DNA-PKi and ɣ-IR showed an amplified p53 response and a corresponding p53-dependent increase in senescence. No apoptosis was observed in the cell lines used, consistent with the results from Purvis et al. What is the molecular mechanism that decodes p53 dynamics in order to decide the cell fate? Purvis et al. proposed that p53 pulses periodically exceed a certain threshold concentration for transcriptional activation of genes involved in senescence. This would mean

that a persistent p53 response would have a higher probability to induce expression of such target genes. This hypothesis cannot apply to the results presented here, as the amplified p53 response occurs only once, in the first pulse.

In this study, where the amplification of only the first p53 pulse was enough for cells to promote senescence, the hypothesis that could be provided is the existence of a low affinity and highly stable p53 target gene involved in senescence. In control cells, mRNA levels of a p53 target gene involved in senescence would increase slowly when p53 reaches its peak level, then decrease or stay constant during the trough of the oscillations (Figure 65), meaning that the transcript will only slowly reach levels high enough to induce senescence (threshold level). In DNA-PKi treated cells, the first amplified p53 pulse would promote a much larger transcript accumulation, as p53 levels are sufficiently high to activate its low affinity promoter for a longer time period. Although p53 dynamics normalize during the later response, mRNA expression of the senescence-related gene would reach its threshold levels much earlier compared to control cells.

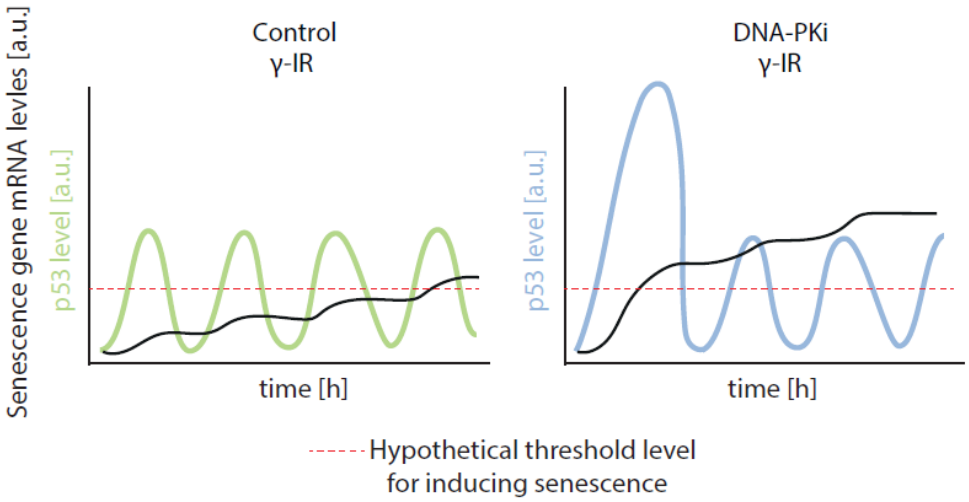

Figure 65. Model proposed for induction of senescence.

4.4 Conclusions

p53 exerts its antitumorigenic functions through different ways, including metabolic control. p53 inhibits glycolysis and promotes mitochondrial respiration in order to counteract the Warburg effect, characteristic of many cancer cells. The present study has documented a broader role than previously described for p53 in controlling energy metabolism upon genotoxic stress, especially fatty acid catabolism. The genes and proteins described here probably contribute to curbing the Warburg effect upon DNA damage induction, and thus could be further studied as potential metabolic targets in cancer therapy.

The induction of terminal cell fates such as senescence is another way for p53 to prevent tumor development. In this study, inhibition of the upstream kinase DNA-PKcs sensitized cells for radiation by hyper-activating ATM that caused an altered p53 response and promoted senescence. Although DNA-PKcs based sensitization to DNA damage is well established, it has been mainly attributed to its function in cNHEJ. Only few studies reported that in some instance the radio-sensitizing effect to DNA-PKcs inhibition depends on the genotype, for example the p53 status (Shaheen et al., 2011). The results presented here have implications for the use of DNA-PKcs inhibitors in cancer therapies. While tumors that retained a wild-type copy of p53 may respond well to a combination of radiotherapy and DNA-PKi, cells with mutated p53 may be less affected. On the contrary, neighboring healthy cells with intact p53 may be more severely affected in this scenario, increasing the side effects of tumor therapy. It will therefore be important to characterize the individual state of a given tumor to devise an efficient strategy to specifically kill transformed cells while ensuring survival of neighboring tissues.

5 SUMMARY – ZUSAMMENFASSUNG

5.1 Summary

p53 has been called “the guardian of the genome” or “cellular gatekeeper” because of its prominent role in responding to a wide range of cellular stress signals. It is a key tumor suppressor in mammalian cells and one of the most studied human genes, as loss of p53 function is a common feature in the majority of cancers. Upon genotoxic stress, p53 accumulates in the nucleus and acts as a transcription factor activating the expression of genes involved in cell cycle arrest, apoptosis and senescence in order to maintain genome integrity. Three kinases belonging to the PI3K-like kinase family, ATM, ATR and DNA-PKcs, are responsible for p53 phosphorylation and stabilization. However, it is at present unclear how these kinases act in concert to regulate p53. Using specific inhibitors and quantitative analysis at the single cell level, the contribution of each kinase for regulating p53 activity upon genotoxic stress was characterized. ATM and ATR loss was compensated by the remaining kinases, while DNA-PKcs inhibition led to an amplification in the p53 response. DNA-PKcs loss caused ATM hyper-activation, which was responsible for the increased p53 accumulation that sensitized cells for damage-induced senescence.

Although the role of p53 as a tumor suppressor has been mainly attributed to its ability to induce terminal cell fates, such as senescence, in recent years p53 has emerged as a regulator of several aspects of cellular homeostasis including cell metabolism. Many cancer cells primarily use glycolysis for energy production instead of oxidative phosphorylation (Warburg effect). Interestingly, p53 has been reported to inhibit glycolysis and promote mitochondrial respiration through different mechanisms, facts that can help cells to curb the acquisition of the Warburg effect. However, the way p53 exerts its homeostatic functions is not completely known. In this thesis, a combination of genome- and proteome-wide approaches were used to systematically investigate how p53 controls metabolism upon double strand breaks induction. Several novel genes and proteins controlled by p53 and involved in pathways related to oxidative phosphorylation were discovered, especially from fatty acid β-oxidation. Moreover, in this study p53 was described for the first time as a positive regulator of kallikreins, serine proteases whose dysregulation is clearly associated with cancer.

5.2 Zusammenfassung

p53 wurde wegen seiner wichtigen Rolle, auf eine Vielzahl von zellulären Stress-Signalen zu reagieren, „der Wächter des Genoms" oder „zellulärer Pförtner" genannt. p53 ist ein Haupttumorsuppressor in Säugerzellen und eines der am meisten untersuchten menschlichen Gene, da der Verlust der p53-Funktion ein gemeinsames Merkmal bei den meisten Krebsarten ist. In der zellulären Signalantwort auf genotoxischen Stress akkumuliert p53 im Zellkern und reguliert die Expression von Zielgenen, die an Zellzyklusarrest, Apoptose und Senesenz beteiligt sind, um die Integrität des Genoms aufrechtzuerhalten. Drei Kinasen, die zur Familie der PI3K-like-Kinasen gehören (ATM, ATR und DNA-PKcs), sind verantwortlich für die Phosphorylierung und dadurch bedingte Stabilisierung von p53. Allerdings ist es derzeit unklar, wie diese Kinasen gemeinsam agieren, um p53 zu regulieren. Unter Verwendung spezifischer Inhibitoren und quantitativer Analyse auf Einzelzellebene wurde der Effekt jeder einzelnen Kinase zur Regulierung der p53-Aktivität in der Signalantwort nach genotoxischem Stress charakterisiert. Der Verlust von ATM und ATR wurde durch die verbleibenden Kinasen kompensiert, während DNA-PKcs-Hemmung zu einer Verstärkung in der p53-Antwort geführt hat. Der Verlust von DNA-PKcs verursacht eine Hyperaktivierung von ATM, die für die erhöhte p53 Akkumulation verantwortlich ist und Zellen für schadensinduzierte Seneszenz sensibilisiert.

Obwohl die Rolle von p53 als Tumorsuppressor hauptsächlich seiner Fähigkeit zur Induktion von terminalen Zellschicksalsentscheidungen zugeschrieben wird (wie Seneszenz), hat sich in den letzten Jahren p53 als Regulator in mehreren Aspekten der zellulären Homöostase einschließlich des Zellstoffwechsels herausgestellt. Viele Krebszellen verwenden statt der oxidativen Phosphorylierung (Warburg-Effekt) in erster Linie Glykolyse zur Energieerzeugung. Interessanterweise wurde berichtet, p53 würde Glykolyse hemmen und die mitochondriale Atmung durch verschiedene Mechanismen fördern. Diese Faktoren können den Warburg-Effekt auf zellulärer Ebene eindämmen. Jedoch ist die Art und Weise, wie p53 seine homöostatische Funktionen ausübt, nicht vollständig bekannt. In dieser Arbeit wurde durch eine Kombination von genom- und proteomweiten Messungen systematisch untersucht, wie p53 nach Induktion von DNA-Doppelstrangbrüchen den intrazellulären Stoffwechsel reguliert. Mehrere neue Gene und Proteine, die von p53 kontrolliert werden, wurden entdeckt. Diese stehen im Zusammenhang mit Signalkaskaden, die an der oxidativen Phosphorylierung beteiligt sind, insbesondere an der β-Oxidation von Fettsäure. Außerdem wurde p53 in dieser Arbeit

zum ersten Mal als positiver Regulator von Kallikreins beschrieben, das sind Serinproteasen, deren Dysregulation eindeutig mit Krebs assoziiert ist.

6 BIBLIOGRAPHY

Allen, C., Halbrook, J., Nickoloff, J.A., 2003. Interactive competition between homologous recombination and non-homologous end joining. Mol Cancer Res 1, 913–920.

Ashburner, M., Ball, C.A., Blake, J.A., Botstein, D., Butler, H., Cherry, J.M., Davis, A.P., Dolinski, K., Dwight, S.S., Eppig, J.T., Harris, M.A., Hill, D.P., et al., 2011. The Gene Ontology Consortium. Gene ontology: tool for the unification of biology. Nat. Genet. 25, 25–29. doi:10.1038/75556

Assaily, W., Rubinger, D.A., Wheaton, K., Lin, Y., Ma, W., Xuan, W., Brown-Endres, L., Tsuchihara, K., Mak, T.W., Benchimol, S., 2011. ROS-mediated p53 induction of Lpin1 regulates fatty acid oxidation in response to nutritional stress. Mol. Cell 44, 491–501. doi:10.1016/j.molcel.2011.08.038

Avgeris, M., Papachristopoulou, G., Polychronis, A., Scorilas, A., 2011. Down-regulation of kallikrein-related peptidase 5 (KLK5) expression in breast cancer patients: a biomarker for the differential diagnosis of breast lesions. Clin. Proteomics 8. doi:10.1186/1559-0275-8-5

Baker, S., Fearon, E., Nigro, J., Hamilton, S., Preisinger, A., Jessup, J., VanTuinen, P., Ledbetter, D., Barker, D., Nakamura, Y., White, R., Vogelstein, B., 1989. Chromosome 17 deletions and p53 gene mutations in colorectal carcinomas. Science 244, 217–221.

Batchelor, E., Mock, C.S., Bhan, I., Loewer, A., Lahav, G., 2008. Recurrent Initiation: A Mechanism for Triggering p53 Pulses in Response to DNA Damage. Mol. Cell 30, 277–289. doi:10.1016/j.molcel.2008.03.016

Baumann, P., Benson, F.E., West, S.C., 1996. Human Rad51 protein promotes ATP-dependent homologous pairing and strand transfer reactions in vitro. Cell 87, 757–766. doi:10.1016/S0092-8674(00)81394-X

Behar, M., Hoffmann, A., 2010. Understanding the Temporal Codes of Intra-cellular Signals. Curr Opin Genet Dev 20, 684–693. doi:10.1016/j.gde.2010.09.007.Understanding

Bensaad, K., Tsuruta, A., Selak, M.A., Vidal, M.N.C., Nakano, K., Bartrons, R., Gottlieb, E., Vousden, K.H., 2006. TIGAR, a p53-Inducible Regulator of Glycolysis and Apoptosis. Cell 126, 107–120. doi:10.1016/j.cell.2006.05.036

Bentley, D.R., Balasubramanian, S., Swerdlow, H.P., Smith, G.P., Milton, J., Brown, C.G., Hall, K.P., Evers, D.J., Barnes, C.L., Bignell, H.R., Boutell, J.M., Bryant, J., et al., 2008. Accurate whole human genome sequencing using reversible terminator chemistry. Nature

456, 53–9. doi:10.1038/nature07517

Bode, A., Dong, Z., 2004. Post-translational modification of p53 in tumorigenesis. Nat Rev Cancer 4, 793–805.

Boehme, K.A., Kulikov, R., Blattner, C., 2008. p53 stabilization in response to DNA damage requires Akt/PKB and DNA-PK. Proc. Natl. Acad. Sci. U. S. A. 105, 7785–7790. doi:10.1073/pnas.0703423105

Borcherds, W., Theillet, F., Katzer, A., Finzel, A., Mishall, K.M., Powell, A.T., Wu, H., Manieri, W., Dieterich, C., Selenko, P., Loewer, A., Daughdrill, G.W., 2014. Disorder and residual helicity alter p53-Mdm2 binding affinity and signaling in cells. Nat. Chem. Biol. 10, 1000–1002. doi:10.1038/nchembio.1668

Borgoño, C.A., Michael, I.P., Diamandis, E.P., 2004. Human tissue kallikreins: physiologic roles and applications in cancer. Mol. cancer Res. 2, 257–280. doi:2/5/257 [pii]

Brummelkamp, T.R., Bernards, R., Agami, R., 2002. Stable suppression of tumorigenicity by virus-mediated RNA interference. Cancer Cell 2, 243–247. doi:10.1016/S1535-6108(02)00122-8

Budanov, A. V, Shoshani, T., Faerman, A., Zelin, E., Kamer, I., Kalinski, H., Gorodin, S., Fishman, A., Chajut, A., Einat, P., Skaliter, R., Gudkov, A. V, et al., 2002. Identification of a novel stress-responsive gene Hi95 involved in regulation of cell viability. Oncogene 21, 6017–6031. doi:10.1038/sj.onc.1205877

Callén, E., Jankovic, M., Wong, N., Zha, S., Chen, H.T., Difilippantonio, S., Di Virgilio, M., Heidkamp, G., Alt, F.W., Nussenzweig, A., Nussenzweig, M., 2009. Essential Role for DNA-PKcs in DNA Double-Strand Break Repair and Apoptosis in ATM-Deficient Lymphocytes. Mol. Cell 34, 285–297. doi:10.1016/j.molcel.2009.04.025

Carpenter, A.E., Jones, T.R., Lamprecht, M.R., Clarke, C., Kang, I.H., Friman, O., Guertin, D.A., Chang, J.H., Lindquist, R.A., Moffat, J., Golland, P., Sabatini, D.M., 2006. CellProfiler: image analysis software for identifying and quantifying cell phenotypes. Genome Biol. 7, R100. doi:10.1186/gb-2006-7-10-r100

Celeste, A., Petersen, S., Romanienko, P.J., Fernandez-Capetillo, O., Chen, H.T., Sedelnikova, O.A., Reina-San-Martin, B., Coppola, V., Meffre, E., Difilippantonio, M.J., Redon, C., Pilch, D.R., et al., 2002. Genomic instability in mice lacking histone H2AX. Science 296, 922–927. doi:10.1126/science.1069398.Genomic

Chen, X., Chen, J., Gan, S., Guan, H., Zhou, Y., Ouyang, Q., Shi, J., 2013. DNA damage strength modulates a bimodal switch of p53 dynamics for cell-fate control. BMC Biol. 11. doi:10.1186/1741-7007-11-73

Chène, P., 2001. The role of tetramerization in p53 function. Oncogene 20, 2611–2617. doi:10.1038/sj.onc.1204373

Chiruvella, K.K., Liang, Z., Wilson, T.E., 2013. Repair of double-strand breaks by end joining. Cold Spring Harb. Perspect. Biol. 5. doi:10.1101/cshperspect.a012757

Ciccia, A., Elledge, S.J., 2010. The DNA Damage Response: Making It Safe to Play with Knives. Mol. Cell 40, 179–204. doi:10.1016/j.molcel.2010.09.019

Cimprich, K.A., Cortez, D., 2008. ATR: an essential regulator of genome integrity. Nat. Rev. Mol. Cell Biol. 9, 616–627. doi:10.1038/nrm2450

Contractor, T., Harris, C.R., 2012. p53 negatively regulates transcription of the pyruvate dehydrogenase kinase Pdk2. Cancer Res. 72, 560–567. doi:10.1158/0008-5472.CAN-11-1215

Cox, J., Hein, M.Y., Luber, C.A., Paron, I., 2014. Accurate proteome-wide label-free quantification by delayed normalization and maximal peptide ratio extraction, termed MaxLFQ. Mol Cell Proteomics 13, 2513–2526. doi:10.1074/mcp.M113.031591

Cox, J., Mann, M., 2008. MaxQuant enables high peptide identification rates, individualized p.p.b.-range mass accuracies and proteome-wide protein quantification. Nat. Biotechnol. 26, 1367–72. doi:10.1038/nbt.1511

Cox, J., Neuhauser, N., Michalski, A., Scheltema, R.A., Olsen, J. V., Mann, M., 2011. Andromeda: A peptide search engine integrated into the MaxQuant environment. J. Proteome Res. 10, 1794–1805. doi:10.1021/pr101065j

Cruz-García, A., López-Saavedra, A., Huertas, P., 2014. BRCA1 accelerates CtIP-ediated DNA-end resection. Cell Rep. 9, 451–459. doi:10.1016/j.celrep.2014.08.076

Daoud, S.S., Munson, P.J., Reinhold, W., Young, L., Prabhu, V. V, Yu, Q., Larose, J., Kohn, K.W., Weinstein, J.N., Pommier, Y., 2003. Impact of p53 Knockout and Topotecan Treatment on Gene Expression Profiles in Human Colon Carcinoma Cells : A Pharmacogenomic Study Cancer Res, 2782–2793.

De Stanchina, E., Querido, E., Narita, M., Davuluri, R. V., Pandolfi, P.P., Ferbeyre, G., Lowe, S.W., 2004. PML is a direct p53 target that modulates p53 effector functions. Mol. Cell 13, 523–535. doi:10.1016/S1097-2765(04)00062-0

DeBerardinis, R.J., Lum, J.J., Hatzivassiliou, G., Thompson, C.B., 2008. The Biology of Cancer: Metabolic Reprogramming Fuels Cell Growth and Proliferation. Cell Metab. 7, 11–20. doi:10.1016/j.cmet.2007.10.002

Debnath, J., Muthuswamy, S.K., Brugge, J.S., 2003. Morphogenesis and oncogenesis of MCF-10A mammary epithelial acini grown in three-dimensional basement membrane cultures.

Methods 30, 256–268. doi:10.1016/S1046-2023(03)00032-X

DeLeo, A., Jay, G., Appella, E., Dubois, G., Law, L., Old, L., 1979. Detection of a transformation-related antigen in chemically induced sarcomas and other transformed cells of the mouse. Proc. Natl Acad. Sci. USA 76, 2420–2424.

Dhar, S., Bhargava, R., Yunes, M., Wazer, D.E., Band, V., 2001. Analysis of Normal Epithelial Cell Specific-1 (NES1)/ Kallikrein 10 mRNA Expression by in Situ Hybridization , a Novel Marker for Breast Cancer. Clin Cancer Res 1, 3393–3398.

Dobin, A., Davis, C.A., Schlesinger, F., Drenkow, J., Zaleski, C., Jha, S., Batut, P., Chaisson, M., Gingeras, T.R., 2013. STAR: ultrafast universal RNA-seq aligner. Bioinformatics 29, 15–21. doi:doi: 10.1093/bioinformatics/bts635

Doherty, A.J., Jackson, S.P., 2001. DNA repair: How Ku makes ends meet. Curr. Biol. 11, 920–924. doi:10.1016/S0960-9822(01)00555-3

el-Deiry, W., Kern, S., Pietenpo, l J., Kinzle, r K., Vogelstein, B., 1992. Definition of a consensus binding site for p53. Nat Genet. 1, 45–9.

El-Deiry, W.S., Tokino, T., Velculescu, V.E., Levy, D.B., Parsons, R., Trent, J.M., Lin, D., Mercer, W.E., Kinzler, K.W., Vogelstein, B., 1993. WAF1, a potential mediator of p53 tumor suppression. Cell 75, 817–825. doi:10.1016/0092-8674(93)90500-P

Emami, N., Diamandis, E.P., 2007. New insights into the functional mechanisms and clinical applications of the kallikrein-related peptidase family. Mol. Oncol. 1, 269–287. doi:10.1016/j.molonc.2007.09.003

EpiTect ChIP qPCR Primers - SABiosciences, QIAGEN [WWW Document], 2016a. URL http://www.sabiosciences.com/chipqpcrsearch.php?species_id=0&nfactor=n&ninfo=n&ngene=n&B2=Search&src=genecard&factor=p53&gene=DECR1

EpiTect ChIP qPCR Primers - SABiosciences, QIAGEN [WWW Document], 2016b. URL http://www.sabiosciences.com/chipqpcrsearch.php?species_id=0&nfactor=n&ninfo=n&ngene=n&B2=Search&src=genecard&factor=p53&gene=NDUFB11

FastQC - Babraham Bioinformatics [WWW Document], 2016. URL http://www.bioinformatics.babraham.ac.uk/projects/fastqc/

Feng, Y., Li, X., Sun, B., Wang, Y., Zhang, L., Pan, X., Chen, X., Wang, X., Wang, J., Hao, X., 2010. Evidence for a transcriptional signature of breast cancer. Breast Cancer Res. Treat. 122, 65–75. doi:10.1007/s10549-009-0505-z

Fernandez-Capetillo, O., Lee, A., Nussenzweig, M., Nussenzweig, A., 2004. H2AX: the histone guardian of the genome. DNA Repair (Amst). 3, 959–67.

Finck, B.N., Gropler, M.C., Chen, Z., Leone, T.C., Croce, M.A., Harris, T.E., Lawrence, J.C.,

Kelly, D.P., 2006. Lipin 1 is an inducible amplifier of the hepatic PGC-1alpha/PPARalpha regulatory pathway. Cell Metab. 4, 199–210. doi:10.1016/j.cmet.2006.08.005

Finlay, C.A., Hinds, P.W., Levine, A.J., 1989. The p53 proto-oncogene can act as a suppressor of transformation. Cell 57, 1083–1093. doi:10.1016/0092-8674(89)90045-7

Fujimoto, H., Onishi, N., Kato, N., Takekawa, M., Xu, X.Z., Kosugi, A., Kondo, T., Imamura, M., Oishi, I., Yoda, A., Minami, Y., 2006. Regulation of the antioncogenic Chk2 kinase by the oncogenic Wip1 phosphatase. Cell Death Differ. 13, 1170–1180. doi:10.1038/sj.cdd.4401801

Galluzzi, L., Kepp, O., Vander Heiden, M.G., Kroemer, G., 2013. Metabolic targets for cancer therapy. Nat. Rev. Drug Discov. 12, 829–46. doi:10.1038/nrd4145

Garber, K., 2006. Energy deregulation: licensing tumors to grow. Science 312, 1158–1159.

Gasser, S., Raulet, D., 2006. The DNA damage response, immunity and cancer. Semin Cancer Biol 16, 344–7.

Goettig, P., Magdolen, V., Brandstetter, H., 2010. Natural and synthetic inhibitors of kallikrein-related peptidases (KLKs). Biochimie 92, 1546–1567. doi:10.1016/j.biochi.2010.06.022

Goyal, J., Smith, K.M., Cowan, J.M., Wazer, D.E., Lee, S.W., Band, V., 1998. The Role for NES1 Serine Protease as a Novel Tumor Suppressor. Cancer Res 58, 4782–4786.

Gu, B., Zhu, W.G., 2012. Surf the Post-translational Modification Network of p53 Regulation. Int. J. Biol. Sci. 8, 672–684. doi:10.7150/ijbs.4283

Gundry, R.L., White, M.Y., Murray, C.I., Kane, L.A., Fu, Q., Stanley, B.A., Eyk, J.E. Van, 2010. Preparation of Proteins and Peptides for Mass Spectrometry Analysis in a Bottom-Up Proteomics Workflow. Curr Protoc Mol Biol Chapter 10. doi:10.1002/0471142727.mb1025s88.Preparation

Hanahan, D., Weinberg, R.A., 2011. Hallmarks of Cancer : The Next Generation. Cell 144, 646–674. doi:10.1016/j.cell.2011.02.013

Hardcastle, I.R., Cockcroft, X., Curtin, N.J., El-Murr, M.D., Leahy, J.J.J., Stockley, M., Golding, B.T., Rigoreau, L., Richardson, C., Smith, G.C.M., Griffin, R.J., 2005. Discovery of potent chromen-4-one inhibitors of the DNA-dependent protein kinase (DNA-PK) using a small-molecule library approach. J. Med. Chem. 48, 7829–7846. doi:10.1021/jm050444b

Harper, J.W., Elledge, S.J., 2007. The DNA Damage Response: Ten Years After. Mol. Cell 28, 739–745. doi:10.1016/j.molcel.2007.11.015

Harris, C.R., Dewan, A., Zupnick, A., Normart, R., Gabriel, A., Prives, C., Levine, A.J., Hoh, J., 2009. P53 Responsive Elements in Human Retrotransposons. Oncogene 28, 3857–65.

doi:10.1038/onc.2009.246

Hickson, I., Zhao, Y., Richardson, C.J., Green, S.J., Martin, N.M.B., Orr, A.I., Reaper, P.M., Jackson, S.P., Curtin, N.J., Smith, G.C.M., 2004. Identification and Characterization of a Novel and Specific Inhibitor of the Ataxia-Telangiectasia Mutated Kinase ATM. Cancer Res. 64, 9152–9159. doi:10.1158/0008-5472.CAN-04-2727

Horn, H.F., Vousden, K.H., 2007. Coping with stress: multiple ways to activate p53. Oncogene 26, 1306–1316. doi:10.1038/sj.onc.1210263

Hsu, P.P., Sabatini, D.M., 2008. Cancer cell metabolism: Warburg and beyond. Cell 134, 703–707. doi:10.1016/j.cell.2008.08.021

Hu, J., Lei, H., Fei, X., Liang, S., Xu, H., Qin, D., Wang, Y., Wu, Y., Li, B., 2015. NES1/KLK10 gene represses proliferation, enhances apoptosis and down-regulates glucose metabolism of PC3 prostate cancer cells. Sci. Rep. 5. doi:10.1038/srep17426

Hu, W., Zhang, C., Wu, R., Sun, Y., Levine, A., Feng, Z., 2010. Glutaminase 2, a novel p53 target gene regulating energy metabolism and antioxidant function. Proc. Natl. Acad. Sci. U. S. A. 107, 7455–7460. doi:10.1073/pnas.1001006107

Huang, D.W., Lempicki, R.A., Sherman, B.T., 2009a. Systematic and integrative analysis of large gene lists using DAVID bioinformatics resources. Nat. Protoc. 4, 44–57. doi:10.1038/nprot.2008.211

Huang, D.W., Sherman, B.T., Lempicki, R.A., 2009b. Bioinformatics enrichment tools: Paths toward the comprehensive functional analysis of large gene lists. Nucleic Acids Res. 37, 1–13. doi:10.1093/nar/gkn923

Jen, K.Y., Cheung, V.G., 2005. Identification of novel p53 target genes in ionizing radiation response. Cancer Res. 65, 7666–7673.

Jiang, W., Crowe, J.L., Liu, X., Nakajima, S., Wang, Y., Li, C., Lee, B.J., Dubois, R.L., Liu, C., Yu, X., Lan, L., Zha, S., 2015. Differential Phosphorylation of DNA-PKcs Regulates the Interplay between End-Processing and End-Ligation during Nonhomologous End-Joining. Mol. Cell 58, 172–185. doi:10.1016/j.molcel.2015.02.024

Jones, R.G., Thompson, C.B., 2009. Tumor suppressors and cell metabolism: A recipe for cancer growth. Genes Dev. 23, 537–548. doi:10.1101/gad.1756509

Jordan, J.J., Menendez, D., Inga, A., Nourredine, M., Bell, D., Resnick, M.A., 2008. Noncanonical DNA motifs as transactivation targets by wild type and mutant p53. PLoS Genet. 4. doi:10.1371/journal.pgen.1000104

Kalinska, M., Meyer-Hoffert, U., Kantyka, T., Potempa, J., 2016. Kallikreins - The melting pot of activity and function. Biochimie 122, 270–282. doi:10.1016/j.biochi.2015.09.023

Kawauchi, K., Araki, K., Tobiume, K., Tanaka, N., 2008. p53 regulates glucose metabolism through an IKK-NF-kappaB pathway and inhibits cell transformation. Nat Cell Biol 10, 611–8. doi:10.1038/ncb1724

Kelley, K.D., Miller, K.R., Todd, A., Kelley, A.R., Tuttle, R., Berberich, S.J., 2010. YPEL3, a p53-regulated gene that induces cellular senescence. Cancer Res. 70, 3566–3575. doi:10.1158/0008-5472.CAN-09-3219

Kenzelmann Broz, D., Mello, S.S., Bieging, K.T., Jiang, D., Dusek, R.L., Brady, C.A., Sidow, A., Attardi, L.D., 2013. Global genomic profiling reveals an extensive p53-regulated autophagy program contributing to key p53 responses. Genes Dev. 27, 1016–1031. doi:10.1101/gad.212282.112

Kote-Jarai, Z., Amin Al Olama, A., Leongamornlert, D., Tymrakiewicz, M., Saunders, E., Guy, M., Giles, G.G., Severi, G., Southey, M., Hopper, J.L., Sit, K.C., Harris, et al., 2011. Identification of a novel prostate cancer susceptibility variant in the KLK3 gene transcript. Hum. Genet. 129, 687–694. doi:10.1007/s00439-011-0981-1

Krause, K., Wasner, M., Reinhard, W., Haugwitz, U., Dohna, C.L., Mössner, J., Engeland, K., 2000. The tumour suppressor protein p53 can repress transcription of cyclin B. Nucleic Acids Res. 28, 4410–4418.

Kruiswijk, F., Labuschagne, C.F., Vousden, K.H., 2015. P53 in Survival, Death and Metabolic Health: a Lifeguard With a Licente To Kill. Nat Rev Mol Cell Biol 16, 393–405. doi:10.1038/nrm4007

Kruse, J.P., Gu, W., 2009. Modes of p53 Regulation. Cell 137, 609–622. doi:10.1016/j.cell.2009.04.050

Kubbutat, M.H., Jones, S.N., Vousden, K.H., 1997. Regulation of p53 stability by Mdm2. Nature 387, 299–303. doi:10.1038/387299a0

Lahav, G., 2004. The Strength of Indecisiveness: Oscillatory Behavior for Better Cell Fate Determination. Sci. Signal. 2004. doi:10.1126/stke.2642004pe55

Lahav, G., Rosenfeld, N., Sigal, A., Geva-Zatorsky, N., Levine, A.J., Elowitz, M.B., Alon, U., 2004. Dynamics of the p53-Mdm2 feedback loop in individual cells. Nat. Genet. 36, 147–150. doi:10.1038/ng1293

Lane, D.P., 1992. Cancer. p53, guardian of the genome. Nature 358, 15–16.

Lane, D.P., Crawford, L. V., 1979. T antigen is bound to a host protein in SV40-transformed cells. Nature 278, 261–263.

Lavin, M.F., Delia, D., Chessa, L., 2006. ATM and the DNA damage response. EMBO Rep 7, 154–160. doi:10.1038/sj.embor.7400629

Lawrence, M.G., Lai, J., Clements, J.A., 2010. Kallikreins on steroids: Structure, function, and hormonal regulation of prostate-specific antigen and the extended kallikrein locus. Endocr. Rev. 31, 407–446. doi:10.1210/er.2009-0034

Leahy, J.J.J., Golding, B.T., Griffin, R.J., Hardcastle, I.R., Richardson, C., Rigoreau, L., Smith, G.C.M., 2004. Identification of a highly potent and selective DNA-dependent protein kinase (DNA-PK) inhibitor (NU7441) by screening of chromenone libraries. Bioorganic Med. Chem. Lett. 14, 6083–6087. doi:10.1016/j.bmcl.2004.09.060

Lee, J.-H., Paull, T.T., 2005. ATM activation by DNA double-strand breaks through the Mre11-Rad50-Nbs1 complex. Science 308, 551–554. doi:10.1126/science.1108297

Lee, K.-H., Li, M., Michalowski, A.M., Zhang, X., Liao, H., Chen, L., Xu, Y., Wu, X., Huang, J., 2010. A genomewide study identifies the Wnt signaling pathway as a major target of p53 in murine embryonic stem cells. Proc. Natl. Acad. Sci. U. S. A. 107, 69–74. doi:10.1073/pnas.0909734107

Lev Bar-Or, R., Maya, R., Segel, L.A., Alon, U., Levine, A.J., Oren, M., 2000. Generation of oscillations by the p53-Mdm2 feedback loop: a theoretical and experimental study. Proc. Natl. Acad. Sci. U. S. A. 97, 11250–11255. doi:10.1073/pnas.210171597

Levine, A.J., 2009. The common mechanisms of transformation by the small DNA tumor viruses: The inactivation of tumor suppressor gene products: p53. Virology 384, 285–293. doi:10.1016/j.virol.2008.09.034

Levine, A.J., 1997. P53, the Cellular Gatekeeper for Growth and Division. Cell 88, 323–331. doi:10.1016/S0092-8674(00)81871-1

Li, J., Stern, D.F., 2005. Regulation of CHK2 by DNA-dependent protein kinase. J. Biol. Chem. 280, 12041–12050. doi:10.1074/jbc.M412445200

Li, X., Liu, J., Wang, Y., Zhang, L., Ning, L., Feng, Y., 2009. Parallel underexpression of kallikrein 5 and kallikrein 7 mRNA in breast malignancies. Cancer Sci. 100, 601–607. doi:10.1111/j.1349-7006.2009.01090.x

Liang, Y., Liu, J., Feng, Z., 2013. The regulation of cellular metabolism by tumor suppressor p53. Cell Biosci. 3. doi:10.1186/2045-3701-3-9

Linzer, D.I., Levine, A.J., 1979. Characterization of a 54Kdalton cellular SV40 tumor antigen present in SV40-transformed cells and uninfected embryonal carcinoma cells. Cell 17, 43–52.

Liu, X.L., Wazer, D.E., Watanabe, K., Band, V., 1996. Identification of a novel serine protease-like gene, the expression of which is down-regulated during breast cancer progression. Cancer Res 56, 3371–3379.

Liu, Y., He, Y., Jin, A., Tikunov, A.P., Zhou, L., Tollini, L.A., Leslie, P., Kim, T.-H., Li, L.O., Coleman, R.A., Gu, Z., Chen, et al., 2014. Ribosomal protein-Mdm2-p53 pathway coordinates nutrient stress with lipid metabolism by regulating MCD and promoting fatty acid oxidation. Proc. Natl. Acad. Sci. U. S. A. 111, 2414–2422. doi:10.1073/pnas.1315605111

Loewer, A., Batchelor, E., Gaglia, G., Lahav, G., 2010. Basal Dynamics of p53 Reveal Transcriptionally Attenuated Pulses in Cycling Cells. Cell 142, 89–100. doi:10.1016/j.cell.2010.05.031

Loewer, A., Karanam, K., Mock, C., Lahav, G., 2013. The p53 response in single cells is linearly correlated to the number of DNA breaks without a distinct threshold. BMC Biol. 11. doi:10.1186/1741-7007-11-114

Lopez-Contreras, A.J., Fernandez-Capetillo, O., 2012. Signalling DNA Damage. Intech Chapter 8, 233–262. doi:10.5772/50863

Lou, Z., Minter-Dykhouse, K., Franco, S., Gostissa, M., Rivera, M.A., Celeste, A., Manis, J.P., Van Deursen, J., Nussenzweig, A., Paull, T.T., Alt, F.W., Chen, J., 2006. MDC1 maintains genomic stability by participating in the amplification of ATM-dependent DNA damage signals. Mol. Cell 21, 187–200. doi:10.1016/j.molcel.2005.11.025

Lu, X., Ma, O., Nguyen, T.A., Jones, S.N., Oren, M., Donehower, L.A., 2007. The Wip1 Phosphatase Acts as a Gatekeeper in the p53-Mdm2 Autoregulatory Loop. Cancer Cell 12, 342–354. doi:10.1016/j.ccr.2007.08.033

Lundwall, A., Brattsand, M., 2008. Kallikrein-related peptidases. Cell. Mol. Life Sci. 65, 2019–2038. doi:10.1007/s00018-008-8024-3

Mahaney, B.L., Meek, K., Lees-Miller, S.P., 2009. Repair of ionizing radiation-induced DNA double strand breaks by non-homologous end-joing. Biochem. J. 417, 639–650. doi:10.1042/BJ20080413.Repair

Marchenko, N.D., Hanel, W., Li, D., Becker, K., Reich, N., Moll, U.M., 2010. Stress-mediated nuclear stabilization of p53 is regulated by ubiquitination and importin-alpha3 binding. Cell Death Differ. 17, 255–67. doi:10.1038/cdd.2009.173

Martin, I. V, MacNeill, S.A., 2002. ATP-dependent DNA ligases. Genome Biol. 3, 3005.1–3005.7. doi:10.1186/gb-2002-3-4-reviews3005

Matoba, S., Kang, U.-G., Patino, W.D., Wragg, A., Boehm, M., Gavrilova, O., Hurley, P.J., Bunz, F., Hwang, P.M., 2006. p53 Regulates Mitochondrial Respiration. Science 312, 1650–1653.

Meek, D.W., 2004. The p53 response to DNA damage. DNA Repair (Amst). 3, 1049–1056.

doi:10.1016/j.dnarep.2004.03.027

Menendez, D., Nguyen, T.A., Freudenberg, J.M., Mathew, V.J., Anderson, C.W., Jothi, R., Resnick, M.A., 2013. Diverse stresses dramatically alter genome-wide p53 binding and transactivation landscape in human cancer cells. Nucleic Acids Res. 41, 7286–7301. doi:10.1093/nar/gkt504

Metzker, M.L., 2010. Sequencing technologies — the next generation. Nat. Rev. Genet. 11, 31–46.

Meyer-Hoffert, U., Wu, Z., Kantyka, T., Fischer, J., Latendorf, T., Hansmann, B., Bartels, J., He, Y., Gläser, R., Schröder, J.M., 2010. Isolation of SPINK6 in human skin: Selective inhibitor of kallikrein-related peptidases. J. Biol. Chem. 285, 32174–32181. doi:10.1074/jbc.M109.091850

Mortazavi, A., Williams, B.A., McCue, K., Schaeffer, L., Wold, B., 2008. Mapping and quantifying mammalian transcriptomes by RNA-Seq. Nat. Methods 5, 621–628. doi:10.1038/nmeth.1226

Muller, P.A.J., Vousden, K.H., 2013. P53 Mutations in Cancer. Nat. Cell Biol. 15, 2–8. doi:10.1038/ncb2641

Nakano, K., Bálint, E., Ashcroft, M., Vousden, K.H., 2000. A ribonucleotide reductase gene is a transcriptional target of p53 and p73. Oncogene 19, 4283–4289. doi:10.1038/sj.onc.1203774

Nikulenkov, F., Spinnler, C., Li, H., Tonelli, C., Shi, Y., Turunen, M., Kivioja, T., Ignatiev, I., Kel, A., Taipale, J., Selivanova, G., 2012. Insights into p53 transcriptional function via genome-wide chromatin occupancy and gene expression analysis. Cell Death Differ. 19, 1992–2002. doi:10.1038/cdd.2012.89

Oliva-Trastoy, M., Berthonaud, V., Chevalier, A., Ducrot, C., Marsolier-Kergoat, M.-C., Mann, C., Leteurtre, F., 2007. The Wip1 phosphatase (PPM1D) antagonizes activation of the Chk2 tumour suppressor kinase. Oncogene 26, 1449–58. doi:10.1038/sj.onc.1209927

Paliouras, M., Borgono, C., Diamandis, E.P., 2007. Human tissue kallikreins: The cancer biomarker family. Cancer Lett. 249, 61–79. doi:10.1016/j.canlet.2006.12.018

Pampalakis, G., Obasuyi, O., Papadodima, O., Chatziioannou, A., Zoumpourlis, V., Sotiropoulou, G., 2014. The KLK5 protease suppresses breast cancer by repressing the mevalonate pathway. Oncotarget 5, 2390–2403. doi:10.18632/oncotarget.1235

Pampalakis, G., Sotiropoulou, G., 2007. Tissue kallikrein proteolytic cascade pathways in normal physiology and cancer. Biochim. Biophys. Acta - Rev. Cancer 1776, 22–31. doi:10.1016/j.bbcan.2007.06.001

Polyak, K., Xia, Y., Zweier, J.L., Kinzler, K.W., Vogelstein, B., 1997. A model for p53-induced apoptosis. Nature 389, 300–305. doi:10.1038/38525

Potter, V., 1958. The biochemical approach to the cancer problem. Fed Proc. 17, 691–7.

Prassas, I., Eissa, A., Poda, G., Diamandis, E.P., 2015. Unleashing the therapeutic potential of human kallikrein-related serine proteases. Nat Rev Drug Discov 14, 183–202. doi:10.1038/nrd4534

Purvis, J.E., Karhohs, K.W., Mock, C., Batchelor, E., Loewer, A., Lahav, G., 2012. p53 Dynamics Control Cell Fate. Science 336, 1440–1444. doi:10.1126/science.1218351

Purvis, J.E., Lahav, G., 2013. Encoding and decoding cellular information through signaling dynamics. Cell 152, 945–956. doi:10.1016/j.cell.2013.02.005

Rajagopalan, S., Huang, F., Fersht, A.R., 2011. Single-molecule characterization of oligomerization kinetics and equilibria of the tumor suppressor p53. Nucleic Acids Res. 39, 2294–2303. doi:10.1093/nar/gkq800

Rappsilber, J., Ishihama, Y., Mann, M., 2003. Stop and Go Extraction Tips for Matrix-Assisted Laser Desorption/Ionization, Nanoelectrospray, and LC/MS Sample Pretreatment in Proteomics. Anal. Chem. 75, 663–670.

Reaper, P.M., Griffiths, M.R., Long, J.M., Charrier, J.-D., Maccormick, S., Charlton, P.A., Golec, J.M.C., Pollard, J.R., 2011. Selective killing of ATM- or p53-deficient cancer cells through inhibition of ATR. Nat. Chem. Biol. 7, 428–430. doi:10.1038/nchembio.573

Roe, C.R., Roe, D.S., 1999. Recent developments in the investigation of inherited metabolic disorders using cultured human cells. Mol. Genet. Metab. 68, 243–257. doi:10.1006/mgme.1999.2911

Sanchez-Macedo, N., Feng, J., Faubert, B., Chang, N., Elia, A., Rushing, E.J., Tsuchihara, K., Bungard, D., Berger, S.L., Jones, R.G., Mak, T.W., Zaugg, K., 2013. Depletion of the novel p53-target gene carnitine palmitoyltransferase 1C delays tumor growth in the neurofibromatosis type I tumor model. Cell Death Differ. 20, 659–68. doi:10.1038/cdd.2012.168

Schroeder, A., Mueller, O., Stocker, S., Salowsky, R., Leiber, M., Gassmann, M., Lightfoot, S., Menzel, W., Granzow, M., Ragg, T., 2006. The RIN: an RNA integrity number for assigning integrity values to RNA measurements. BMC Mol. Biol. 7. doi:10.1186/1471-2199-7-3

Schwartzenberg-Bar-Yoseph, F., Armoni, M., Karnieli, E., 2004. The tumor suppressor p53 down-regulates glucose transporters GLUT1 and GLUT4 gene expression. Cancer Res. 64, 2627–33.

Serrano, M.A., Li, Z., Dangeti, M., Musich, P.R., Patrick, S., Roginskaya, M., Cartwright, B., Zou, Y., 2012. DNA-PK, ATM and ATR collaboratively regulate p53–RPA interaction to facilitate homologous recombination DNA repair. Oncogene 32, 2452–2462. doi:10.1038/onc.2012.257

Shaheen, F.S., Znojek, P., Fisher, A., Webster, M., Plummer, R., Gaughan, L., Smith, G.C.M., Leung, H.Y., Curtin, N.J., Robson, C.N., 2011. Targeting the DNA double strand break repair machinery in prostate cancer. PLoS One 6. doi:10.1371/journal.pone.0020311

Shreeram, S., Demidov, O.N., Hee, W.K., Yamaguchi, H., Onishi, N., Kek, C., Timofeev, O.N., Dudgeon, C., Fornace, A.J., Anderson, C.W., Minami, Y., Appella, E., Bulavin, D. V., 2006. Wip1 Phosphatase Modulates ATM-Dependent Signaling Pathways. Mol. Cell 23, 757–764. doi:10.1016/j.molcel.2006.07.010

Specification Sheet: Sequencing - cBot Illumina [WWW Document], 2011. URL http://www.illumina.com/documents/products/datasheets/datasheet_cbot.pdf9A-9E20-43E1-BB8E-7B4E35D0E965

Srivastava, M., Nambiar, M., Sharma, S., Karki, S.S., Goldsmith, G., Hegde, M., Kumar, S., Pandey, M., Singh, R.K., Ray, P., Natarajan, R., Kelkar, M., et al., 2012. An inhibitor of nonhomologous end-joining abrogates double-strand break repair and impedes cancer progression. Cell 151, 1474–1487. doi:10.1016/j.cell.2012.11.054

Stambolsky, P., Weisz, L., Shats, I., Klein, Y., Goldfinger, N., Oren, M., Rotter, V., 2006. Regulation of AIF expression by p53. Cell Death Differ. 13, 2140–2149. doi:10.1038/sj.cdd.4401965

Steen, H., Mann, M., 2004. The ABC’s (and XYZ's) of peptide sequencing. Nat. Rev. Mol. Cell Biol. 5, 699–711. doi:10.1038/nrm1468

Stommel, J.M., Marchenko, N.D., Jimenez, G.S., Moll, U.M., Hope, T.J., Wahl, G.M., 1999. A leucine-rich nuclear export signal in the p53 tetramerization domain: regulation of subcellular localization and p53 activity by NES masking. EMBO J. 18, 1660–72. doi:10.1093/emboj/18.6.1660

Stommel, J.M., Wahl, G.M., 2004. Accelerated MDM2 auto-degradation induced by DNA-damage kinases is required for p53 activation. EMBO J. 23, 1547–1556. doi:10.1038/sj.emboj.7600145

Stucki, M., Clapperton, J.A., Mohammad, D., Yaffe, M.B., Smerdon, S.J., Jackson, S.P., 2005. MDC1 directly binds phosphorylated histone H2AX to regulate cellular responses to DNA double-strand breaks. Cell 123, 1213–1226. doi:10.1016/j.cell.2005.09.038

Sun, Y., Yi, H., Zhang, P.F., Li, M.Y., Li, C., Li, F., Peng, F., Feng, X.P., Yang, Y.X., Yang,

F., Xiao, Z.Q., Chen, Z.C., 2007. Identification of differential proteins in nasopharyngeal carcinoma cells with p53 silence by proteome analysis. FEBS Lett. 581, 131–139. doi:10.1016/j.febslet.2006.12.008

Suzuki, S., Tanaka, T., Poyurovsky, M. V, Nagano, H., Mayama, T., Ohkubo, S., Lokshin, M., Hosokawa, H., Nakayama, T., Suzuki, Y., Sugano, S., Sato, E., et al., 2010. Phosphate-activated glutaminase (GLS2), a p53-inducible regulator of glutamine metabolism and reactive oxygen species. Proc. Natl. Acad. Sci. U. S. A. 107, 7461–7466. doi:10.1073/pnas.1002459107

Tan, M., Wang, Y., Guan, K., Sun, Y., 2000. PTGF-beta, a type beta transforming growth factor (TGF-beta) superfamily member, is a p53 target gene that inhibits tumor cell growth via TGF-beta signaling pathway. Proc. Natl. Acad. Sci. U. S. A. 97, 109–114. doi:10.1073/pnas.97.1.109

Tanaka, H., Arakawa, H., Yamaguchi, T., Shiraishi, K., Fukuda, S., Matsui, K., Takei, Y., Nakamura, Y., 2000. A ribonucleotide reductase gene involved in a p53-dependent cell-cycle checkpoint for DNA damage. Nature 404, 42–49. doi:10.1038/35003506

Tao, W., Levine, A.J., 1999. P19(ARF) stabilizes p53 by blocking nucleo-cytoplasmic shuttling of Mdm2. Proc. Natl. Acad. Sci. U. S. A. 96, 6937–41. doi:10.1073/pnas.96.12.6937

Technology Spotlight: Illumina Sequencing - Illumina Sequencing Technology [WWW Document], 2010. URL http://www.illumina.com/documents/products/techspotlights/techspotlight_sequencing.pdf

Tomimatsu, N., Mukherjee, B., Burma, S., 2009. Distinct roles of ATR and DNA-PKcs in triggering DNA damage responses in ATM-deficient cells. EMBO Rep. 10, 629–35. doi:10.1038/embor.2009.60

Torgovnick, A., Schumacher, B., 2015. DNA repair mechanisms in cancer development and therapy. Front. Genet. 6. doi:10.3389/fgene.2015.00157

TruSeq RNA Access Library Prep Kit Support - Questions & Answers [WWW Document], 2016. URL http://support.illumina.com/sequencing/sequencing_kits/truseq_rna_access_library_prep_kit/questions.html

TruSeq RNA Sample Preparation v2 Guide - Illumina [WWW Document], 2014. URL http://support.illumina.com/content/dam/illumina-support/documents/documentation/chemistry_documentation/samplepreps_truseq/truseqrna/truseq-rna-sample-prep-v2-guide-15026495-f.pdf

Tyni, T., Pourfarzam, M., Turnbull, D.M., 2002. Analysis of mitochondrial fatty acid oxidation intermediates by tandem mass spectrometry from intact mitochondria prepared from homogenates of cultured fibroblasts, skeletal muscle cells, and fresh muscle. Pediatr. Res. 52, 64–70. doi:10.1203/00006450-200207000-00013

Vahsen, N., Candé, C., Brière, J.-J., Bénit, P., Joza, N., Larochette, N., Mastroberardino, P.G., Pequignot, M.O., Casares, N., Lazar, V., Feraud, O., Debili, N., et al., 2004. AIF deficiency compromises oxidative phosphorylation. EMBO J. 23, 4679–89. doi:10.1038/sj.emboj.7600461

van den Bosch, M., Bree, R.T., Lowndes, N.F., 2003. The MRN complex: coordinating and mediating the response to broken chromosomes. EMBO Rep. 4, 844–9. doi:10.1038/sj.embor.embor925

Vander Heiden, M., Cantley, L., Thompson, C., 2009. Understanding the Warburg effect: The metabolic Requirements of cell proliferation. Science 324, 1029–1033. doi:10.1126/science.1160809.Understanding

Vassilev, L.T., Vu, B.T., Craves, B., Carvajal, D., Podlaski, F., Filipovic, Z., Kong, N., Kammlott, U., Lukacs, C., Klein, C., Fotouhi, N., Liu, E.A., 2004. In Vivo Activation of the p53 Pathway by Small-MoleculeAntagonists of MDM2. Science 303, 844–848. doi:10.1126/science.1092472

Velasco-Miguel, S., Buckbinder, L., Jean, P., Gelbert, L., Talbott, R., Laidlaw, J., Seizinger, B., Kley, N., 1999. PA26, a novel target of the p53 tumor suppressor and member of the GADD family of DNA damage and growth arrest inducible genes. Oncogene 18, 127–137. doi:10.1038/sj.onc.1202274

Vogelstein, B., Lane, D., Levine, A.J., 2000. Surfing the p53 network. Nature 408, 307–310.

Vousden, K.H., Prives, C., 2009. Blinded by the Light: The Growing Complexity of p53. Cell 137, 413–431. doi:10.1016/j.cell.2009.04.037

Wang, Z., Gerstein, M., Snyder, M., 2009. RNA-Seq: a revolutionary tool for transcriptomics. Nat. Rev. Genet. 10, 57–63. doi:10.1038/nrg2484

Warburg, O., 1956. On the Origin of Cancer Cells. Science 123, 309–14. doi:10.1126/science.123.3191.309

Weinberg, R.L., Veprintsev, D.B., Bycroft, M., Fersht, A.R., 2005. Comparative binding of p53 to its promoter and DNA recognition elements. J. Mol. Biol. 348, 589–596. doi:10.1016/j.jmb.2005.03.014

Williams, R.S., Williams, J.S., Tainer, J.A., 2007. Mre11–Rad50–Nbs1 is a keystone complex connecting DNA repair machinery, double-strand break signaling, and the chromatin

template. Biochem. Cell Biol. 85, 509–520. doi:10.1139/O07-069

Yoon, K.A., Nakamura, Y., Arakawa, H., 2004. Identification of ALDH4 as a p53-inducible gene and its protective role in cellular stresses. J. Hum. Genet. 49, 134–140. doi:10.1007/s10038-003-0122-3

Yousef, G.M., 2001. The New Human Tissue Kallikrein Gene Family: Structure, Function, and Association to Disease. Endocr. Rev. 22, 184–204. doi:10.1210/er.22.2.184

Yousef, G.M., Yacoub, G.M., Polymeris, M.-E., Popalis, C., Soosaipillai, A., Diamandis, E.P., 2004. Kallikrein gene downregulation in breast cancer. Br. J. Cancer 90, 167–72. doi:10.1038/sj.bjc.6601451

Zahra Bathaie, S., Ashrafi, M., Azizian, M., Tamanoi, F., 2016. Mevalonate Pathway and Human Cancers. Curr Mol Pharmacol.

Zhang, Y., 2001. A p53 Amino-Terminal Nuclear Export Signal Inhibited by DNA Damage-Induced Phosphorylation. Science 292, 1910–1915. doi:10.1126/science.1058637

Zhao, Y., Butler, E.B., Tan, M., 2013. Targeting cellular metabolism to improve cancer therapeutics. Cell Death Dis. 4. doi:10.1038/cddis.2013.60

Zheng, J., Weng, J., Sun, X., Hao, M., Ding, T., Xiong, D., Wang, X., Zhu, Y., Xiao, G., Cheng, G., Zhao, M., Zhang, J., et al., 2013. HIC1 modulates prostate cancer progression by epigenetic modification. Clin. Cancer Res. 19, 1400–1410. doi:10.1158/1078-0432.CCR-12-2888

Zhu, H., Gooderham, N.J., 2006. Mechanisms of induction of cell cycle arrest and cell death by cryptolepine in human lung adenocarcinoma A549 cells. Toxicol. Sci. 91, 132–139. doi:10.1093/toxsci/kfj146

6.1 References consulted for plotting the different metabolic pathways and mapping the corresponding genes and proteins

Berg, J.M., Tymoczko, J.L., Stryer, L., 2012. Biochemistry, 7th ed. W. H. Freeman and Company, New York.

Bhagavan, N.V., Ha, C.-E., 2015. Essentials of Medical Biochemistry: With Clinical Cases, 2nd ed. Academic Press, Elsevier.

Brandt, M., 2016. Fatty Acid Breakdown [WWW Document]. URL https://www.rose-hulman.edu/~brandt/Chem331/Lipid_Breakdown.pdf

Budanov, A.V., Karin, M., 2008. The p53-regulated Sestrin gene products inhibit mTOR signaling. Cell 134, 451–460. doi:10.1016/j.cell.2008.06.028.

Crocetti, M., Barone, M.A. (Eds.)., 2004. Oski's Essential Pediatrics, 2nd ed. Lippincott Williams & Wilkins, Philadelphia.

Das, D., 2012. Biochemistry, 14th ed. Academic Publishers, Kolkata.

Feldman, M., Friedman, L.S., Brandt, L.J., 2010. Sleisenger and Fordtran's Gastrointestinal and Liver Disease, 9th ed. Saunders, Elsevier Inc., Philadelphia.

Fillmore, N., Alrob, O.A., Lopaschuk, G.D., 2011. Fatty Acid beta-Oxidation [WWW Document]. URL http://lipidlibrary.aocs.org/Biochemistry/content.cfm?ItemNumber=39187

GeneCards - Human Gene Database [WWW Document], 2016. URL http://www.genecards.org/

Houten, S.M., Wanders, R.J.A., 2010. A general introduction to the biochemistry of mitochondrial fatty acid β-oxidation. J. Inherit. Metab. Dis. 33, 469–477. doi:10.1007/s10545-010-9061-2

Hunt, M.C., Alexson, S.E.H., 2002. The role Acyl-CoA thioesterases play in mediating intracellular lipid metabolism. Prog. Lipid Res. 41, 99–130. doi:10.1016/S0163-7827(01)00017-0

King, M.W., 2016. Lipolysis and the Oxidation of Fatty Acids. [WWW Document]. URL http://themedicalbiochemistrypage.org/fatty-acid-oxidation.php

Komoda, T., Matsunaga, T., 2015. Biochemistry for Medical Professionals, 1st ed. Academic Press, Elsevier.

Liu, W., Phang, J.M., 2013. MiRNA and Proline Metabolism in Cancer, in: Siregar, Y. (Ed.), Oncogene and Cancer - From Bench to Clinic. Intech.

MacLaren, D., Morton, J., 2012. Biochemistry for Sport and Exercise Metabolism, 1st ed. John Wiley & Sons, Ltd., Chichester.

Nelson, D.L., Cox, M.M., 2013. Lehninger Principles of Biochemistry, 6th ed. W. H. Freeman and Company, New York.

Numa, S. (Ed.), 1984. Fatty Acid Metabolism and its Regulation. Elsevier Science, Amsterdam.

Poirier, Y., Antonenkov, V.D., Glumoff, T., Hiltunen, J.K., 2006. Peroxisomal beta-oxidation-A metabolic pathway with multiple functions. Biochim. Biophys. Acta 1763, 1413–1426. doi:10.1016/j.bbamcr.2006.08.034

PubMed - NCBI Literature [WWW Document], 2016. URL http://www.ncbi.nlm.nih.gov/pubmed

Sacksteder, K.A., Morrell, J.C., Wanders, R.J.A., Matalon, R., Gould, S.J., 1999. MCD encodes peroxisomal and cytoplasmic forms of malonyl-CoA decarboxylase and is mutated in malonyl-CoA decarboxylase deficiency. J. Biol. Chem. 274, 24461–24468. doi:10.1074/jbc.274.35.24461

Saggerson, D., 2008. Malonyl-CoA, a key signaling molecule in mammalian cells. Annu. Rev. Nutr. 28, 253–272. doi:10.1146/annurev.nutr.28.061807.155434.

Schell, J.C., Rutter, J., 2013. The long and winding road to the mitochondrial pyruvate carrier. Cancer Metab. 1. doi:10.1186/2049-3002-1-6.

Visser, W.F., van Roermund, C.W.T., Ijlst, L., Waterham, H.R., Wanders, R.J.A., 2007. Metabolite transport across the peroxisomal membrane. Biochem. J. 401, 365–375. doi:10.1042/BJ20061352

Walther, T.C., Farese Jr., R.V., 2012. Lipid Droplets And Cellular Lipid Metabolism. Annu Rev Biochem 81, 687–714. doi:10.1146/annurev-biochem-061009-102430.

Wanders, R.J.A., Ruiter, J.P.N., Ijlst, L., Waterham, H.R., Houten, S.M., 2010. The enzymology of mitochondrial fatty acid beta-oxidation and its application to follow-up analysis of positive neonatal screening results. J. Inherit. Metab. Dis. 33, 479–494. doi:10.1007/s10545-010-9104-8

Wanders, R.J.A., Waterham, H.R., 2006. Biochemistry of mammalian peroxisomes revisited. Annu. Rev. Biochem. 75, 295–332. doi:10.1146/annurev.biochem.74.082803.133329

Westin, M.A.K., Hunt, M.C., Alexson, S.E.H, 2008. Short- and medium-chain carnitine acyltransferases and acyl-CoA thioesterases in mouse provide complementary systems for transport of beta-oxidation products out of peroxisomes. Cell. Mol. Life Sci. 65, 982–990. doi:10.1007/s00018-008-7576-6

7 LIST OF PUBLICATIONS

Borcherds, W., Theillet, F., Katzer, A., **Finzel, A.**, Mishall, K.M., Powell, A.T., Wu, H., Manieri, W., Dieterich, C., Selenko, P., Loewer, A., Daughdrill, G.W., 2014. Disorder and residual helicity alter p53-Mdm2 binding affinity and signaling in cells. Nat. Chem. Biol. 10, 1000–1002. https://dx.doi.org/10.1038/nchembio.1668

Finzel, A., Grybowski, A., Strasen, J., Cristiano, E., Loewer, A., 2016. Hyper-activation of ATM upon DNA-PKcs inhibition modulates p53 dynamics and cell fate in response to DNA damage. Mol Biol Cell 27, 2360-2367. http://dx.doi.org/10.1091/mbc.E16-01-0032

Schueler, M., Munschauer, M., Gregersen, L.H., **Finzel, A.**, Loewer, A., Chen, W., Landthaler, M., Dieterich, C., 2014. Differential protein occupancy profiling of the mRNA transcriptome. Genome Biol. 15. http://dx.doi.org/10.1186/gb-2014-15-1-r15

8 APPENDIX

8.1 List of abbreviations

ACADVL	acyl-CoA dehydrogenase, very long chain
ACC	acetyl-CoA carboxylase
ADP	adenosine diphosphate
AIFM2	apoptosis-inducing factor, mitochondrion-associated, 2
ALDH4A1	aldehyde dehydrogenase 4 family, member A1
AMP	adenosine monophosphate
AMPK	AMP-activated protein kinase
ATM	ataxia telangiectasia-mutated
ATMi	ATM inhibitor
ATP	adenosine triphosphate
ATR	ataxia telangiectasia and Rad3-related
ATRi	ATR inhibitor
a.u.	arbitrary units
Bis-Tris	2,2-bis(hydroxymethyl)-2,2′,2″-nitrilotriethanol
bp	base pair
BRCA1	breast cancer 1
BSA	bovine serum albumin
CAPS	3-(cyclohexylamino)-1-propanesulfonic acid
CBP	CREB-binding protein
CCNB2	cyclin B2
cDNA	complementary DNA
CFP	cyan fluorescent protein
ChIP	chromatin immunoprecipitation
Chk1	checkpoint kinase 1
Chk2	checkpoint kinase 2
Chk2i II	Chk2 inhibitor II
cNHEJ	canonical non-homologous end joining
CoA	coenzyme A
COX20	cytochrome c oxidase assembly factor
CPT1	carnitine palmitoyltransferase 1 (acyltransferase)
CPT1B	carnitine palmitoyltransferase 1B (acyltransferase 1B)
CPT1C	carnitine palmitoyltransferase 1C (acyltransferase 1C)
DDR	DNA damage response
DECR1	2,4-dienoyl CoA reductase 1
DECR2	2,4-dienoyl CoA reductase 2
DEPC	diethylpyrocarbonate
DMEM/F-12	Dulbecco's modified eagle medium/nutrient mixture F-12
DMSO	dimethyl sulfoxide
DNA	deoxyribonucleic acid
DNA-PKcs	DNA-dependent protein kinase catalytic subunit
DNA-PKi	DNA-PKcs inhibitor
dNTP	deoxynucleotide
ds	double strand
DSB	double strand break

dT	deoxythymidine
DTT	dithiothreitol
EF1αp	elongation factor-1 α promoter
EGF	epidermal growth factor
ETFDH	electron-transferring-flavoprotein dehydrogenase
FAD	flavin adenine dinucleotide
FCS	fetal calf serum
FWHM	full-width at half-maximum
G2 phase	Gap 2 phase
G418	geneticin disulphate
GAPDH	glyceraldehyde-3-phosphate dehydrogenase
GDF15	growth differentiation factor 15
GLS2	glutaminase 2
GLUT1	glucose transporter type 1
GLUT3	glucose transporter type 3
GLUT4	glucose transporter type 4
Gy	gray
HADHA	hydroxyacyl-CoA dehydrogenase/3-ketoacyl-CoA thiolase/enoyl-CoA hydratase (trifunctional protein), alpha subunit
HEPES	4-(2-hydroxyethyl)-1-piperazineethanesulfonic acid
HR	homologous recombination
HRP	horseradish peroxidase
HS	horse serum
IR	irradiation
iRFP	near-infrared fluorescent protein
KLK3	kallikrein-related peptidase 3
KLK5	kallikrein-related peptidase 5
KLK7	kallikrein-related peptidase 7
KLK8	kallikrein-related peptidase 8
KLK10	kallikrein-related peptidase 10
LC-MS/MS	liquid chromatography-tandem mass spectrometry
LDS	lithium dodecyl sulfate
LFQ	label-free quantification
LigIV	ligase IV
LigIVi	ligase IV inhibitor
LIPA	lipase A
MDC1	mediator of DNA-damage checkpoint 1
Mdm2	mouse double minute 2, human homolog
Mdm4	mouse double minute 4, human homolog
MES	2-(N-morpholino)ethanesulfonic acid
MLYCD	malonyl-CoA decarboxylase
MNF1	mitochondrial nucleoid factor 1
MRE11A	meiotic recombination 11 homolog A
MRN	MRE11A–RAD50–NBN
mRNA	messenger RNA
MT-ATP8	mitochondrially encoded ATP synthase 8
MT-ND4	mitochondrially encoded NADH dehydrogenase 4
m/z	mass-to-charge ratio
n	number of cells

NA	numerical aperture
NAD	nicotinamide adenine dinucleotide
NBN	nibrin
NDUFA4	NADH dehydrogenase (ubiquinone) 1 alpha subcomplex, 4
NDUFA5	NADH dehydrogenase (ubiquinone) 1 alpha subcomplex, 5
NDUFA9	NADH dehydrogenase (ubiquinone) 1 alpha subcomplex, 9
NDUFA11	NADH dehydrogenase (ubiquinone) 1 alpha subcomplex, 11
NDUFB6	NADH dehydrogenase (ubiquinone) 1 beta subcomplex, 6
NDUFB7	NADH dehydrogenase (ubiquinone) 1 beta subcomplex, 7
NDUFB11	NADH dehydrogenase (ubiquinone) 1 beta subcomplex, 11
NDUFC2	NADH dehydrogenase (ubiquinone) 1, subcomplex unknown, 2
NDUFS6	NADH dehydrogenase (ubiquinone) Fe-S Protein 6
NES	nuclear export signal
NLS	nuclear localization signal
OXPHOS	oxidative phosphorylation
pATM	phosphorylated ATM
PBS	phosphate buffered saline
pChk1	phosphorylated Chk1
pChk2	phosphorylated Chk2
PCR	polymerase chain reaction
PDH	pyruvate dehydrogenase
PDK	pyruvate dehydrogenase kinase
PDK2	pyruvate dehydrogenase kinase, isozyme 2
PDK4	pyruvate dehydrogenase kinase, isozyme 4
pDNA-PKcs	phosphorylated DNA-PKcs
PDP1	pyruvate dehyrogenase phosphatase catalytic subunit 1
PDVF	polyvinylidene difluoride
pH2A.X	phosphorylated H2A.X
PI3K	phosphatidylinositol 3-kinase
pp53	phosphorylated p53
PPARG	peroxisome proliferator activated receptor gamma
PRKAB1	protein kinase, AMP-activated, beta 1 non-catalytic subunit
PRKAG2	protein kinase, AMP-activated, gamma 2 non-catalytic subunit
PRODH	proline dehydrogenase 1
PSA	prostate-specific antigen
RBBP8	retinoblastoma binding protein 8
RIN	RNA integrity number
RNA	ribonucleic acid
RNA-seq	RNA sequencing
RPKM	reads per kilobase per million mapped reads
RPM	revolutions per minute
RPMI	Roswell Park Memorial Institute
RRM2B	ribonucleotide reductase M2 B
rRNA	ribosomal RNA
RT-qPCR	real-time quantitative PCR
SDHAF1	succinate dehydrogenase complex assembly factor 1
SDS	sodium dodecyl sulfate
Ser	serine

SESN1	sestrin 1
SESN2	sestrin 2
sh	shRNA (cells where p53 was knocked down with a shRNA)
shRNA	small hairpin RNA
siRNA	small interfering RNA
S phase	synthesis phase
SPINK6	serine peptidase inhibitor, Kazal type 6
STAGE	stop and go extraction
TBST	tris-buffered saline with Tween20
TCA	tricarboxylic acid
Thr	threonine
TIGAR	TP53-induced glycolysis regulator
TP53BP1	tumor protein p53 binding protein 1
Tris	tris(hydroxymethyl)aminomethane
UbCp	ubiquitin C promoter
UV	ultraviolet
wt	wild-type
w/w	weight/weight
x g	times gravity
XLF	XRCC4-like factor
XRCC4	X-ray repair complementing defective repair in Chinese hamster cells 4
YFP	yellow fluorescent protein
YPEL3	yippee-like 3

8.2 List of clusters obtained after gene enrichment analysis for biological process with DAVID across time points

Enrichment score 9.50 **Annotation Cluster 1** **Cell fate and DNA damage**	*Term*	*Count*	*p-value*
	cell cycle	178	3.6exp-15
	cell cycle process	136	2.3exp-13
	cell cycle phase	108	4.3exp-13
	mitotic cell cycle	94	8.0exp-11
	M phase	83	1.6exp-09
	organelle fission	62	1.5exp-08
	nuclear division	60	2.0exp-08
	mitosis	60	2.0exp-08
	M phase of mitotic cell cycle	60	4.0exp-08
	cell division	69	9.4exp-07
Enrichment score 6.47 **Annotation Cluster 2** **Others**	*Term*	*Count*	*p-value*
	ectoderm development	65	1.0exp-12
	epidermis development	61	2.6exp-12
	epidermal cell differentiation	25	6.2exp-06
	keratinocyte differentiation	23	1.5exp-05
	epithelial cell differentiation	37	1.8exp-05
	epithelium development	50	1.7exp-04
	keratinization	15	6.9exp-04
Enrichment score 6.14 **Annotation Cluster 3** **Cell fate and DNA damage**	*Term*	*Count*	*p-value*
	mitotic cell cycle	94	8.0exp-11
	interphase of mitotic cell cycle	33	1.1exp-06
	interphase	33	2.2exp-06
	G1/S transition of mitotic cell cycle	17	1.4exp-03
Enrichment score 5.66 **Annotation Cluster 4** **Cell fate and DNA damage**	*Term*	*Count*	*p-value*
	regulation of cell growth	54	5.3exp-08
	negative regulation of growth	36	1.8exp-07
	negative regulation of cell growth	31	7.6exp-07
	negative regulation of cell size	31	4.2exp-06
	regulation of cell size	51	5.6exp-06
	regulation of growth	73	1.3exp-05
	regulation of cellular component size	58	1.1exp-04
Enrichment score 4.68 **Annotation Cluster 5** **Cell fate and DNA damage**	*Term*	*Count*	*p-value*
	apoptosis	115	1.2exp-05
	programmed cell death	116	1.4exp-05
	cell death	131	2.9exp-05
	death	131	4.1exp-05

Enrichment score 4.60 **Annotation Cluster 6** **Others**	*Term*	*Count*	*p-value*
	angiogenesis	40	7.6exp-06
	blood vessel morphogenesis	50	2.5exp-05
	blood vessel development	55	4.6exp-05
	vasculature development	56	4.6exp-05
Enrichment score 4.09 **Annotation Cluster 7** **Cell fate and DNA damage**	*Term*	*Count*	*p-value*
	DNA metabolic process	104	1.1exp-06
	response to DNA damage stimulus	78	1.5exp-05
	cellular response to stress	99	1.3exp-03
	DNA repair	55	2.0exp-03
Enrichment score 4.04 **Annotation Cluster 8** **Cell fate and DNA damage**	*Term*	*Count*	*p-value*
	regulation of apoptosis	153	4.2exp-07
	regulation of programmed cell death	153	8.0exp-07
	regulation of cell death	153	9.8exp-07
	anti-apoptosis	47	1.2exp-04
	positive regulation of apoptosis	82	2.5exp-04
	negative regulation of apoptosis	70	2.6exp-04
	positive regulation of programmed cell death	82	3.1exp-04
	positive regulation of cell death	82	3.6exp-04
	negative regulation of programmed cell death	70	3.9exp-04
	negative regulation of cell death	70	4.2exp-04
	induction of apoptosis	60	2.7exp-03
	induction of programmed cell death	60	2.9exp-03
Enrichment score 3.85 **Annotation Cluster 9** **Others**	*Term*	*Count*	*p-value*
	response to wounding	109	5.9exp-07
	inflammatory response	69	3.0exp-05
	defense response	89	1.6exp-01
Enrichment score 3.23 **Annotation Cluster 10** **Cell fate and DNA damage**	*Term*	*Count*	*p-value*
	spindle organization	19	4.9exp-06
	microtubule cytoskeleton organization	36	2.0exp-04
	cytoskeleton organization	76	5.3exp-03
	microtubule-based process	45	2.3exp-02
Enrichment score 2.83 **Annotation Cluster 11** **Others**	*Term*	*Count*	*p-value*
	negative regulation of neurogenesis	15	1.1exp-03
	negative regulation of cell differentiation	45	1.3exp-03
	negative regulation of cell development	15	2.3exp-03

Enrichment score 2.82 **Annotation Cluster 12** **Cell fate and DNA damage**	*Term*	*Count*	*p-value*
	DNA damage response, signal transduction	24	1.3exp-04
	DNA damage response, signal transduction by p53 class mediator	11	9.3exp-04
	induction of apoptosis by intracellular signals	17	9.4exp-04
	DNA damage response, signal transduction resulting in induction of apoptosis	12	2.0exp-03
	DNA damage response, signal transduction by p53 class mediator resulting in induction of apoptosis	6	3.5exp-02
Enrichment score 2.81 **Annotation Cluster 13** **Cell fate and DNA damage**	*Term*	*Count*	*p-value*
	regulation of cell cycle	86	1.7exp-10
	regulation of mitotic cell cycle	40	1.5exp-05
	regulation of cell cycle process	32	3.3exp-05
	positive regulation of cell cycle	15	1.2exp-02
	regulation of mitosis	14	2.4exp-02
	regulation of nuclear division	14	2.4exp-02
	regulation of organelle organization	37	6.7exp-02
	positive regulation of mitosis	7	9.4exp-02
	positive regulation of nuclear division	7	9.4exp-02
	positive regulation of organelle organization	14	2.7exp-01
Enrichment score 2.75 **Annotation Cluster 14** **Fatty acid metabolism**	*Term*	*Count*	*p-value*
	fatty acid metabolic process	44	3.6exp-04
	organic acid biosynthetic process	34	2.3exp-03
	carboxylic acid biosynthetic process	34	2.3exp-03
	fatty acid biosynthetic process	20	4.8exp-03
Enrichment score 2.67 **Annotation Cluster 15** **Cell fate and DNA damage**	*Term*	*Count*	*p-value*
	chromosome segregation	26	1.8exp-05
	mitotic sister chromatid segregation	13	1.3exp-03
	sister chromatid segregation	13	1.7exp-03
	establishment of organelle localization	10	5.4exp-01
Enrichment score 2.66 **Annotation Cluster 16** **Cell fate and DNA damage**	*Term*	*Count*	*p-value*
	cell cycle checkpoint	29	6.3exp-06
	DNA damage response, signal transduction	24	1.3exp-04
	DNA integrity checkpoint	16	1.8exp-03
	DNA damage checkpoint	14	6.4exp-03
	G1 DNA damage checkpoint	6	8.4exp-03
	G1/S transition checkpoint	7	1.6exp-02
	DNA damage response, signal transduction by p53 class mediator resulting in cell cycle arrest	3	1.8exp-01

Enrichment score 2.28 **Annotation Cluster 17** **Cell fate and DNA damage**	*Term*	*Count*	*p-value*
	DNA duplex unwinding	8	5.1exp-03
	DNA geometric change	8	5.1exp-03
	DNA unwinding during replication	7	5.5exp-03
Enrichment score 2.05 **Annotation Cluster 18** **Others**	*Term*	*Count*	*p-value*
	response to hormone stimulus	66	4.6exp-03
	response to endogenous stimulus	71	6.1exp-03
	response to estrogen stimulus	24	7.0exp-03
	response to steroid hormone stimulus	38	7.7exp-03
	response to organic substance	116	8.4exp-03
	response to estradiol stimulus	13	4.0exp-02
Enrichment score 2.03 **Annotation Cluster 19** **Others**	*Term*	*Count*	*p-value*
	iron ion transport	11	2.4exp-03
	transition metal ion transport	18	7.8exp-03
	di-, tri-valent inorganic cation transport	32	4.3exp-02
Enrichment score 1.98 **Annotation Cluster 20** **Others**	*Term*	*Count*	*p-value*
	positive regulation of locomotion	24	2.9exp-03
	positive regulation of cell migration	22	4.0exp-03
	positive regulation of cell motion	23	6.1exp-03
	regulation of cell motion	37	1.4exp-02
	regulation of locomotion	35	3.3exp-02
	regulation of cell migration	31	4.2exp-02
Enrichment score 1.88 **Annotation Cluster 21** **Others**	Term	*Count*	*p-value*
	negative regulation of hydrolase activity	16	7.3exp-04
	negative regulation of peptidase activity	7	4.5exp-02
	negative regulation of caspase activity	6	7.2exp-02
Enrichment score 1.85 **Annotation Cluster 22** **Fatty acid metabolism**	*Term*	*Count*	*p-value*
	unsaturated fatty acid metabolic process	17	4.7exp-04
	icosanoid metabolic process	15	1.8exp-03
	prostanoid metabolic process	8	7.2exp-03
	prostaglandin metabolic process	8	7.2exp-03
	prostanoid biosynthetic process	3	4.2exp-01
	prostaglandin biosynthetic process	3	4.2exp-01

Enrichment score 1.80 **Annotation Cluster 23** **Others**	*Term*	*Count*	*p-value*
	regulation of cell development	47	1.0exp-04
	regulation of neurogenesis	39	2.6exp-04
	regulation of nervous system development	40	2.5exp-03
	regulation of neuron differentiation	28	1.1exp-02
	regulation of axonogenesis	14	2.7exp-02
	positive regulation of cell development	16	2.8exp-02
	regulation of cell projection organization	19	3.4exp-02
	positive regulation of neurogenesis	14	3.5exp-02
	regulation of cell morphogenesis	25	4.7exp-02
	regulation of neuron projection development	15	6.1exp-02
	regulation of cell morphogenesis involved in differentiation	16	6.6exp-02
	positive regulation of cell projection organization	10	1.4exp-01
	positive regulation of axonogenesis	6	2.1exp-01
Enrichment score 1.77 **Annotation Cluster 24** **Others**	*Term*	*Count*	*p-value*
	regulation of blood coagulation	13	1.3exp-03
	regulation of coagulation	14	1.4exp-03
	negative regulation of coagulation	8	4.2exp-02
	fibrinolysis	5	5.8exp-02
	negative regulation of blood coagulation	7	6.7exp-02
	positive regulation of coagulation	5	7.6exp-02
Enrichment score 1.69 **Annotation Cluster 25** **Others**	*Term*	*Count*	*p-value*
	limb morphogenesis	23	6.9exp-03
	appendage morphogenesis	23	6.9exp-03
	appendage development	23	1.1exp-02
	limb development	23	1.1exp-02
	embryonic limb morphogenesis	19	2.8exp-02
	embryonic appendage morphogenesis	19	2.8exp-02
	embryonic morphogenesis	44	3.0exp-01
Enrichment score 1.57 **Annotation Cluster 26** **Others**	*Term*	*Count*	*p-value*
	biological adhesion	112	1.2exp-02
	cell adhesion	111	1.5exp-02
	cell-cell adhesion	44	1.1exp-01

Enrichment score 1.55 **Annotation Cluster 27** **Others**	*Term*	*Count*	*p-value*
	regulation of peptidase activity	24	4.2exp-04
	regulation of endopeptidase activity	22	1.4exp-03
	regulation of caspase activity	21	2.0exp-03
	positive regulation of caspase activity	12	1.3exp-01
	positive regulation of peptidase activity	12	1.3exp-01
	activation of caspase activity	11	1.5exp-01
	regulation of hydrolase activity	50	2.0exp-01
	positive regulation of hydrolase activity	23	6.3exp-01
Enrichment score 1.48 **Annotation Cluster 28** **Others**	*Term*	*Count*	*p-value*
	regeneration	19	2.3exp-03
	tissue regeneration	9	4.6exp-02
	developmental growth	14	3.3exp-01
Enrichment score 1.47 **Annotation Cluster 29** **Cell fate and DNA damage**	*Term*	*Count*	*p-value*
	response to UV	17	2.6exp-03
	response to radiation	36	3.6exp-02
	response to light stimulus	20	4.2exp-01
Enrichment score 1.40 **Annotation Cluster 30** **Others**	*Term*	*Count*	*p-value*
	neutrophil chemotaxis	9	1.0exp-03
	leukocyte migration	15	1.2exp-02
	leukocyte chemotaxis	11	1.6exp-02
	cell chemotaxis	11	2.3exp-02
	chemotaxis	29	5.6exp-02
	taxis	29	5.6exp-02
	macrophage chemotaxis	4	9.9exp-02
	locomotory behavior	44	9.9exp-02
	lymphocyte chemotaxis	3	2.3exp-01
	behavior	65	3.3exp-01
Enrichment score 1.39 **Annotation Cluster 31** **Others**	*Term*	*Count*	*p-value*
	wound healing	43	3.2exp-04
	regulation of body fluid levels	25	9.4exp-02
	hemostasis	19	1.5exp-01
	coagulation	18	1.6exp-01
	blood coagulation	18	1.6exp-01
Enrichment score 1.33 **Annotation Cluster 32** **Cell fate and DNA damage**	*Term*	*Count*	*p-value*
	regulation of DNA metabolic process	26	5.0exp-03
	regulation of DNA replication	15	2.4exp-02
	positive regulation of DNA metabolic process	13	5.1exp-02
	negative regulation of DNA metabolic process	9	1.2exp-01
	positive regulation of DNA replication	6	2.9exp-01

	Term	*Count*	*p-value*
Enrichment score 1.33 **Annotation Cluster 33** **Others**	M phase of meiotic cell cycle	21	2.4exp-02
	Meiosis	21	2.4exp-02
	meiotic cell cycle	21	2.9exp-02
	meiosis I	8	2.9exp-01
	Term	*Count*	*p-value*
Enrichment score 1.32 **Annotation Cluster 34** **Cell fate and DNA damage**	release of cytochrome c from mitochondria	10	6.6exp-04
	apoptotic mitochondrial changes	11	4.2exp-03
	mitochondrion organization	24	1.2exp-01
	regulation of mitochondrial membrane permeability	4	1.6exp-01
	mitochondrial membrane organization	6	4.0exp-01
	mitochondrial transport	10	5.4exp-01

8.3 List of clusters obtained after gene enrichment analysis for biological process with DAVID 24 hours after irradiation

Enrichment Score: 5.49 **Annotation Cluster 1**	*Term*	*Count*	*p-value*
	ectoderm development	63	7.4exp-12
	epidermis development	58	6.7exp-11
	epithelial cell differentiation	35	9.0exp-05
	epidermal cell differentiation	22	1.8exp-04
	keratinocyte differentiation	20	4.4exp-04
	epithelium development	48	5.2exp-04
	keratinization	14	2.1exp-03
Enrichment Score: 4.96 **Annotation Cluster 2**	*Term*	*Count*	*p-value*
	negative regulation of growth	34	1.5exp-06
	negative regulation of cell growth	30	2.1exp-06
	regulation of cell growth	49	3.9exp-06
	negative regulation of cell size	30	1.1exp-05
	regulation of growth	72	1.9exp-05
	regulation of cell size	48	4.7exp-05
	regulation of cellular component size	57	1.7exp-04
Enrichment Score: 3.90 **Annotation Cluster 3**	*Term*	*Count*	*p-value*
	angiogenesis	38	3.8exp-05
	vasculature development	54	1.4exp-04
	blood vessel development	53	1.4exp-04
	blood vessel morphogenesis	46	3.4exp-04
Enrichment Score: 3.07 **Annotation Cluster 4**	*Term*	*Count*	*p-value*
	apoptosis	105	7.5exp-04
	cell death	122	8.1exp-04
	programmed cell death	106	8.5exp-04
	death	122	1.0exp-03
Enrichment Score: 2.84 **Annotation Cluster 5**	*Term*	*Count*	*p-value*
	response to wounding	101	3.3exp-05
	inflammatory response	63	7.5exp-04
	defense response	90	1.2exp-01
Enrichment Score: 2.53 **Annotation Cluster 6**	*Term*	*Count*	*p-value*
	release of cytochrome c from mitochondria	11	1.1exp-04
	apoptotic mitochondrial changes	12	1.1exp-03
	mitochondrion organization	22	2.3exp-01
Enrichment Score: 2.31 **Annotation Cluster 7**	*Term*	*Count*	*p-value*
	regulation of cell cycle	64	7.2exp-04
	regulation of mitotic cell cycle	32	5.4exp-03
	regulation of cell cycle process	23	3.1exp-02

	Term	*Count*	*p-value*
Enrichment Score: 2.30 **Annotation Cluster 8**	anti-apoptosis	47	9.7exp-05
	regulation of apoptosis	136	4.5exp-04
	negative regulation of apoptosis	68	5.9exp-04
	regulation of programmed cell death	136	6.8exp-04
	regulation of cell death	136	8.1exp-04
	negative regulation of programmed cell death	68	8.7exp-04
	negative regulation of cell death	68	9.4exp-04
	induction of apoptosis	50	1.0exp-01
	induction of programmed cell death	50	1.1exp-01
	positive regulation of apoptosis	65	1.1exp-01
	positive regulation of programmed cell death	65	1.2exp-01
	positive regulation of cell death	65	1.3exp-01
Enrichment Score: 2.12 **Annotation Cluster 9**	*Term*	*Count*	*p-value*
	regulation of peptidase activity	25	1.4exp-04
	regulation of endopeptidase activity	24	1.8exp-04
	negative regulation of hydrolase activity	17	1.9exp-04
	regulation of caspase activity	23	2.7exp-04
	negative regulation of peptidase activity	10	6.3exp-04
	negative regulation of caspase activity	9	9.4exp-04
	positive regulation of caspase activity	11	2.2exp-01
	positive regulation of peptidase activity	11	2.2exp-01
	activation of caspase activity	10	2.5exp-01
	regulation of hydrolase activity	42	6.6exp-01
	positive regulation of hydrolase activity	19	8.9exp-01
Enrichment Score: 1.92 **Annotation Cluster 10**	*Term*	*Count*	*p-value*
	induction of apoptosis by intracellular signals	16	2.5exp-03
	DNA damage response, signal transduction	19	1.1exp-02
	DNA damage response, signal transduction by p53 class mediator	9	1.3exp-02
	DNA damage response, signal transduction resulting in induction of apoptosis	10	2.0exp-02
	DNA damage response, signal transduction by p53 class mediator resulting in induction of apoptosis	6	3.4exp-02

Enrichment Score: 1.72 **Annotation Cluster 11**	*Term*	*Count*	*p-value*
	regulation of blood coagulation	12	4.1exp-03
	regulation of coagulation	13	4.1exp-03
	negative regulation of coagulation	8	4.1exp-02
	fibrinolysis	5	5.7exp-02
	negative regulation of blood coagulation	7	6.4exp-02
Enrichment Score: 1.65 **Annotation Cluster 12**	*Term*	*Count*	*p-value*
	negative regulation of neurogenesis	15	1.1exp-03
	regulation of neurogenesis	36	1.8exp-03
	negative regulation of cell development	15	2.1exp-03
	regulation of cell development	41	4.0exp-03
	regulation of neuron differentiation	28	9.6exp-03
	regulation of axonogenesis	15	1.1exp-02
	regulation of nervous system development	37	1.1exp-02
	regulation of cell morphogenesis	26	2.6exp-02
	regulation of neuron projection development	16	3.0exp-02
	negative regulation of axonogenesis	8	3.3exp-02
	negative regulation of cell differentiation	38	3.9exp-02
	regulation of cell projection organization	18	5.8exp-02
	negative regulation of cell projection organization	8	5.8exp-02
	regulation of cell morphogenesis involved in differentiation	16	6.2exp-02
	positive regulation of neurogenesis	13	6.8exp-02
	positive regulation of cell development	14	9.7exp-02
	positive regulation of axonogenesis	6	2.1exp-01
	positive regulation of cell projection organization	8	4.0exp-01
Enrichment Score: 1.50 **Annotation Cluster 13**	*Term*	*Count*	*p-value*
	positive regulation of signal transduction	54	6.3exp-03
	positive regulation of cell communication	57	1.5exp-02
	regulation of protein kinase cascade	43	3.6exp-02
	regulation of I-kappaB kinase/NF-kappaB cascade	21	5.1exp-02
	positive regulation of protein kinase cascade	30	5.3exp-02
	positive regulation of I-kappaB kinase/NF-kappaB cascade	18	1.1exp-01

Enrichment Score: 1.49 **Annotation Cluster 14**	*Term*	*Count*	*p-value*
	cell adhesion	110	1.6exp-02
	biological adhesion	110	1.7exp-02
	cell-cell adhesion	43	1.3exp-01
Enrichment Score: 1.46 **Annotation Cluster 15** **Fatty acid metabolism**	*Term*	*Count*	*p-value*
	fatty acid metabolic process	41	2.1exp-03
	fatty acid biosynthetic process	17	4.1exp-02
	organic acid biosynthetic process	26	1.3exp-01
	carboxylic acid biosynthetic process	26	1.3exp-01
Enrichment Score: 1.42 **Annotation Cluster 16**	*Term*	*Count*	*p-value*
	tissue remodeling	15	9.5exp-03
	bone remodeling	8	1.3exp-02
	bone resorption	6	3.4exp-02
	multicellular organismal homeostasis	18	4.0exp-02
	tissue homeostasis	13	1.0exp-01
	anatomical structure homeostasis	18	1.9exp-01
Enrichment Score: 1.41 **Annotation Cluster 17**	*Term*	*Count*	*p-value*
	positive regulation of locomotion	22	1.1exp-02
	positive regulation of cell migration	20	1.6exp-02
	positive regulation of cell motion	20	4.1exp-02
	regulation of locomotion	33	7.0exp-02
	regulation of cell motion	33	7.4exp-02
	regulation of cell migration	29	9.0exp-02
Enrichment Score: 1.31 **Annotation Cluster 18** **Fatty acid metabolism**	*Term*	*Count*	*p-value*
	unsaturated fatty acid metabolic process	16	1.3exp-03
	icosanoid metabolic process	14	5.0exp-03
	prostanoid metabolic process	8	6.9exp-03
	prostaglandin metabolic process	8	6.9exp-03
	unsaturated fatty acid biosynthetic process	8	1.4exp-01
	leukotriene metabolic process	6	1.4exp-01
	cellular alkene metabolic process	6	1.6exp-01
	icosanoid biosynthetic process	6	3.6exp-01
	leukotriene biosynthetic process	4	4.5exp-01
	alkene biosynthetic process	4	4.5exp-01